Measuring Parameters of Black holes

- **А.Ф.Захаров (Alexander F. Zakharov)**
- Institute of Theoretical and Experimental Physics, Moscow
- ASC FI RAS
- E-mail: zakharov@itep.ru

- Neaples, Italy
- Wednesday, April 20, 2005

NEWS

Published online: 31 March 2005; | doi:10.1038/news050328-8

Black holes 'do not exist'

Philip Ball

These mysterious objects are dark-energy stars, physicist claims.

Black holes are staples of science fiction and many think astronomers have observed them indirectly. But according to a physicist at the Lawrence Livermore National Laboratory in California, these awesome breaches in space-time do not and indeed cannot exist.

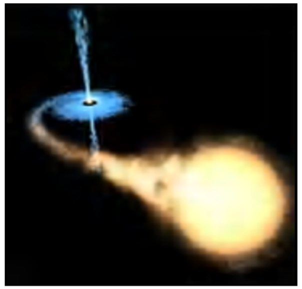

Black holes, such as the one pictured in this artist's impression, may in fact be pockets of 'dark energy'.

© ESA/NASA

Over the past few years, observations of the motions of galaxies have shown that some 70% the Universe seems to be composed of a strange 'dark energy' that is driving the Universe's accelerating expansion.

George Chapline thinks that the collapse of the massive stars, which was long believed to generate black holes, actually leads to the formation of stars that contain dark energy. "It's a near certainty that black holes don't exist," he claims.

Black holes are one of the most celebrated predictions of Einstein's general theory of relativity, which explains gravity as the warping of space-time caused by massive objects. The theory suggests that a sufficiently massive star, when it dies, will collapse under its own gravity to a single point.

But Einstein didn't believe in black holes, Chapline argues. "Unfortunately", he adds, "he couldn't articulate why." At the root of the problem is the other revolutionary theory of twentieth-century physics, which Einstein also helped to formulate: quantum mechanics.

> **It's a near certainty that black holes don't exist.**
>
> George Chapline
> Lawrence Livermore National Laboratory

In general relativity, there is no such thing as a 'universal time' that makes clocks tick at the same rate everywhere. Instead, gravity makes clocks run at different rates in different places. But quantum mechanics, which describes physical phenomena at infinitesimally small scales, is meaningful only if time is universal; if not, its equations make no sense.

This problem is particularly pressing at the boundary, or event horizon, of a black hole. To a far-off observer, time seems to stand still here. A spacecraft falling into a black hole would seem, to someone watching it from afar, to be stuck forever at the event horizon, although the astronauts in the spacecraft would feel as if they were continuing to fall. "General relativity predicts that nothing happens at the event horizon," says Chapline.

Quantum transitions

However, as long ago as 1975 quantum physicists argued that strange things do happen at an event horizon: matter governed by quantum laws becomes hypersensitive to slight disturbances. "The result was quickly forgotten," says Chapline, "because it didn't agree with the prediction of general relativity. But actually, it was absolutely correct."

This strange behaviour, he says, is the signature of a 'quantum phase transition' of space-time. Chapline argues that a star doesn't simply collapse to form a black hole; instead, the space-time inside it becomes filled with dark energy and this has some intriguing gravitational effects.

Outside the 'surface' of a

dark-energy star, it behaves much like a black hole, producing a strong gravitational tug. But inside, the 'negative' gravity of dark energy may cause matter to bounce back out again.

If the dark-energy star is big enough, Chapline predicts, any electrons bounced out will have been converted to positrons, which then annihilate other electrons in a burst of high-energy radiation. Chapline says that this could explain the radiation observed from the centre of our galaxy, previously interpreted as the signature of a huge black hole.

He also thinks that the Universe could be filled with 'primordial' dark-energy stars. These are formed not by stellar collapse but by fluctuations of space-time itself, like blobs of liquid condensing spontaneously out of a cooling gas. These, he suggests, could be stuff that has the same gravitational effect as normal matter, but cannot be seen: the elusive substance known as dark matter.

Top

References

1. Chapline G. *Arxiv*, http://xxx.arxiv.org/abs/astro-ph/0503200 (2005).

Top

Outline of my talk

- History
- Black holes in astrophysics
- The iron K_α -line as a tool for BH characteristics
- Movies

Outline of my talk

- Wrong pictures of black holes
- Mirages around BHs and retro-lensing
- Black Hole Images
- Conclusions

Black hole history (I)

- 1783 : The Reverend John Michell (invisible sphere)
- 1798,1799 : P.S. Laplace (Exposition du Systeme du Monde Part II, p. 305, Allgemeine Geographifche Ephemeriden, 4, S.1, 1799)
- 1915 : K. Schwarzschild
- 1928 : Ya.I Frenkel (EOS for degenerate electron Fermi-gas with arbitrary relativistic degree and typical WD masses)
- 1930 : E. Stoner (the upper limit for masses of white dwarfs for uniform mass distribution)
- 1931 : S. Chandrasekhar (the upper limit for masses of white dwarfs for polytrope mass distribution)
- 1932 : E. Stoner (EOS for degenerate electron Fermi-gas with arbitrary relativistic degree)
- 1934, 1935 : S. Chandrasekhar (the upper limit for masses of white dwarfs for arbitrary relativistic degree)
- 1935 : A.Eddington (rejections of the upper limit for WDs)
- 1939 : R.Oppenheimer & G.Volkoff (the upper limit for NSs and the GR approach)
- 1939 : R.Oppenheimer & R.Snyder (the collapse of pressureless stars and the GR approach) “Every statement of this paper is in accordance with ideas that remain valid today”(Novikov & Frolov, 2001)

Black hole history (II)

- 1939: Einstein considered a possibility "to create a field having
- Schwarzschild singularity by gravitating masses";
- Einstein (1939): "The main result of this investigation is a clear understanding that Schwarzschild singularities do not exits in real conditions";
- 1942: Bergmann:" In reality, mass has no possibility to concentrate
- by the following way that the Schwarzschild singular surface would be in vacuum"
- 1958 : D. Finkelstein & 1960 M.Kruskal (causal structure of Schwarzschild metric)
- 1962 : R. Feynman "Lectures on gravitation" ("it would be interesting to investigate dust collapse" (23 years later OS paper!)
- 1967 : J.A. Wheeler: black holes predicted to result from "continued gravitational collapse of over-compact masses" (the birth of the BH concept)

Таблица 5. Параметры двойных систем с ЧД

Система	Спектр оптической звезды	P_{orb}, сут	$f_v(m)$, в $M_\odot$	m_x, в $M_\odot$	m_v, в $M_\odot$	V_{pec}, км c^{-1}	Примечание
Cyg X-1 V 1357 Cyg	O 9,7 Iab	5,6	$0{,}24 \pm 0{,}01$	16 ± 5	33 ± 9	$2{,}4 \pm 1{,}2$	Стационарная
LMC X-3	B3 Ve	1,7	$2{,}3 \pm 0{,}3$	9 ± 2	6 ± 2	—	Стационарная
LMC X-1	O (7–9) III	4,2	$0{,}14 \pm 0{,}05$	7 ± 3	22 ± 4	—	Стационарная
A0 620–00 (V616 Mon)	K5 V	0,3	$2{,}91 \pm 0{,}08$	10 ± 5	$0{,}6 \pm 0{,}1$	-15 ± 5	Транзиентная
GS 2023+338 (V404 Cyg)	K0 IV	6,5	$6{,}08 \pm 0{,}06$	12 ± 2	$0{,}7 \pm 0{,}1$	$8{,}5 \pm 2{,}2$	Транзиентная
GRS 1124–68 (GU Mus)	K2 V	0,4	$3{,}01 \pm 0{,}15$	$6(+5-2)$	$0{,}8 \pm 0{,}1$	25 ± 5	Транзиентная
GS 2000+25 (QZ Vul)	K5 V	0,3	$4{,}97 \pm 0{,}10$	10 ± 4	$0{,}5 \pm 0{,}1$	—	Транзиентная
GRO J0422+32 (V518 Per)	M2 V	0,2	$1{,}13 \pm 0{,}09$	10 ± 5	$0{,}4 \pm 0{,}1$	—	Транзиентная
GRO J1655–40 (XN Sco 1994)	F5 IV	2,6	$2{,}73 \pm 0{,}09$	$6{,}3 \pm 0{,}5$	$2{,}4 \pm 0{,}4$	-114 ± 19	Транзиентная
H 1705–250 (V2107 Oph)	K5 V	0,5	$4{,}86 \pm 0{,}13$	6 ± 1	$0{,}4 \pm 0{,}1$	38 ± 20	Транзиентная
4U 1543–47 (HL Lup)	A2 V	1,1	$0{,}22 \pm 0{,}02$	4,0–6,7	$\sim 2{,}5$	—	Транзиентная
GRS 1009–45 (MM Vel)	(K6–M0) V	0,3	$3{,}17 \pm 0{,}12$	3,6–4,7	0,5–0,7	—	Транзиентная
SAX J1819.3–2525 (V4641 Sgr)	B9 III	2,8	$2{,}74 \pm 0{,}12$	$9{,}61(+2{,}08-0{,}88)$	$6{,}53(+1{,}6-1{,}03)$	—	Транзиентная
XTE J1118+480	(K7–M0) V	0,17	$6{,}1 \pm 0{,}3$	6,0–7,7	0,09–0,5	145*	Транзиентная
GRS 1915+105	(K–M) III	33,5	$9{,}5 \pm 3{,}0$	14 ± 4	$1{,}2 \pm 0{,}2$		Транзиентная

Таблица 6. Микроквазары в нашей Галактике

Название источника	Компактный объект	$V_{джета}$
GRS 1915 + 105	ЧД	$0{,}92c - 0{,}98c$
GRO J1655 – 40	ЧД	$0{,}92c$
XTE J1748 – 288	ЧД	$0{,}93c - 0{,}23c$
SS 433	ЧД	$0{,}26c$
Cyg X-3	ЧД	$\sim 0{,}3c - \geqslant 0{,}8c$
CI Cam	НЗ?	$\sim 0{,}15c$
Sco X-1	НЗ	$\sim 0{,}5c$
Cir X-1	НЗ	$\geqslant 0{,}1c$
1E 1740.7 – 2942	ЧД	
GRS 1758 – 258	ЧД	
SAX J1819.3 – 2525	ЧД	$\geqslant 0{,}95c$
LS 5039	?	$\geqslant 0{,}15c$
Cyg X-1	ЧД	$> 0{,}6c$
XTE J1550 – 564	ЧД	

- Ho1
- Ho2

Black holes in centers of galaxies

(L.Ho,ApJ 564,120 (2002))

TABLE 1: GALAXIES WITH BLACK HOLE MASSES

Galaxy Name (1)	Hubble Type (2)	T (3)	Spectral Class (4)	cz (km s^{-1}) (5)	D (Mpc) (6)	Ref. (7)	M_{BH} ($M_\odot$) (8)	Method (9)	Ref. (10)
3C 120 (Mrk 1506)	S0:	−1.0	S1	9896	137.8	1	2.3×10^7	R	1
3C 390.3 (VII w 838)	E?	−5.0	S1	16818	241.2	1	3.4×10^8	R	1
Ark 120 (Mrk 1095)	S0/a	0.0	S1	9682	134.6	1	1.84×10^8	R	1
Arp 102B	E0	−5.0	L1.8	7245	99.7	1	2.2×10^8	G	2
Circinus	Sb:	3.0	S2	449	4.0	2	1.3×10^6	M	3
Fairall 9	S?	⋯	S1	14095	199.8	1	8.0×10^7	R	1
IC 342	SABcd	6.0	H	31	1.8	3	$<5.0 \times 10^5$	S	4
IC 1459	E3	−5.0	L2	1691	29.2	4	3.7×10^8	G	5
IC 4329A	S0+	−1.0	S1	4813	65.5	1	5.0×10^6	R	1
Milky Way	Sbc	3.0	⋯	⋯	0.008	5	2.95×10^6	S	6
Mrk 79 (UGC 3973)	SBb	3.0	S1.5	6652	91.3	1	5.2×10^7	R	1
Mrk 110	Pair?	⋯	S1	10580	147.7	1	5.6×10^6	R	1
Mrk 279 (UGC 8823)	S0	−1.0	S1.5	9129	126.6	1	4.2×10^7	R	1
Mrk 335	S0/a	0.0	S1.0	7730	106.6	1	6.3×10^6	R	7
Mrk 509	comp	⋯	S1	10312	143.8	1	5.78×10^7	R	1
Mrk 590 (NGC 863)	Sa:	1.0	S1.2	7910	109.2	1	1.78×10^7	R	1
Mrk 817 (UGC 9412)	S?	⋯	S1.5	9430	131.0	1	4.4×10^7	R	1
NGC 205 (M110)	dE5	−5.0	A	−241	0.74	6	$<9.3 \times 10^4$	S	8
NGC 221 (M32)	E2	−6.0	A	−145	0.81	4	3.9×10^6	S	9
NGC 224 (M31)	Sb	3.0	A	−300	0.76	4	3.3×10^7	S	10

NGC 224 (M31)	Sb	3.0	A	–300	0.76	4	3.3×10^7	S	10
NGC 598 (M33)	Scd	6.0	H	–179	0.87	6	$<1.5 \times 10^3$	S	11
NGC 821	E6?	–5.0	A	1735	24.1	4	5.0×10^7	S	12
NGC 1023	SB0−	–3.0	A	637	11.4	4	3.9×10^7	S	13
NGC 1068 (M77)	Sb	3.0	S1.9	1137	14.4	7	1.6×10^7	M	14
NGC 2778	E	–5.0	···	2049	22.9	4	2.0×10^7	S	12
NGC 2787	SB0+	–1.0	L1.9	696	7.5	4	3.9×10^7	G	15
NGC 3031 (M81)	Sab	2.0	S1.5	–34	3.9	4	6.3×10^7	S	16
NGC 3115	S0−	–3.0	A	720	9.7	4	9.1×10^8	S	17
NGC 3227	SABa	1.0	S1.5	1157	20.6	7	3.9×10^7	R	1
NGC 3245	S0?	–2.0	T2	1358	20.9	4	2.1×10^8	G	18
NGC 3377	E5+	–5.0	A	665	11.2	4	1.0×10^8	S	12
NGC 3379 (M105)	E1	–5.0	L2/T2:	911	10.6	4	1.0×10^8	S	19
NGC 3384	SB0−:	–3.0	A	704	11.6	4	1.8×10^7	S	12
NGC 3516	SB0:	–2.0	S1.2	2649	38.9	7	2.3×10^7	R	7
NGC 3608	E2	–5.0	L2/S2:	1253	22.9	4	1.1×10^8	S	12
NGC 3783	SBa	1.0	S1	2917	38.5	7	9.4×10^6	R	1
NGC 3998	S0?	–2.0	L1.9	1040	14.1	4	5.6×10^8	S	16
NGC 4051	SABbc	4.0	S1.2	725	17.0	7	1.3×10^6	R	1
NGC 4151	SABab	2.0	S1.5	995	20.3	7	1.53×10^7	R	1
NGC 4203	SAB0	–3.0	L1.9	1086	14.1	4	$<1.2 \times 10^7$	G	15
NGC 4258 (M106)	SABbc	4.0	S1.9	448	7.3	4	4.1×10^7	M	20
NGC 4261 (3C 270)	E2+	–5.0	L2	2238	31.6	4	5.2×10^8	G	21
NGC 4291	E	–5.0	A	1757	26.2	4	1.5×10^8	S	12
NGC 4342	S0−	–3.0	···	751	16.8	7	3.4×10^8	S	22
NGC 4374 (M84, 3C 272.1)	E1	–5.0	L2	1060	18.4	4	1.6×10^9	G	23
NGC 4395	Sm:	9.0	S1.5	319	3.6	7	$<1.1 \times 10^5$	S	24
NGC 4459	S0+	–1.0	T2:	1210	16.1	4	6.5×10^7	G	15
NGC 4473	E5	–5.0	A	2244	15.7	4	1.0×10^8	S	12
NGC 4486 (M87, 3C 274)	E0+	–4.0	L2	1307	16.1	4	3.4×10^9	G	25

Galaxy Name (1)	Hubble Type (2)	T (3)	Spectral Class (4)	cz (km s^{-1}) (5)	D (Mpc) (6)	Ref. (7)	M_{BH} ($M_\odot$) (8)	Method (9)	Ref. (10)
NGC 4486B	E0	−6.0	···	1555	16.1	8	6.0×10^8	S	26
NGC 4564	E	−5.0	A	1142	15.0	4	5.7×10^7	S	12
NGC 4593	SBb	3.0	S1	2698	39.5	7	8.1×10^6	R	7
NGC 4594 (M104)	Sa	1.0	L2	1024	9.8	4	1.1×10^9	S	27
NGC 4596	SB0	−1.0	L2::	1874	16.8	7	5.8×10^7	G	15
NGC 4649 (M60)	E2	−5.0	A	1117	16.8	4	2.0×10^9	S	12
NGC 4697	E6	−5.0	···	1241	11.7	4	1.2×10^8	S	12
NGC 4945	SBcd	6.0	S2	560	4.2	9	1.1×10^6	M	28
NGC 5548	S0/a	0.0	S1.5	5149	70.2	1	1.23×10^8	R	1
NGC 5845	E	−5.0	···	1456	25.9	4	3.2×10^8	S	12
NGC 6251	E0	−5.0	S2	6900	94.8	1	5.4×10^8	G	29
NGC 7052	E4	−5.0	···	4672	63.6	1	3.6×10^8	G	30
NGC 7457	S0−?	−3.0	A	812	13.2	4	3.4×10^6	S	12
NGC 7469	SABa	1.0	S1.0	4892	66.6	1	6.5×10^6	R	1
PG 0026+129	···	···	QSO	0.142	627.4	1	5.4×10^7	R	1
PG 0052+251	S	···	QSO	0.155	690.4	1	2.2×10^8	R	1
PG 0804+761	···	···	QSO	0.100	429.9	1	1.89×10^8	R	1
PG 0844+349	···	···	QSO	0.064	268.4	1	2.16×10^7	R	1
PG 0953+414	S	···	QSO	0.239	1118	1	1.84×10^8	R	1
PG 1211+143	···	···	QSO	0.085	361.7	1	4.05×10^7	R	1
PG 1226+023 (3C 273)	E	···	QSO	0.158	705.1	1	5.5×10^8	R	1
PG 1229+204	S	···	QSO	0.064	268.4	1	7.5×10^7	R	1
PG 1307+085	E	···	QSO	0.155	690.4	1	2.8×10^8	R	1
PG 1351+640	···	···	QSO	0.087	370.7	1	4.6×10^7	R	1
PG 1411+442	···	···	QSO	0.089	379.8	1	8.0×10^7	R	1
PG 1426+015 (Mrk 1383)	···	···	QSO	0.086	366.2	1	4.7×10^8	R	1
PG 1613+658 (Mrk 876)	···	···	QSO	0.129	565.3	1	2.41×10^8	R	1
PG 1617+175 (Mrk 877)	···	···	QSO	0.114	494.7	1	2.73×10^8	R	1
PG 1700+518	···	···	QSO	0.292	1406	1	6×10^7	R	1
PG 1704+608 (3C 351)	E	···	QSO	0.371	1857	1	3.7×10^7	R	1
PG 2130+099	···	···	QSO	0.061	255.3	1	1.44×10^8	R	1

Note.— Col. (1) Galaxy name. Col. (2) Revised Hubble type from de Vaucouleurs et al. 1991 (RC3), except for QSOs, which is estimated by Hamilton, Casertano, & Turnshek 2001. Col. (3) Morphological type index from the RC3. Col. (4) Spectral class of the nucleus from Ho et al. 1997, and otherwise from Whittle 1992a and NED, where A = absorption-line nucleus, H = H II nucleus, L = LINER, S = Seyfert, T = "transition object" (LINER/H II), 1 = type 1, 2 = type 2, and a fractional number between 1 and 2 denotes various intermediate types; uncertain and highly uncertain classifications are followed by a single and double colon, respectively. Col. (5) Heliocentric radial velocity (redshift for QSOs) from NED. Col. (6) Adopted distance. Col. (7) Reference for D. Col. (8) Black hole mass, scaled to our adopted distances. Col. (9) Method for determining $M_{\rm BH}$: G, gas kinematics; M, maser kinematics; R, reverberation mapping; S, stellar kinematics. Col. (10) Reference for $M_{\rm BH}$.

References.— *Distance:* (1) Luminosity distance derived from heliocentric redshift, $H_0 = 75$ km s^{-1} Mpc^{-1}, $\Omega_{\rm M} = 0.3$, and $\Omega_\lambda = 0.7$; (2) Freeman et al. 1977; (3) McCall 1989; (4) Tonry et al. 2001; (5) Reid 1993; (6) Ferrarese et al. 2000; (7) Tully 1988, who also uses our value of H_0; (8) Assumed to be at the distance of NGC 4486; (9) Assumed to be at the distance of NGC 5128, which is known from Tonry et al. 2001.

References.— *Black hole mass:* (1) Kaspi et al. 2000; (2) Newman et al. 1997; (3) Greenhill et al. 2000; (4) Böker, van der Marel, & Vacca 1999; (5) Verdoes Kleijn et al. 2000; (6) Genzel et al. 2000; (7) Ho 1999a; (8) Jones et al. 1996; (9) van der Marel et al. 1998; (10) Kormendy & Bender 1999; (11) Gebhardt et al. 2001; (12) Gebhardt et al. 2000a; (13) Bower et al. 2001a; (14) Greenhill et al. 1996; (15) Sarzi et al. 2001; (16) Bower et al. 2001b; (17) Emsellem, Dejonghe, & Bacon 1999; (18) Barth et al. 2001; (19) Gebhardt et al. 2000b; (20) Miyoshi et al. 1995; (21) Ferrarese, Ford, & Jaffe 1996; (22) Cretton & van den Bosch 1999; (23) Bower et al. 1998; (24) Filippenko & Ho 2001; (25) Macchetto et al. 1997; (26) Kormendy et al. 1997a; (27) Kormendy et al. 1997b; (28) Greenhill, Moran, & Herrnstein 1997; (29) Ferrarese & Ford 1999; (30) van der Marel & van den Bosch 1998.

- Macho_96_5_light _curve
- Macho_96_6_light _curve
- Likelihood functions for BH microlenses
- Probable masses and distances for BH microlenses

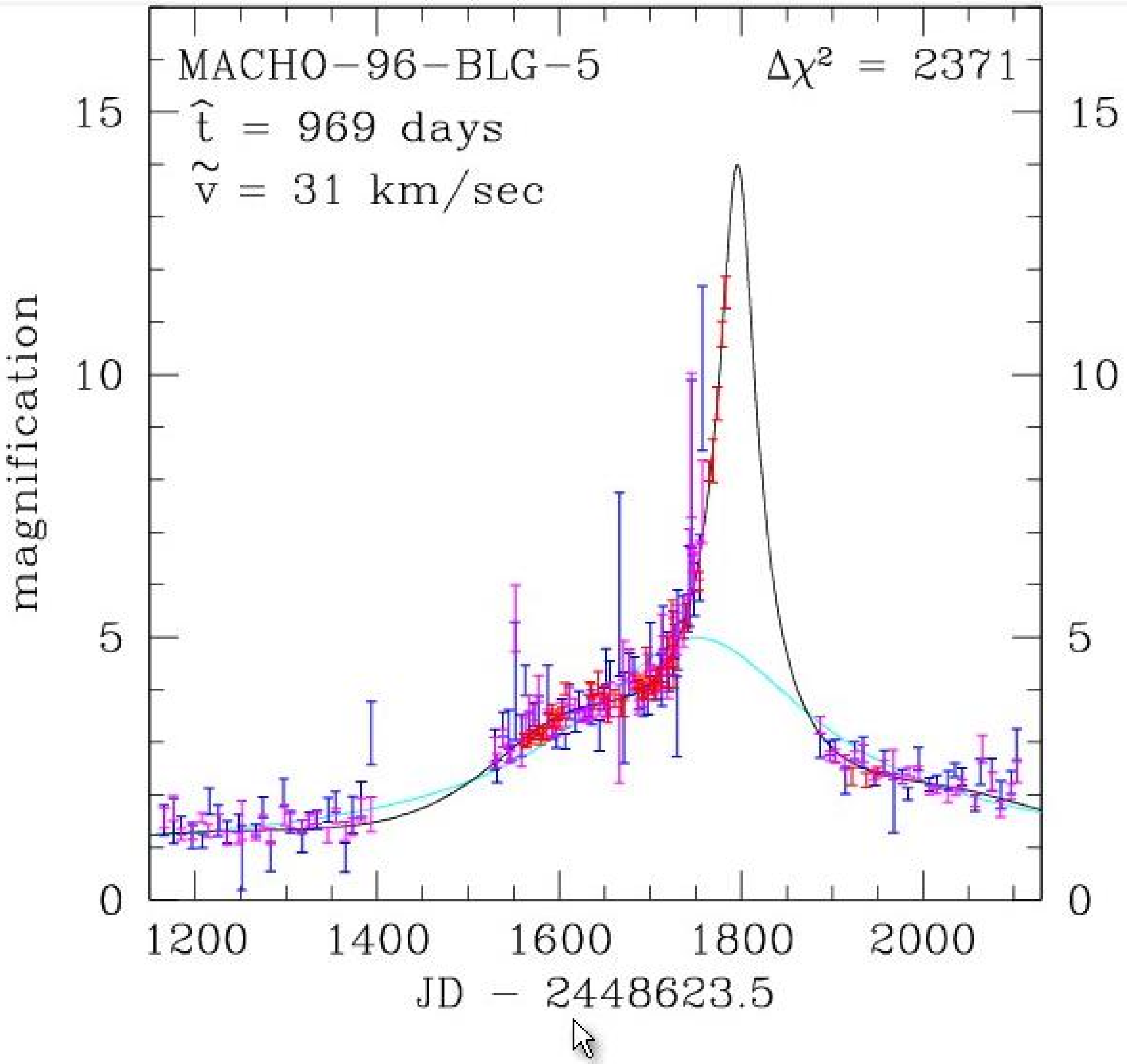

Fig. 7.— MACHO-96-BLG-5 lightcurves normalized to the unlensed flux of the lensed star. The MACHO red and blue data are plotted in magenta and blue, respectively, and the CTIO data are shown in red. The black curve is the parallax fit while the cyan curve is the best fit standard microlensing lightcurve. An additional 4 years of data showing very little photometric variation are not shown.

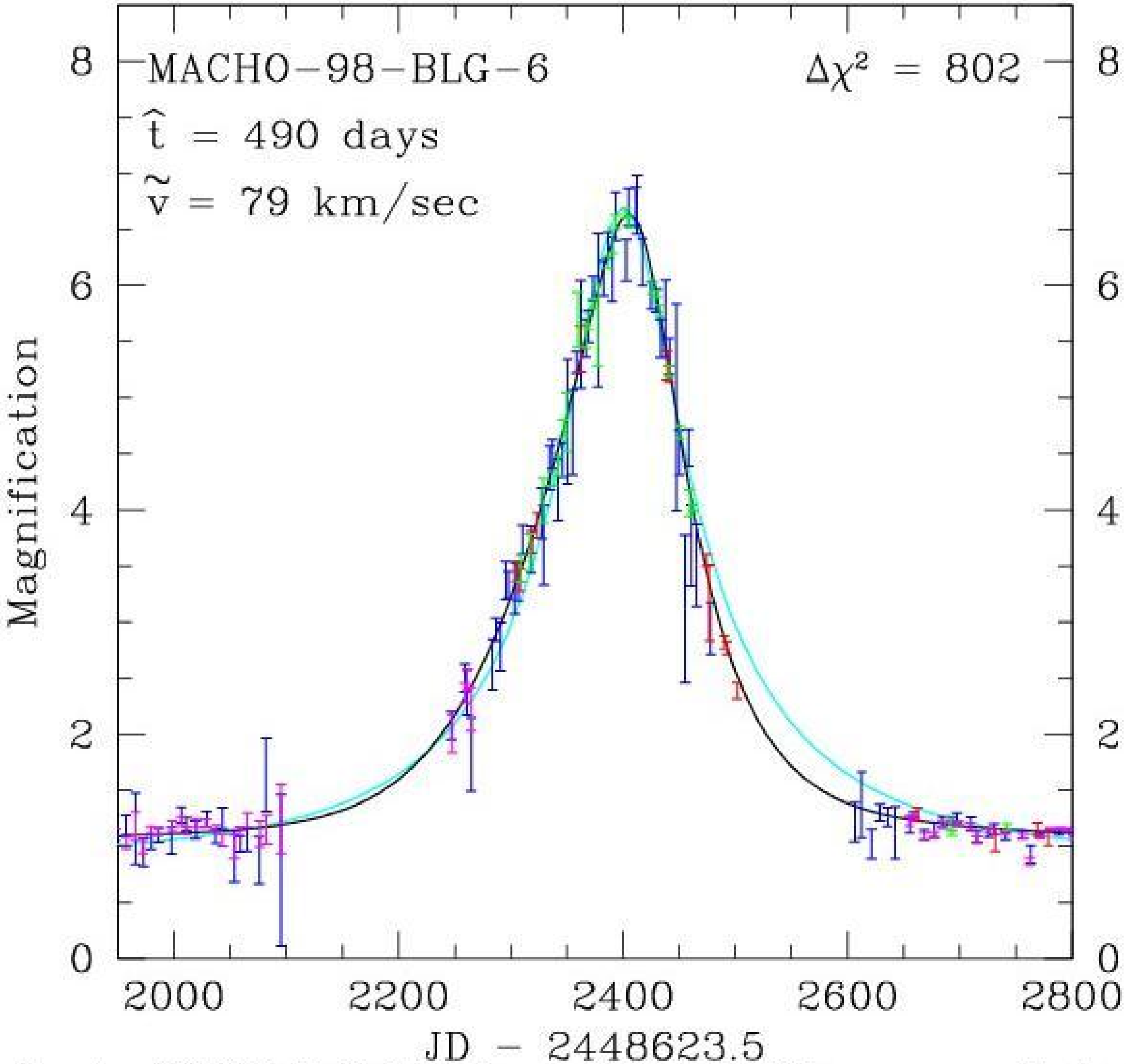

Fig. 4.— MACHO-98-BLG-6 lightcurve closeup with lightcurves normalized to the unlensed flux of the lensed star. The MACHO red and blue data are plotted in magenta and blue, respectively, the CTIO data are shown in red, and the MPS data are shown in green. The black curve is the parallax fit while the cyan curve is the best fit standard microlensing lightcurve. The gap in the MACHO red data during the day 2280-2650 interval is due to a CCD failure. An additional year of data showing no photometric variation is not shown.

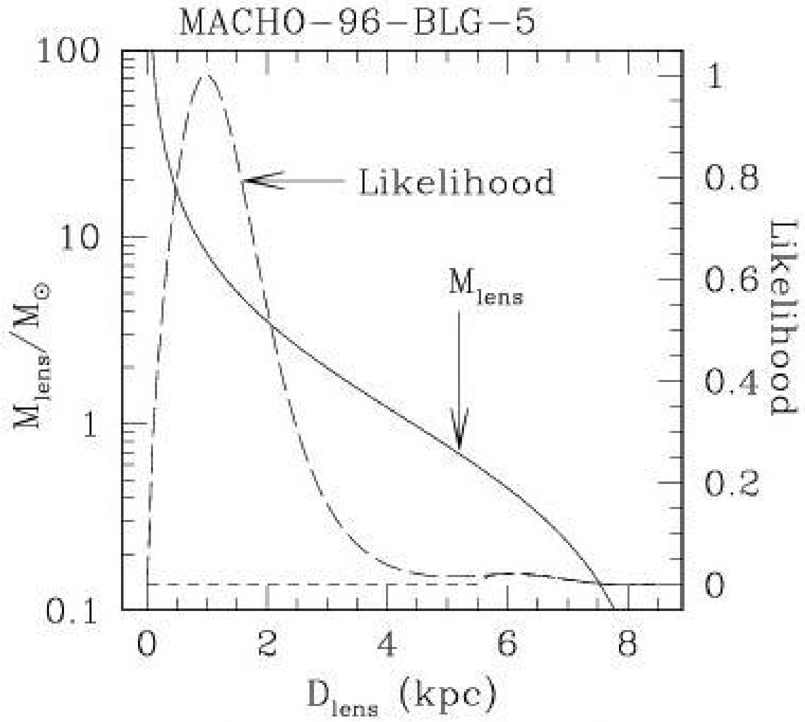

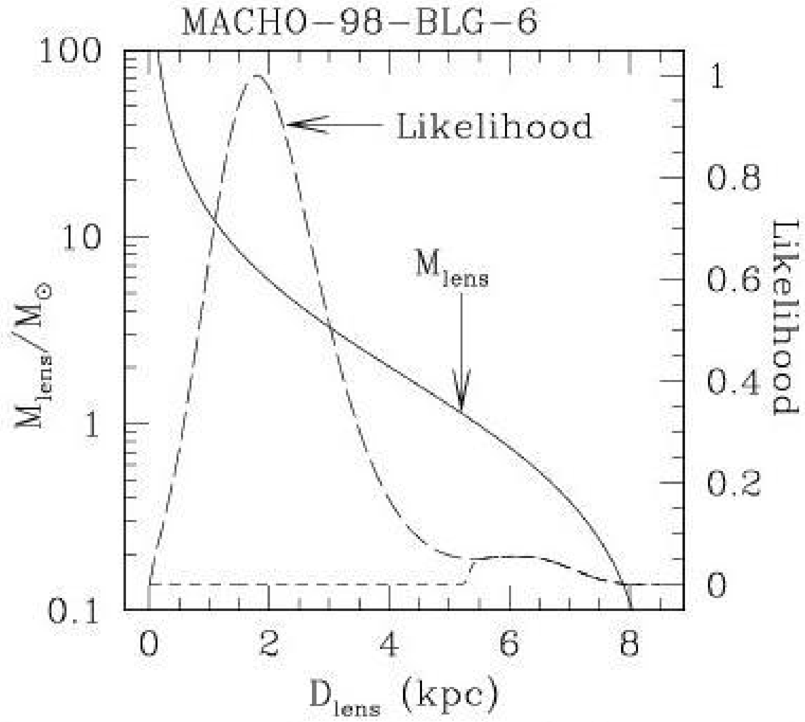

Fig. 11.— The mass vs. distance relations (solid curves) for our candidate black hole lenses are shown along with the likelihood functions (long dashed curves) computed assuming a standard model for the Galactic phase space distribution. The source star is assumed to reside in the bulge for both events. The implied best fit masses are $M = 6^{+10}_{-3} M_{\odot}$ for the MACHO-96-BLG-5 lens and $M = 6^{+7}_{-3} M_{\odot}$ for the MACHO-98-BLG-6. The 95% confidence level lower limits on the masses are $1.6 M_{\odot}$ and $0.94 M_{\odot}$ respectively. The short dashed curves delineate the portion of the likelihood functions that is allowed when the lens is assumed to be a main sequence star. The ratio of the area below this portion to the entire area below the likelihood curve gives a probability that a lens is a main sequence star. For MACHO-96-BLG-5, the upper limit on the lens brightness is very stringent because of the HST images, and a main sequence lens is ruled out.

Table 7. Mass & Magnitude Estimates for the MACHO Microlensing Parallax Events

Event	$M/\mathrm{M}_\odot$	$M_{\mathrm{MS}}/\mathrm{M}_\odot$	$D_{\ell-\mathrm{MS}}$	sep-MS	V_s	$\Delta I_{\ell s}$	$\Delta V_{\ell s}$	$\Delta B_{\ell s}$	$\Delta U_{\ell s}$
104-C	$1.1^{+1.1}_{-0.5}$	0.74	2.7 kpc	40 mas	17.3	3.5	3.5	3.5	3.2
96-BLG-5	6^{+10}_{-3}	-	-	-	-	-	-	-	-
96-BLG-12	$1.3^{+1.8}_{-0.7}$	0.75	2.0 kpc	28 mas	18.0	2.1	2.2	2.2	2.3
98-BLG-6	$2.5^{+1.7}_{-0.9}$	0.88	5.7 kpc	5 mas	20.1	2.2	1.9	1.6	1.1
99-BLG-1	$0.7^{+1.2}_{-0.4}$	0.40	1.7 kpc	17 mas	18.9	1.8	3.2	3.6	3.9
99-BLG-8	$1.2^{+1.6}_{-0.6}$	1.2	1.6 kpc	25 mas	16.3	1.3	0.7	−0.3	−1.1

Note. — These are the parameters of the "most likely" main sequence star lenses for our best microlensing parallax events. For MACHO-96-BLG-5, a main sequence lens is ruled out.

Black holes in galaxy centers

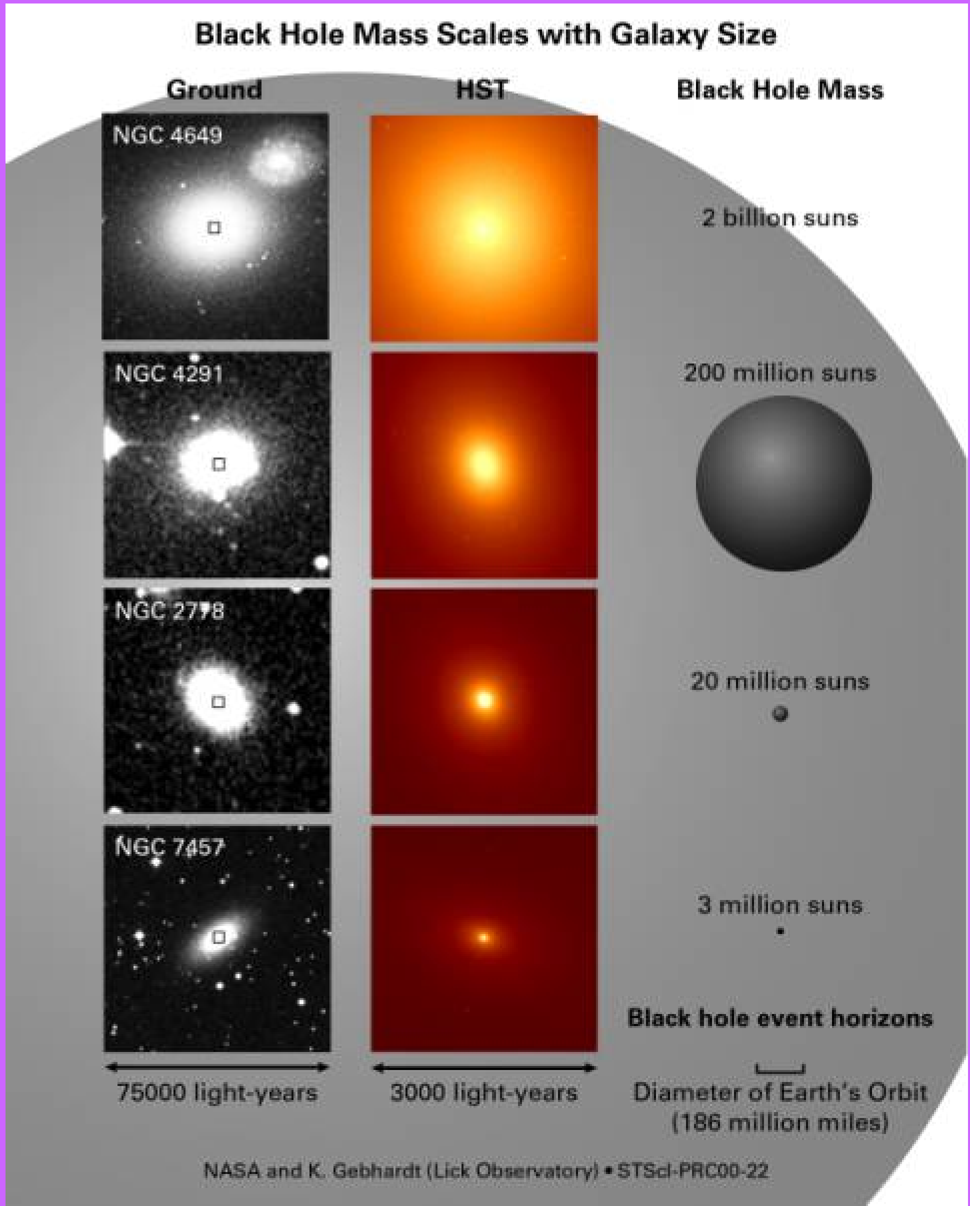

Many galaxies are assumed to have the black holes in their centers.

The black hole masses vary from million to dozens of billion Solar mass.

Because of the small size we cannot observe the black hole itself, but can register the emission of the accretion disk, rotating around the black hole.

Seyfert galaxies and Kα line

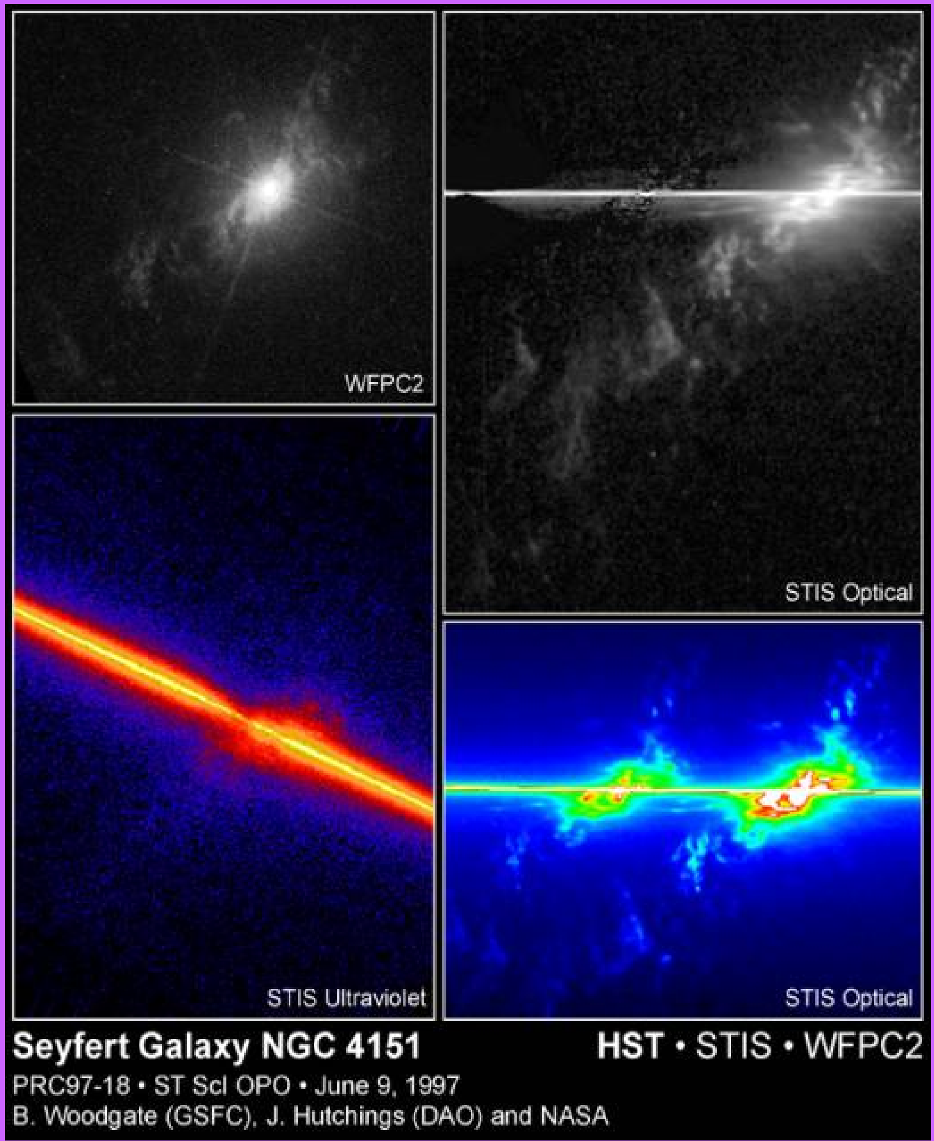

Seyfert galaxies give us a wonderful possibility of direct observations of black holes in their centers.

They often have a wide iron Kα line in their spectra, which seems to arise in the innermost part of the accretion disk close to the event horizon.

Hubble image of Seyfert galaxy NGC 4151 shown at the left.

Fe K α line origin

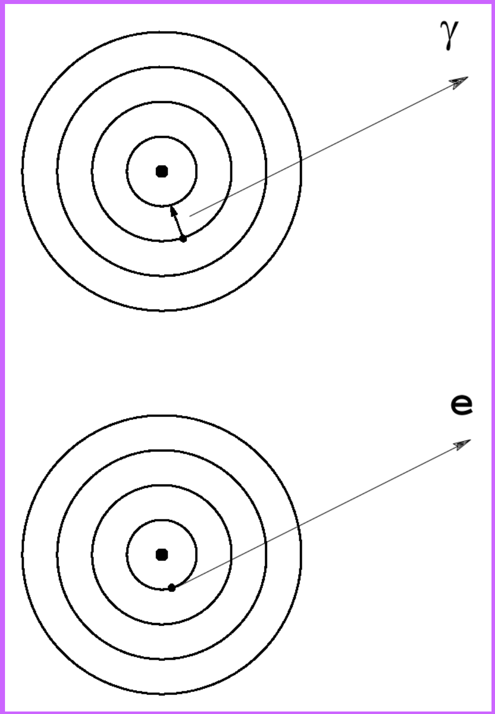

Kα (6.4 keV) analogous to Lα in hydrogen,
electron transition to the lowest level

excitation by electronic shock

hν > 7.1 keV neutral iron
photoionization and recombination

Fe XXV, XXVI – 6.9 keV hydrogen-like Fe

Emission lines in Seyfert galaxies

O VIII	0.653 keV	Fe L	0.7– 0.8 keV
Ne IX	0.915 keV	Ne X	1.02 keV
Fe L	1.03 – 1.25 keV	Mg XI	1.34 keV
Mg XII	1.47 keV	Si XIII	1.85 keV
Si XIV	2.0 keV	S XIV	2.35 keV
S XV	2.45 keV	S XVI	2.62 keV
Ar XVII	3.10 keV	Ar XVIII	3.30 keV

Fe I – Fe XVI	6.4 keV	K α
Fe XVII – Fe XXIII	6.5 keV	
Fe XXV	6.68 keV	
Fe XXVI	6.96 keV	

Turner, George, Nandra, Mushotzky
ApJSS, 113, 23, 1997, November

We find a 6.4 keV emission line in 72% of the sample (18 of 25 sources) at the 99% confidence level. The 5 – 7 keV regime is dominated by emission from neutral iron (< Fe XVI).

Observations

Tanaka, Nandra, Fabian. Nature, 1995, **375**, 659.
Galaxy MCG-6-30-15, ASCA satellite, SIS detectors

Sy 1 type

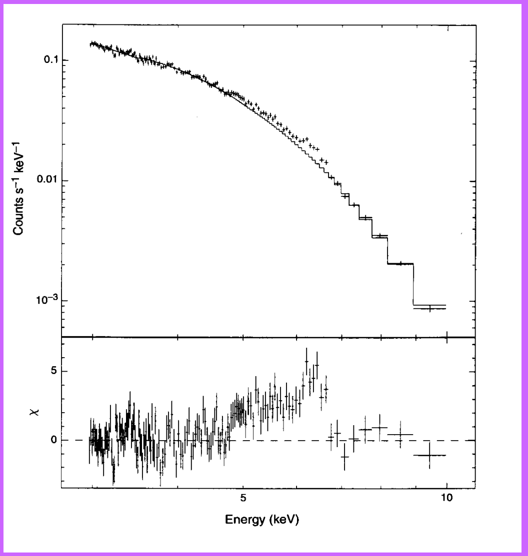

The line profile of iron Kα line in
X-ray emission from MCG-6-30-15.

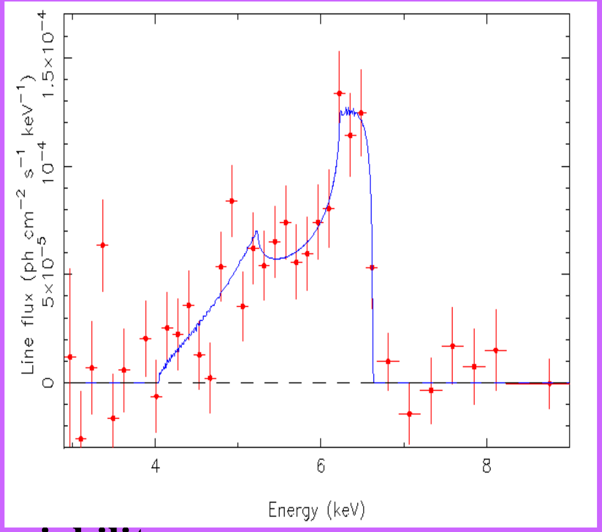

Width corresponds to 80000 – 100000 km/s.

- **Variability**

  Sulentic, Marziani, Calvani. ApJL, 1998, **497**, L65.

Observations

Weaver, Krolik, Pier. ApJ, 1998, **498**, 213. (astro-ph / 9712035).

MCG-5-23-16 Kα FWHM = 48000 km/s RXTE observations (launched Dec.95)

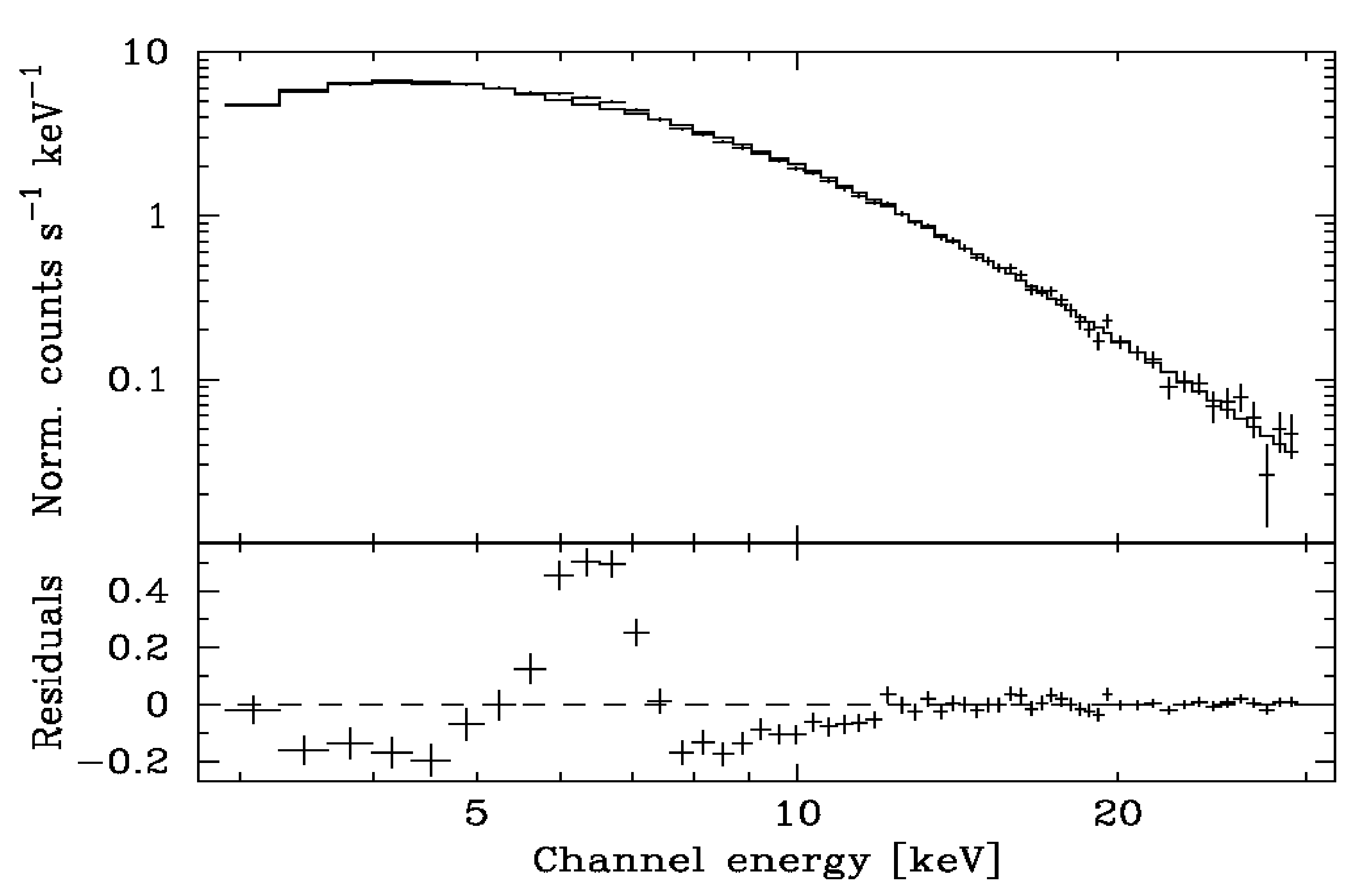

ASCA observations. Seyfert 2 galaxies.

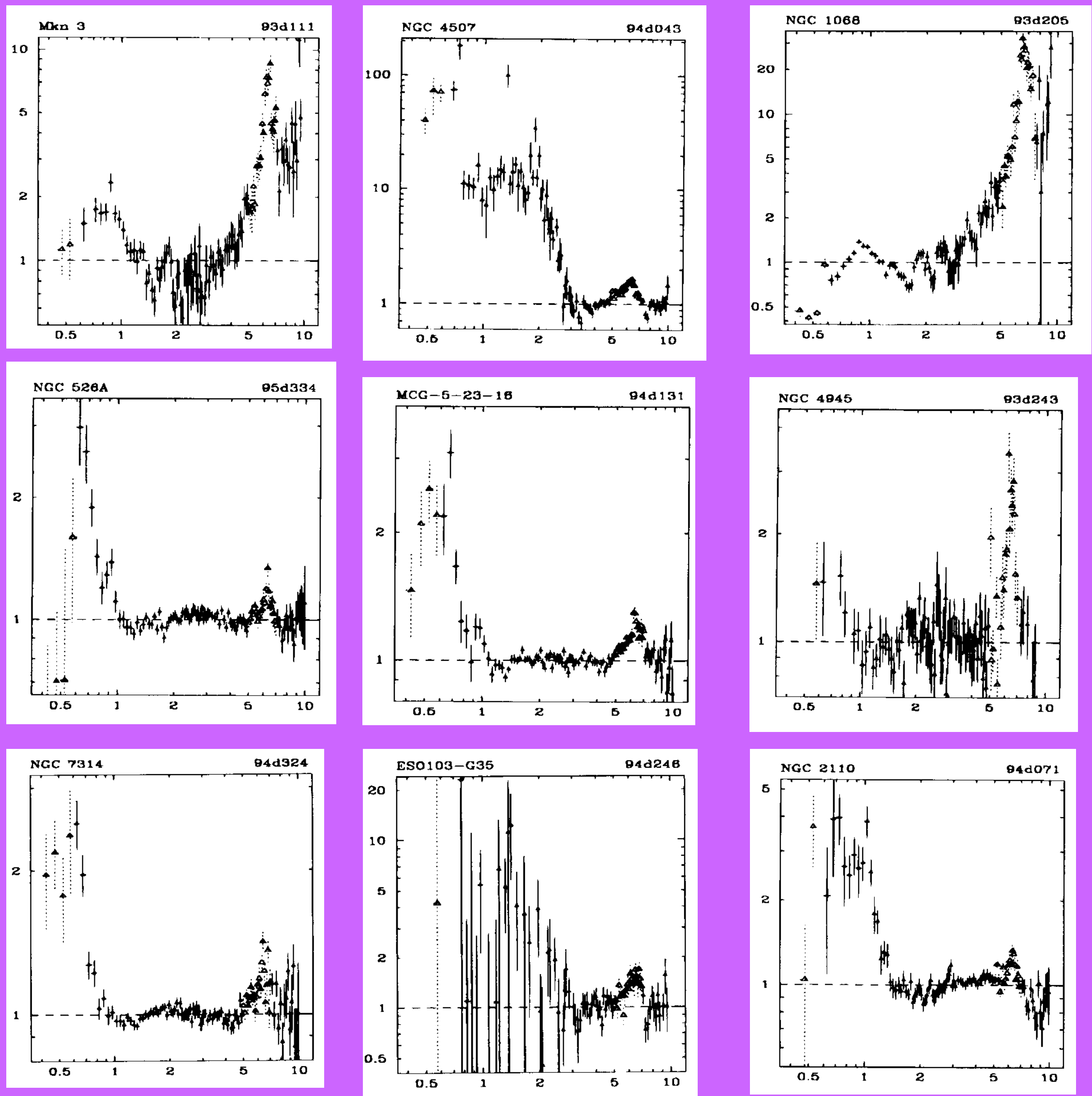

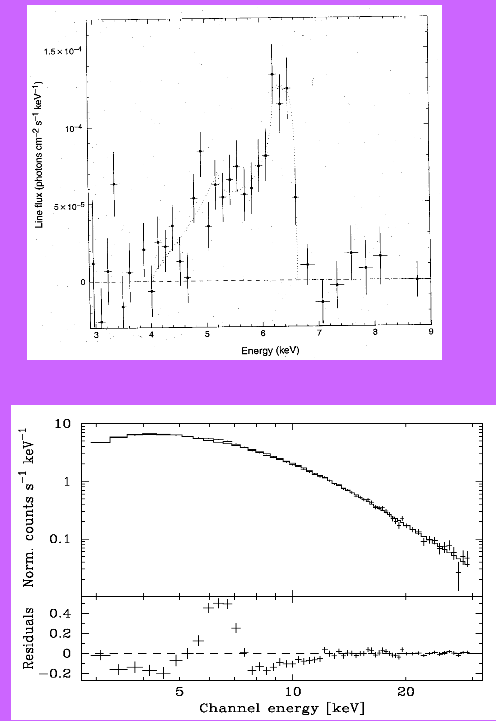

Turner, George,
Nandra, Mushotzky,
ApJSS, **113**, 23, 1997.

<u>Properties of wide lines at 6.4 keV</u>

- Line width corresponds to velocity
  - v ~ 80000 – 100000 km/s   MCG-6-30-15
  - v ~ 48000 km/s   MCG-5-23-16
  - v ~ 20000 – 30000 km/s   many other galaxies

- Asymmetric structure (profile)
  - two-peak shape
  - narrow bright **blue** wing
  - wide faint **red** wing

- Variability of both
  - line shape
  - intensity

Possible interpretation

- iron Kα emission line
  - 6.4 – 6.9 – 7.1 keV

- radiation of inner part of accretion disk around a supermassive **black hole** in the center of the galaxy

$r_{\text{emission}} \sim 1 - 4\ r_g$

$$r_g = \frac{2km}{c^2}$$

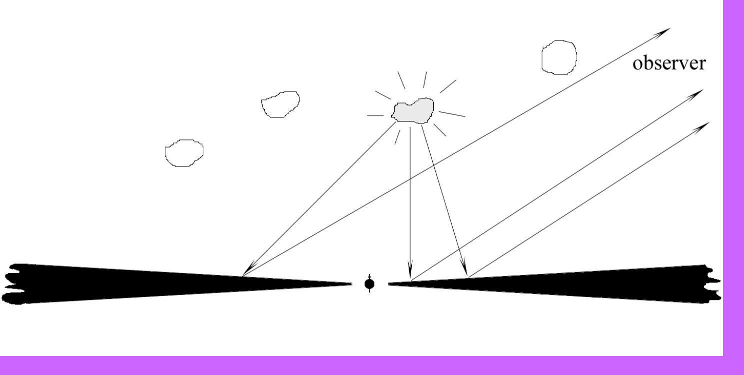

Interpretation

1. Jets

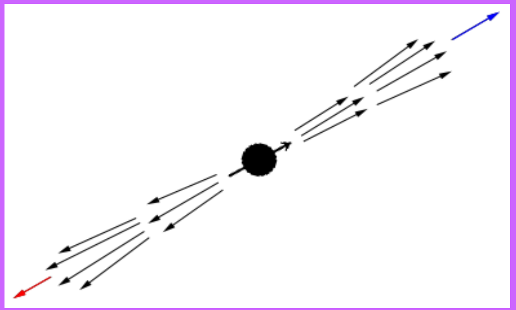

? Blue shift has never been seen

? Broad red wing

2. Multiple Compton scattering

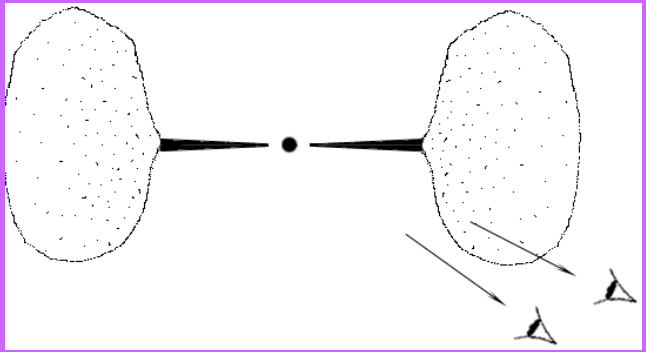

? Line profile

? High frequency variability

3. Accretion disk

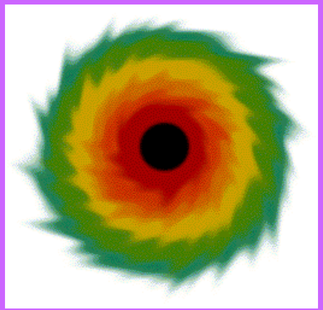

!!! Line profile !!!

Variability !

Equations of motion

Kerr metric

$$ds^2 = -\frac{\Delta}{\rho^2}\left(dt - a\sin^2\theta d\phi\right)^2 + \frac{\rho^2}{\Delta}dr^2 + \rho^2 d\theta^2 +$$

$$+\frac{\sin^2\theta}{\rho^2}\left[\left(r^2 + a^2\right)d\phi - a dt\right]^2$$

or

$$ds^2 = -\left(1 - \frac{2Mr}{\rho^2}\right)dt^2 + \frac{\rho^2}{\Delta}dr^2 + \rho^2 d\theta^2 +$$

$$+\left(r^2 + a^2 + \frac{2Mra^2}{\rho^2}\sin^2\theta\right)\sin^2\theta\, d\phi^2 - \frac{4Mra}{\rho^2}\sin^2\theta\, d\phi dt,$$

Equations of motion

Equations of photon motion:

$$\begin{aligned}
\frac{dt}{d\lambda} &= -\frac{r_g r a}{\rho^2 \Delta} L + \frac{\omega_0}{\Delta}\left(r^2 + a^2 + \frac{r_r r a^2}{\rho^2} \sin^2\theta\right) \\
\frac{d\phi}{d\lambda} &= \frac{L}{\Delta \sin^2\theta}\left(1 - \frac{r_g r}{\rho^2}\right) + \frac{r_g r a}{\rho^2 \Delta} \omega_0 \\
\left(\frac{dr}{d\lambda}\right)^2 &= \frac{1}{\rho^4}\left[\left(r^2 + a^2\right)\omega_0 - aL\right] - \frac{K\Delta}{\rho^4} \\
\left(\frac{d\theta}{d\lambda}\right)^2 &= \frac{K}{\rho^4} - \frac{1}{\rho^4}\left[a\,\omega_0 \sin\theta - \frac{L}{\sin\theta}\right]^2
\end{aligned}$$

where

$$\Delta = r^2 - r_g r + a^2, \qquad \rho^2 = r^2 + a^2 \cos^2\theta,$$

$$r_g = 2km, \qquad a = M/m$$

Equations of motion

For numerical solution the system should be replaced with

$$\begin{aligned}
\frac{dt'}{d\sigma} &= -\hat{a}\left(\hat{a}\sin^2\theta - \xi\right) + \frac{\hat{r}^2+\hat{a}^2}{\hat{\Delta}}\left(\hat{r}^2+\hat{a}^2-\xi\hat{a}\right), \\
\frac{d\hat{r}}{d\sigma} &= r_1, \\
\frac{dr_1}{d\sigma} &= 2\hat{r}^3 + \left(\hat{a}^2-\xi^2-\eta\right)\hat{r} + (\hat{a}-\xi) + \eta, \\
\frac{d\theta}{d\sigma} &= \theta_1, \\
\frac{d\theta_1}{d\sigma} &= \cos\theta\left(\frac{\xi^2}{\sin^3\theta} - \hat{a}^2\sin\theta\right), \\
\frac{d\phi}{d\sigma} &= -\left(\hat{a} - \frac{\xi}{\sin^2\theta}\right) + \frac{\hat{a}}{\hat{\Delta}}\left(\hat{r}^2+\hat{a}^2-\xi\hat{a}\right).
\end{aligned}$$

The system has two integrals:

$$\begin{aligned}
\epsilon_1 &\equiv r_1^2 - \hat{r}^4 - \left(\hat{a}^2-\xi^2-\eta\right)\hat{r}^2 - 2\left[(\hat{a}-\xi)^2+\eta\right]\hat{r} + \hat{a}^2\eta = 0, \\
\epsilon_2 &\equiv \theta_1^2 - \eta - \cos^2\theta\left(\hat{a}^2 - \frac{\xi^2}{\sin^2\theta}\right) = 0,
\end{aligned}$$

Simulation result

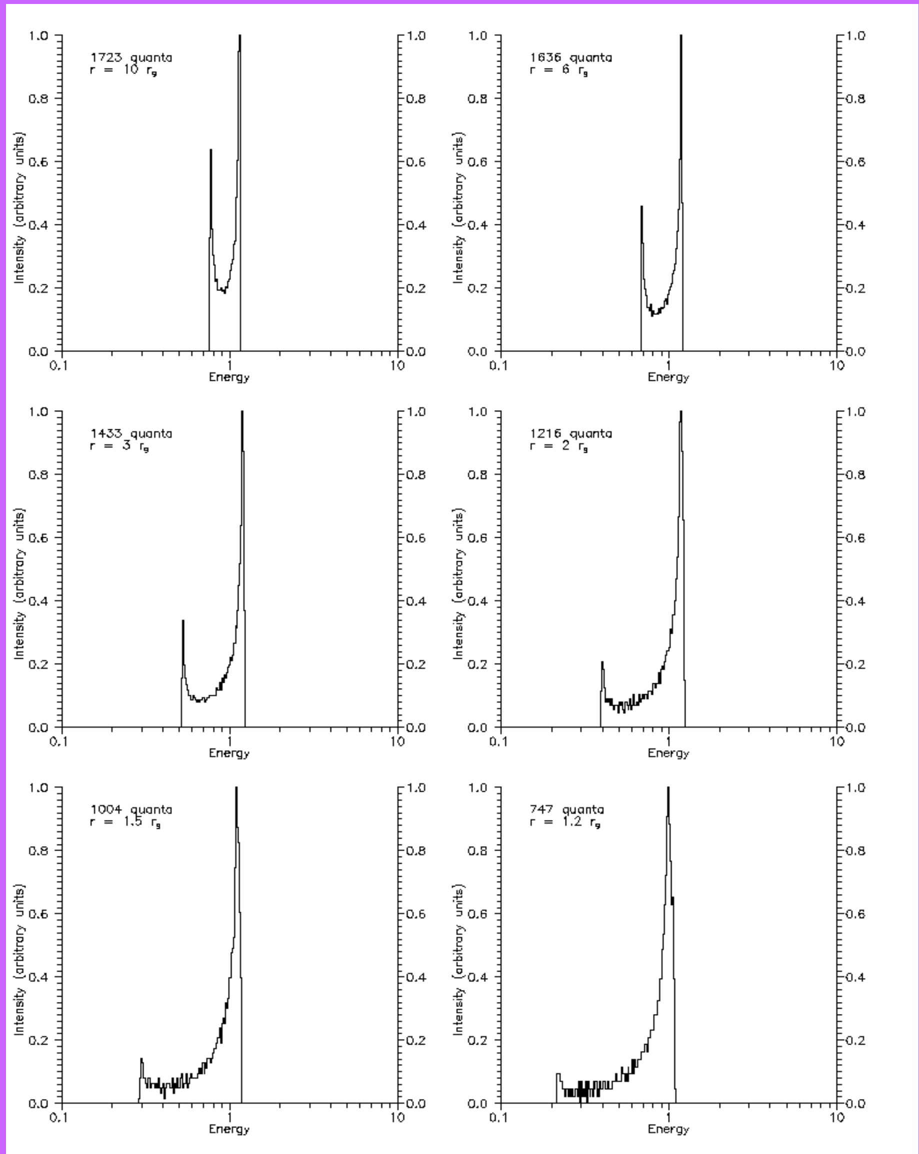

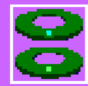

Spectrum of a hot spot for a=0.9, θ=60 deg. and different values of radial coordinate.

Marginally stable orbit lays at r = 1.16 r_g.

Simulation result

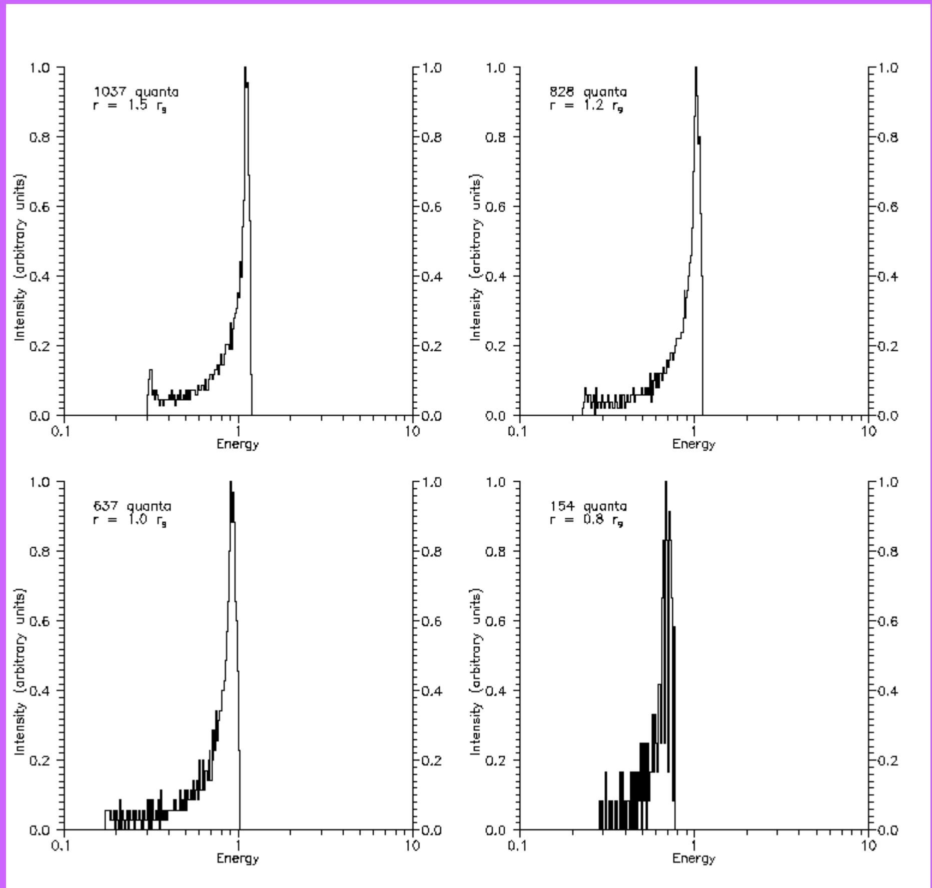

Spectrum of a hot spot for a=0.99, θ=60 deg. and different values of radial coordinate.

Marginally stable orbit lays at r = 0.727 rg.

Simulation result

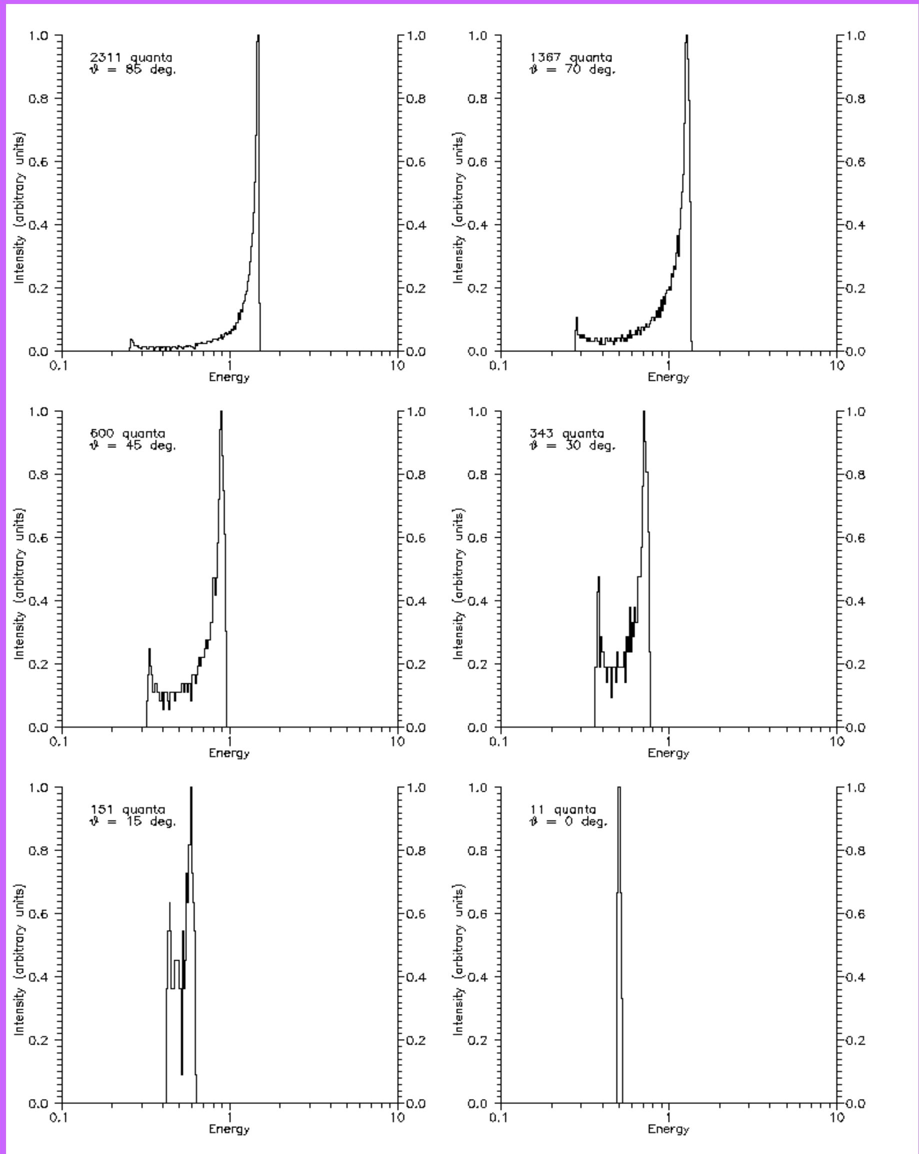

Spectrum of a hot spot for $a=0.99$, $r = 1.5\ r_g$ and different values of θ angle.

Gallery of profiles

with S.V. Repin (in preparation)

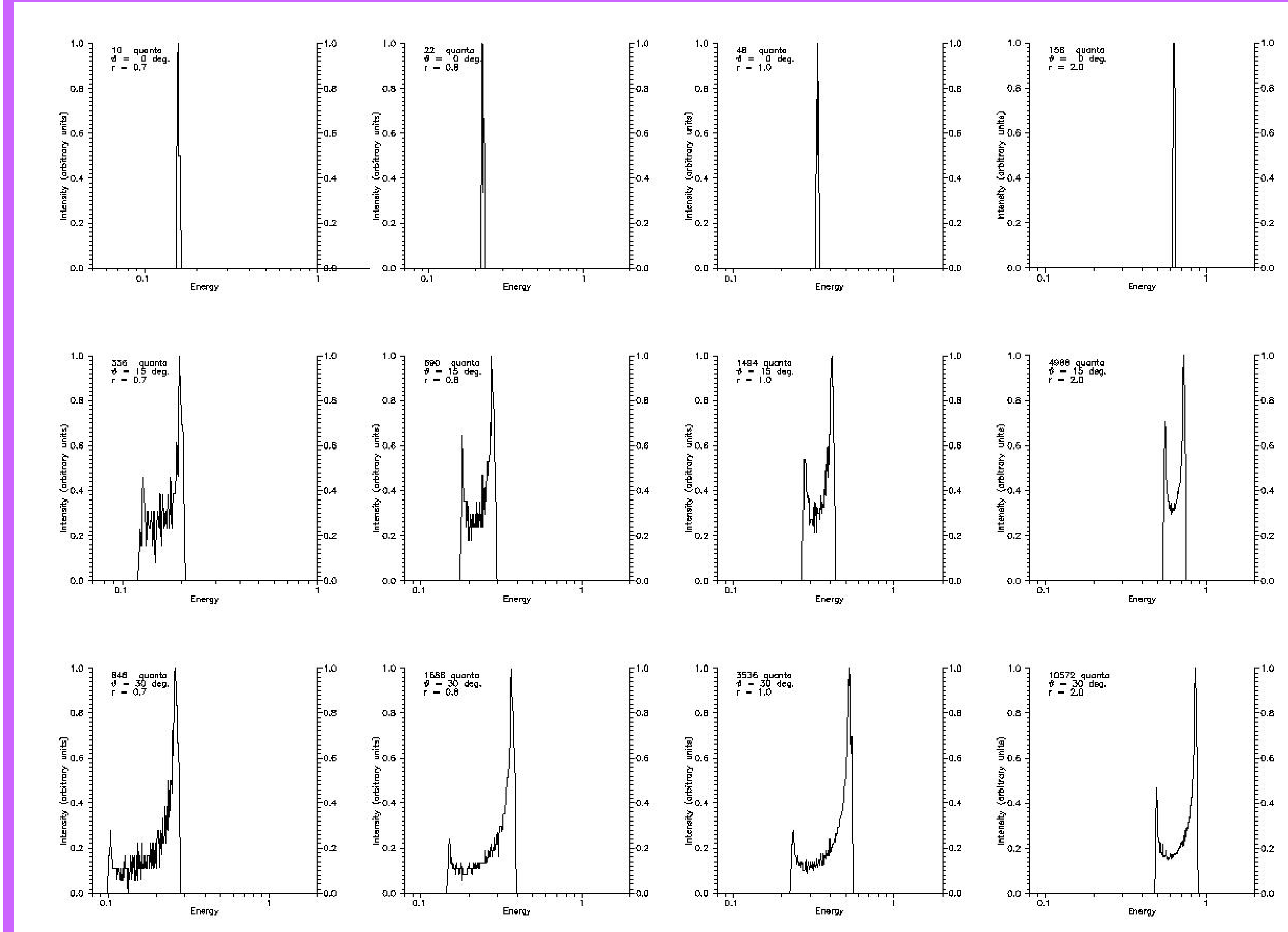

10 quanta ϑ = 0 deg. r = 0.7
22 quanta ϑ = 0 deg. r = 0.8
48 quanta ϑ = 0 deg. r = 1.0
156 quanta ϑ = 0 deg. r = 2.0
336 quanta ϑ = 15 deg. r = 0.7
690 quanta ϑ = 15 deg. r = 0.8
1484 quanta ϑ = 15 deg. r = 1.0
4988 quanta ϑ = 15 deg. r = 2.0
848 quanta ϑ = 30 deg. r = 0.7
1688 quanta ϑ = 30 deg. r = 0.8
3536 quanta ϑ = 30 deg. r = 1.0
10572 quanta ϑ = 30 deg. r = 2.0
Intensity (arbitrary units)
Energy

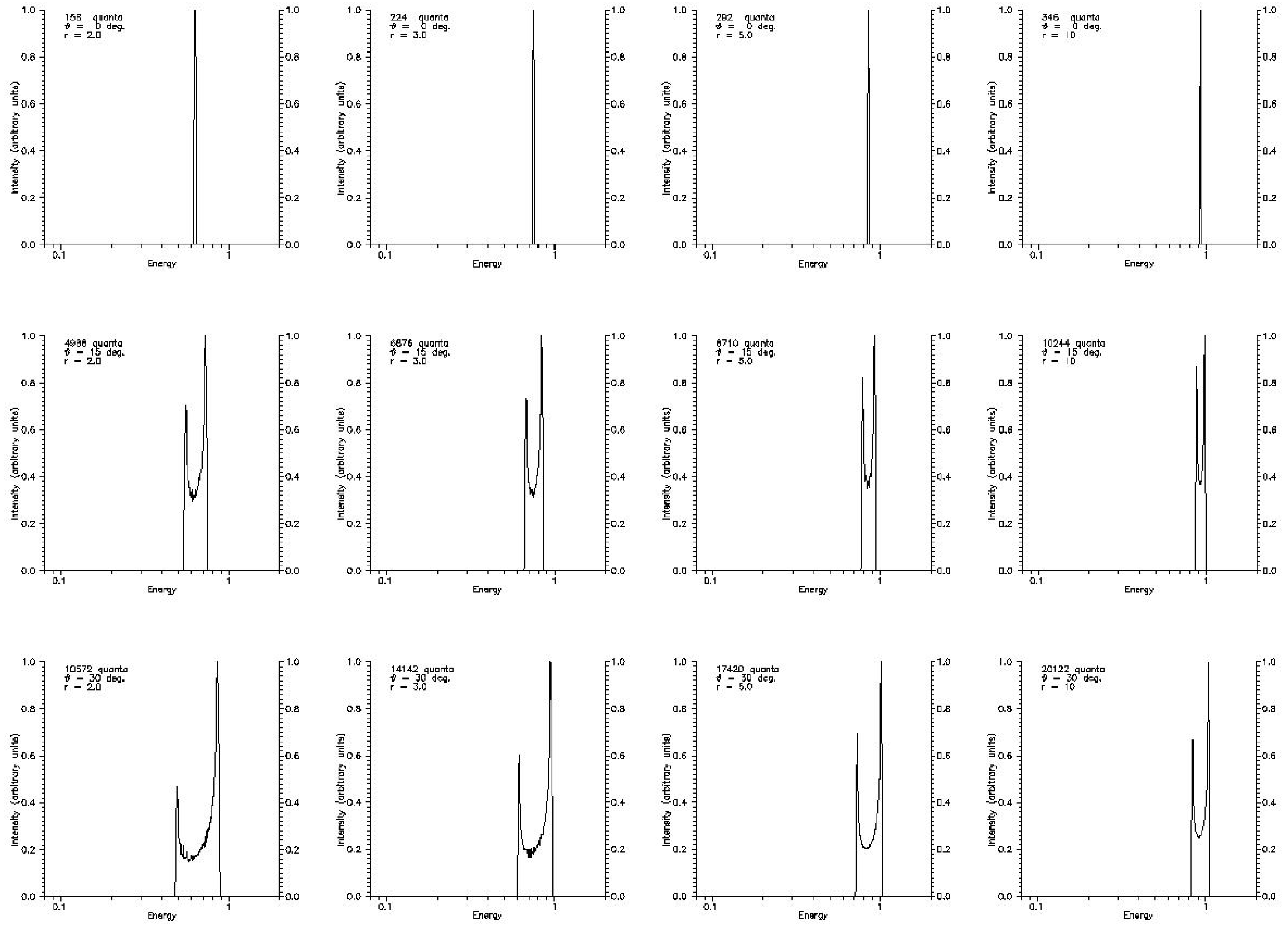

158 quanta
ϑ = 0 deg.
r = 2.0
224 quanta
ϑ = 0 deg.
r = 3.0
292 quanta
ϑ = 0 deg.
r = 5.0
346 quanta
ϑ = 0 deg.
r = 10
4988 quanta
ϑ = 15 deg.
r = 2.0
6876 quanta
ϑ = 15 deg.
r = 3.0
8710 quanta
ϑ = 15 deg.
r = 5.0
10244 quanta
ϑ = 15 deg.
r = 10
10572 quanta
ϑ = 30 deg.
r = 2.0
14142 quanta
ϑ = 30 deg.
r = 3.0
17420 quanta
ϑ = 30 deg.
r = 5.0
20122 quanta
ϑ = 30 deg.
r = 10
Intensity (arbitrary units)
Energy

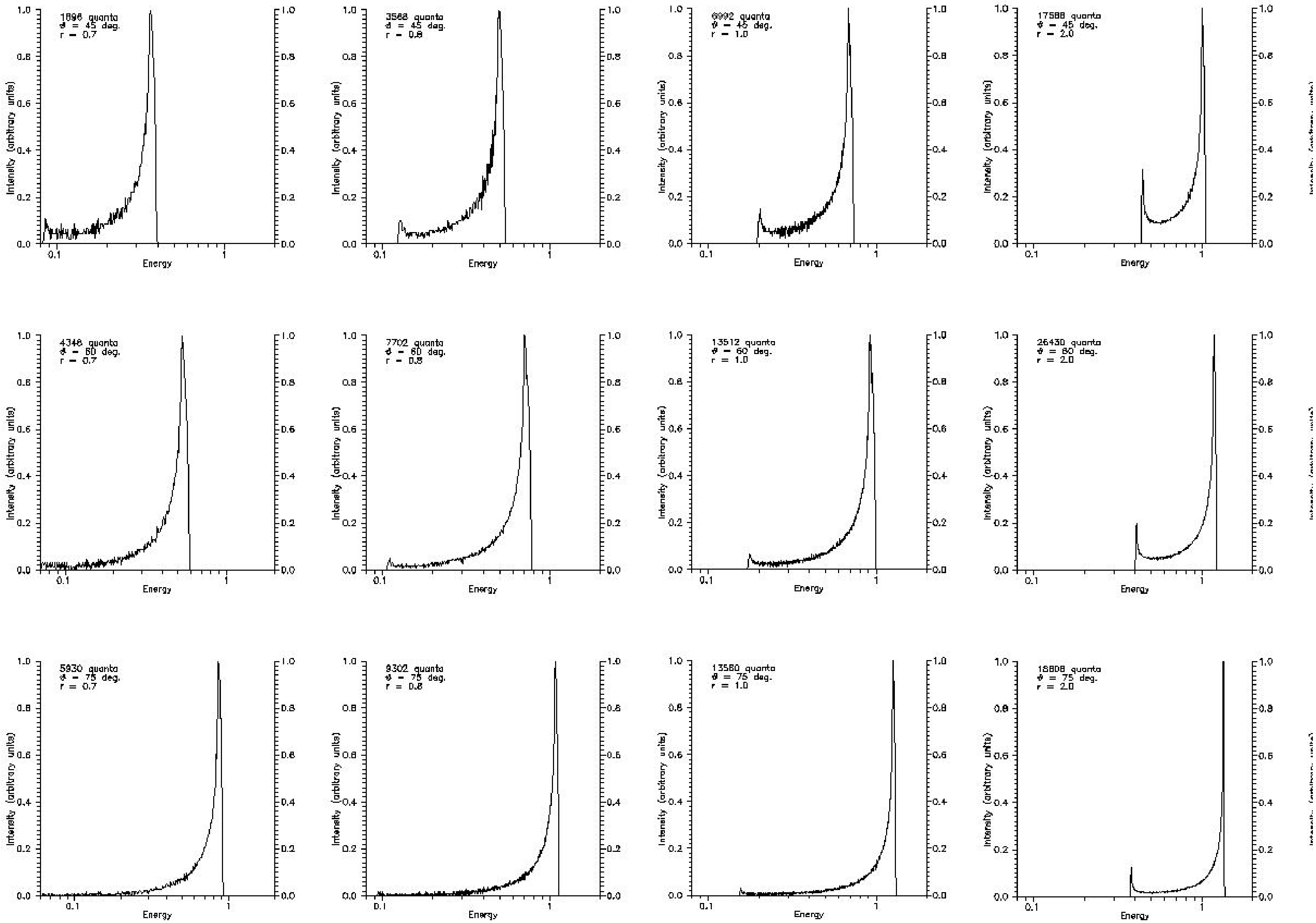
1896 quanta
ϑ = 45 deg.
r = 0.7
3568 quanta
ϑ = 45 deg.
r = 0.8
6992 quanta
ϑ = 45 deg.
r = 1.0
17588 quanta
ϑ = 45 deg.
r = 2.0
4346 quanta
ϑ = 60 deg.
r = 0.7
7702 quanta
ϑ = 60 deg.
r = 0.8
13512 quanta
ϑ = 60 deg.
r = 1.0
26430 quanta
ϑ = 60 deg.
r = 2.0
5930 quanta
ϑ = 75 deg.
r = 0.7
9302 quanta
ϑ = 75 deg.
r = 0.8
13560 quanta
ϑ = 75 deg.
r = 1.0
18808 quanta
ϑ = 75 deg.
r = 2.0
Intensity (arbitrary units)
Energy

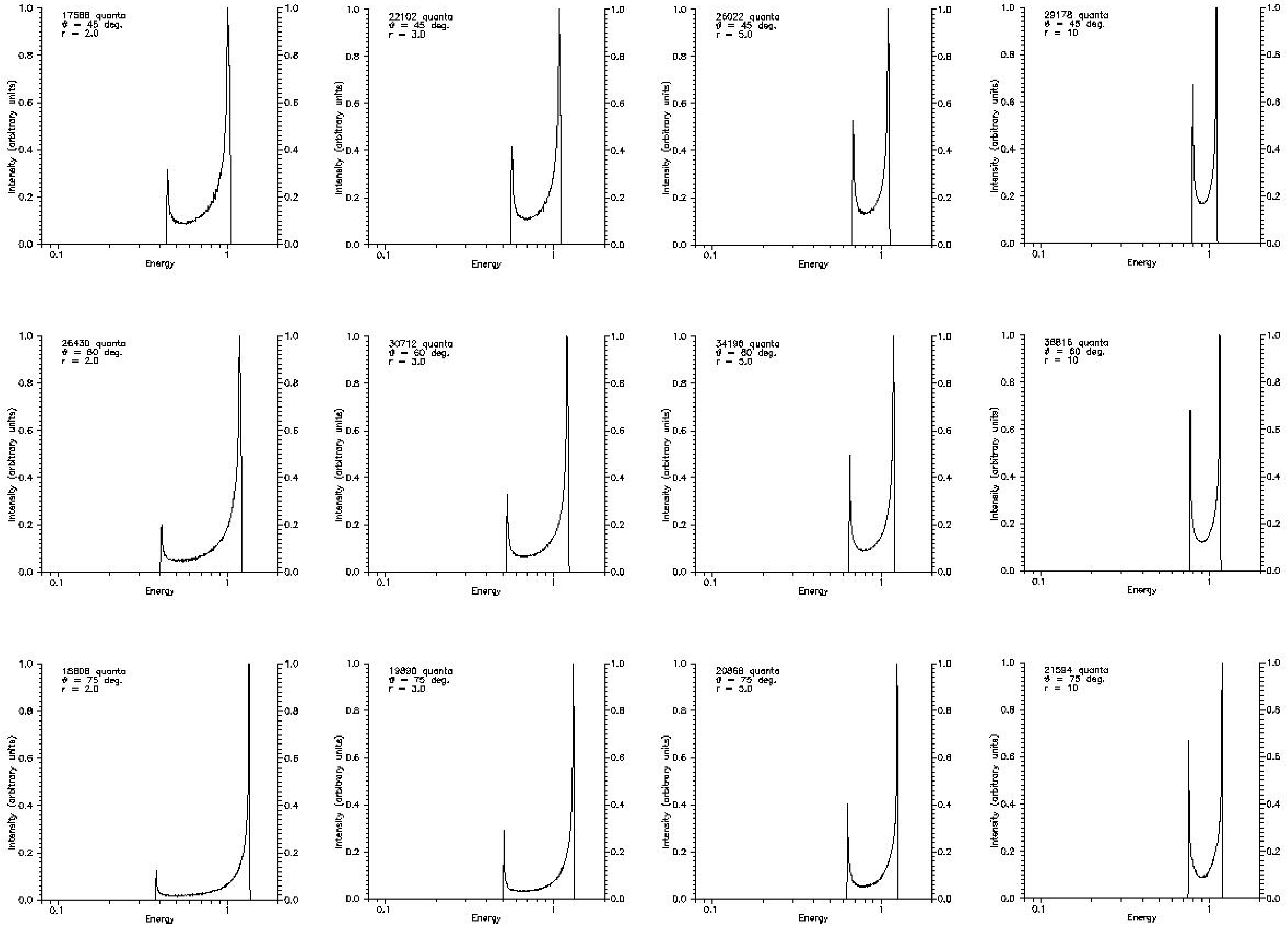

17588 quanta
ϑ = 45 deg.
r = 2.0
22102 quanta
ϑ = 45 deg.
r = 3.0
26022 quanta
ϑ = 45 deg.
r = 5.0
29178 quanta
ϑ = 45 deg.
r = 10
26430 quanta
ϑ = 60 deg.
r = 2.0
30712 quanta
ϑ = 60 deg.
r = 3.0
34196 quanta
ϑ = 60 deg.
r = 5.0
38816 quanta
ϑ = 60 deg.
r = 10
16808 quanta
ϑ = 75 deg.
r = 2.0
19890 quanta
ϑ = 75 deg.
r = 3.0
20968 quanta
ϑ = 75 deg.
r = 5.0
21594 quanta
ϑ = 75 deg.
r = 10
Intensity (arbitrary units)
Energy

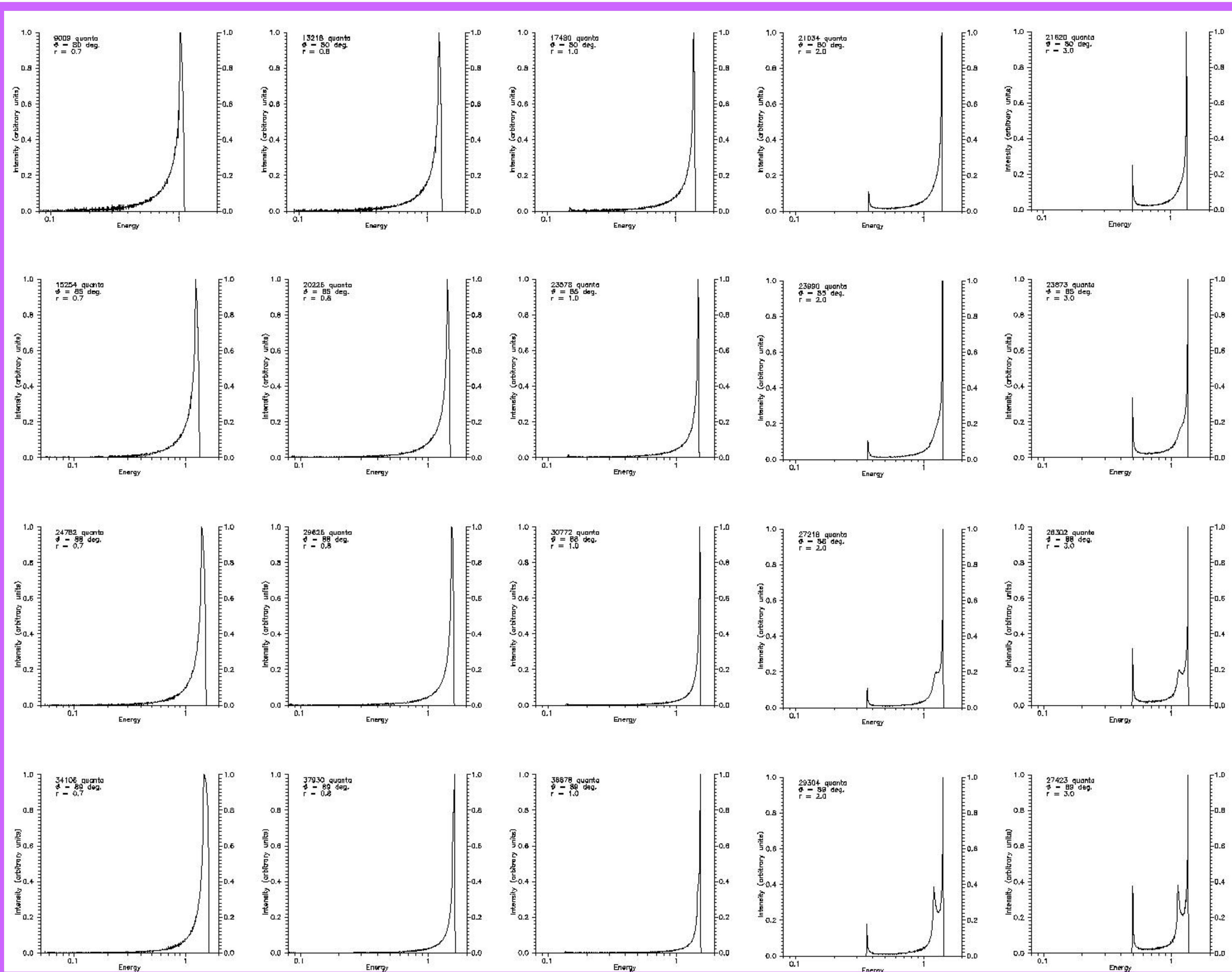
9009 quanta φ = 80 deg. r = 0.7
13218 quanta φ = 80 deg. r = 0.8
17480 quanta φ = 80 deg. r = 1.0
21034 quanta φ = 80 deg. r = 2.0
21620 quanta φ = 80 deg. r = 3.0
15254 quanta φ = 85 deg. r = 0.7
20226 quanta φ = 85 deg. r = 0.8
23578 quanta φ = 85 deg. r = 1.0
23890 quanta φ = 85 deg. r = 2.0
23873 quanta φ = 85 deg. r = 3.0
24782 quanta φ = 88 deg. r = 0.7
29626 quanta φ = 88 deg. r = 0.8
30772 quanta φ = 88 deg. r = 1.0
27218 quanta φ = 88 deg. r = 2.0
28302 quanta φ = 88 deg. r = 3.0
34106 quanta φ = 89 deg. r = 0.7
37930 quanta φ = 89 deg. r = 0.8
38678 quanta φ = 89 deg. r = 1.0
29304 quanta φ = 89 deg. r = 2.0
27423 quanta φ = 89 deg. r = 3.0
Intensity (arbitrary units)
Energy

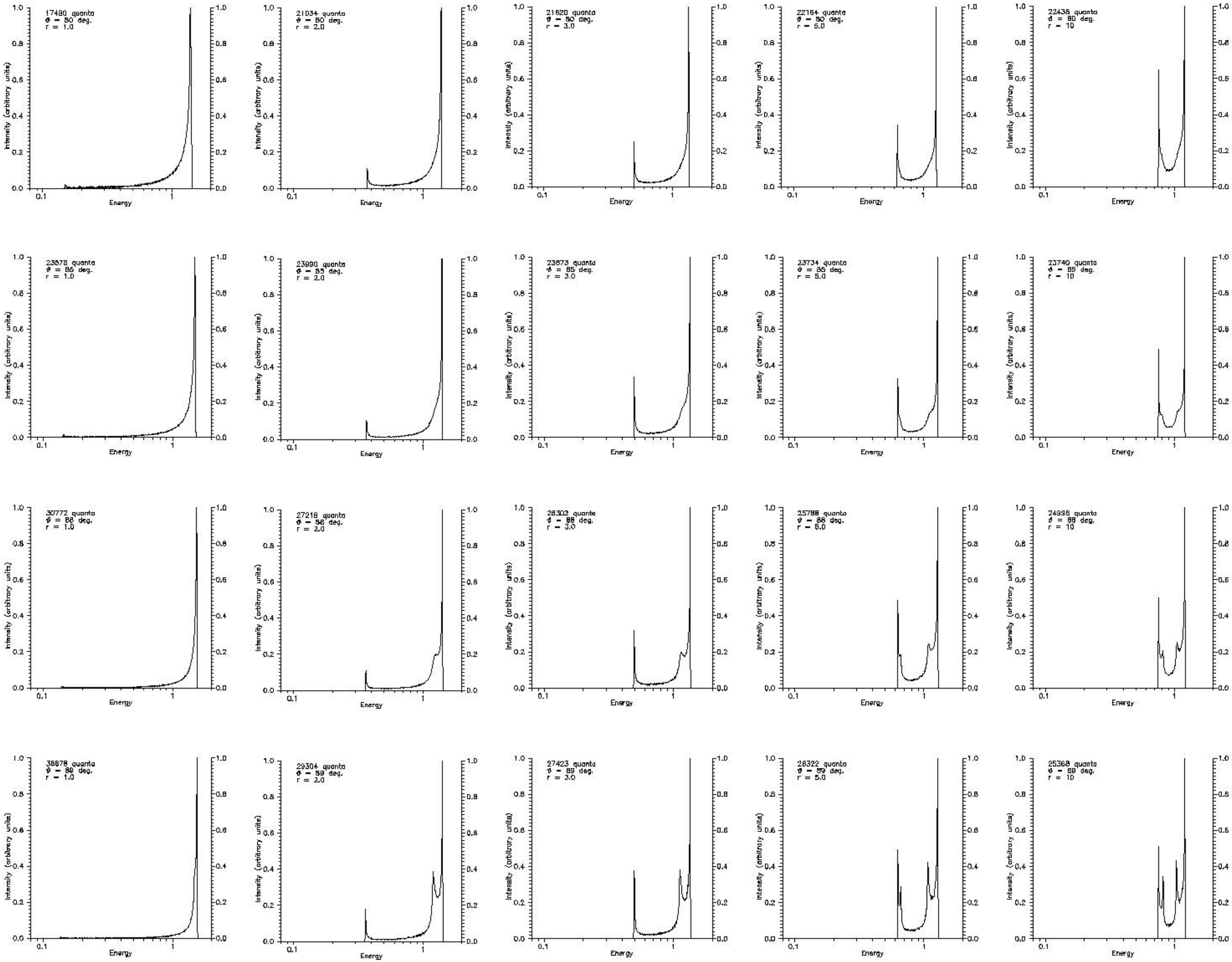
17480 quanta
φ = 80 deg.
r = 1.0
21034 quanta
φ = 80 deg.
r = 2.0
21620 quanta
φ = 80 deg.
r = 3.0
22164 quanta
φ = 80 deg.
r = 5.0
22436 quanta
φ = 80 deg.
r = 10
23878 quanta
φ = 85 deg.
r = 1.0
23990 quanta
φ = 85 deg.
r = 2.0
23873 quanta
φ = 85 deg.
r = 3.0
23734 quanta
φ = 85 deg.
r = 5.0
23740 quanta
φ = 85 deg.
r = 10
30772 quanta
φ = 88 deg.
r = 1.0
27218 quanta
φ = 88 deg.
r = 2.0
26302 quanta
φ = 88 deg.
r = 3.0
25788 quanta
φ = 88 deg.
r = 5.0
24998 quanta
φ = 88 deg.
r = 10
36878 quanta
φ = 89 deg.
r = 1.0
29304 quanta
φ = 89 deg.
r = 2.0
27423 quanta
φ = 89 deg.
r = 3.0
26322 quanta
φ = 89 deg.
r = 5.0
25368 quanta
φ = 89 deg.
r = 10
Intensity (arbitrary units)
Energy

Rings summation

Classical expression for the ring area

$$dS = 2\pi r\, dr$$

should be replaced in General Relativity with

$$dS = \frac{2\pi \left(r^2 + a^2\right)}{\sqrt{r^2 - r r_g + a^2}}\, dr$$

where

$$f_{GR} = \frac{r^2 + a^2}{r\sqrt{r^2 - r r_g + a^2}}$$

is the additional relativistic factor, appearing due to the frame dragging.

Simulation result

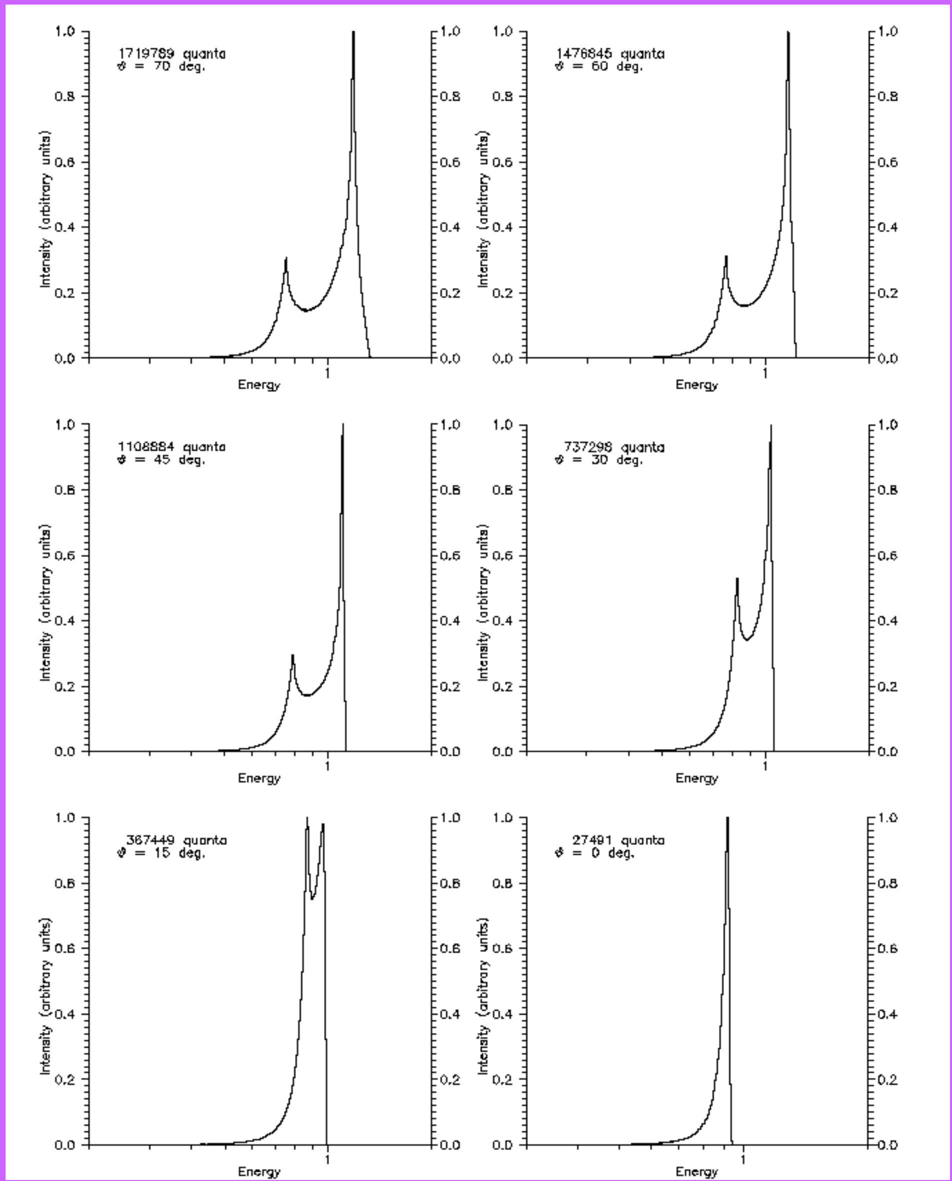

Spectrum of Fe Kα line in isothermal disk with a = 0.9 and emission region between 10 r_g and marginally stable orbit at 1.16 r_g.

The figure presents the dependence on θ angle.

Simulation result

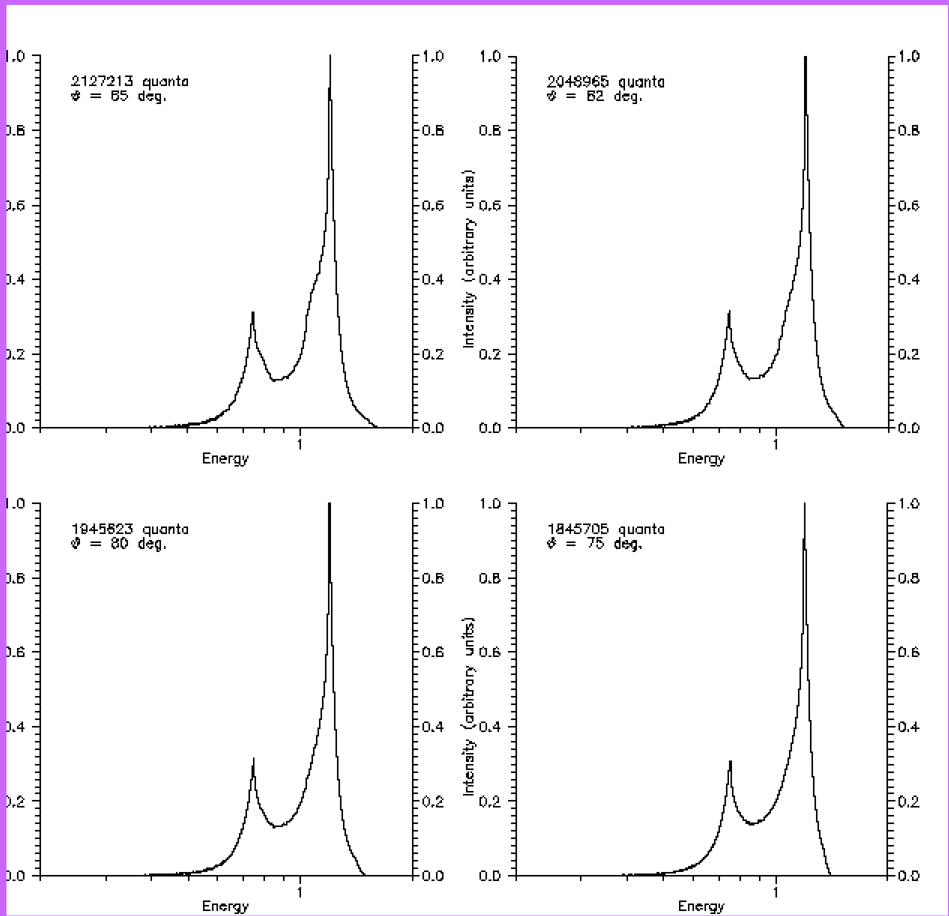

Spectrum of Fe Kα line in isothermal disk with a = 0.9 and emission region between 10 r_g and marginally stable orbit at 1.16 r_g.

The figure presents the dependence on θ angle (large θ values).

Simulation result

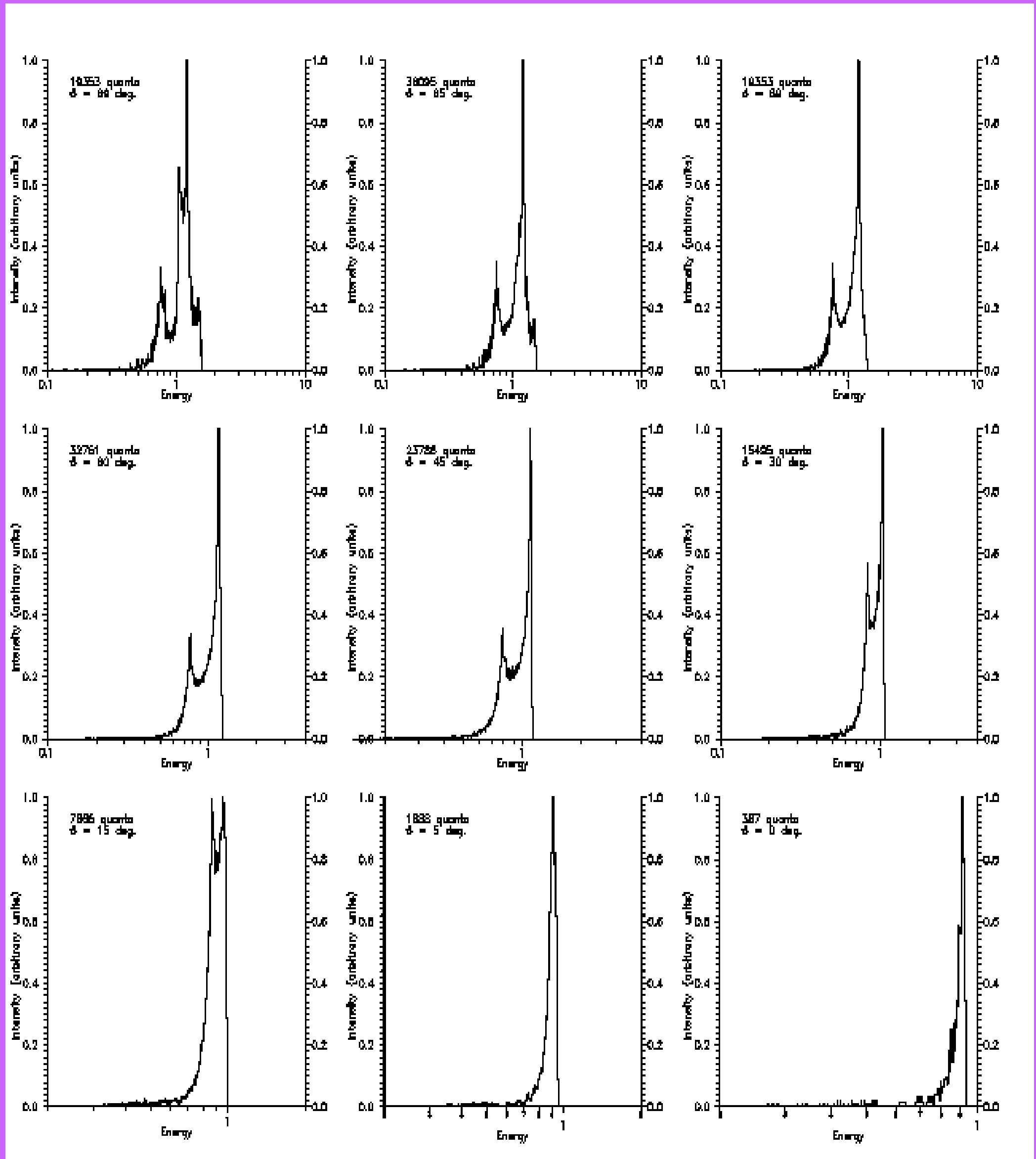

Spectrum of Fe Kα line in isothermal disk with a = 0.99 and emission region between 10 r_g and marginally stable orbit at 0.727 r_g.

At large θ one can see the lensing effect.

Simulation result

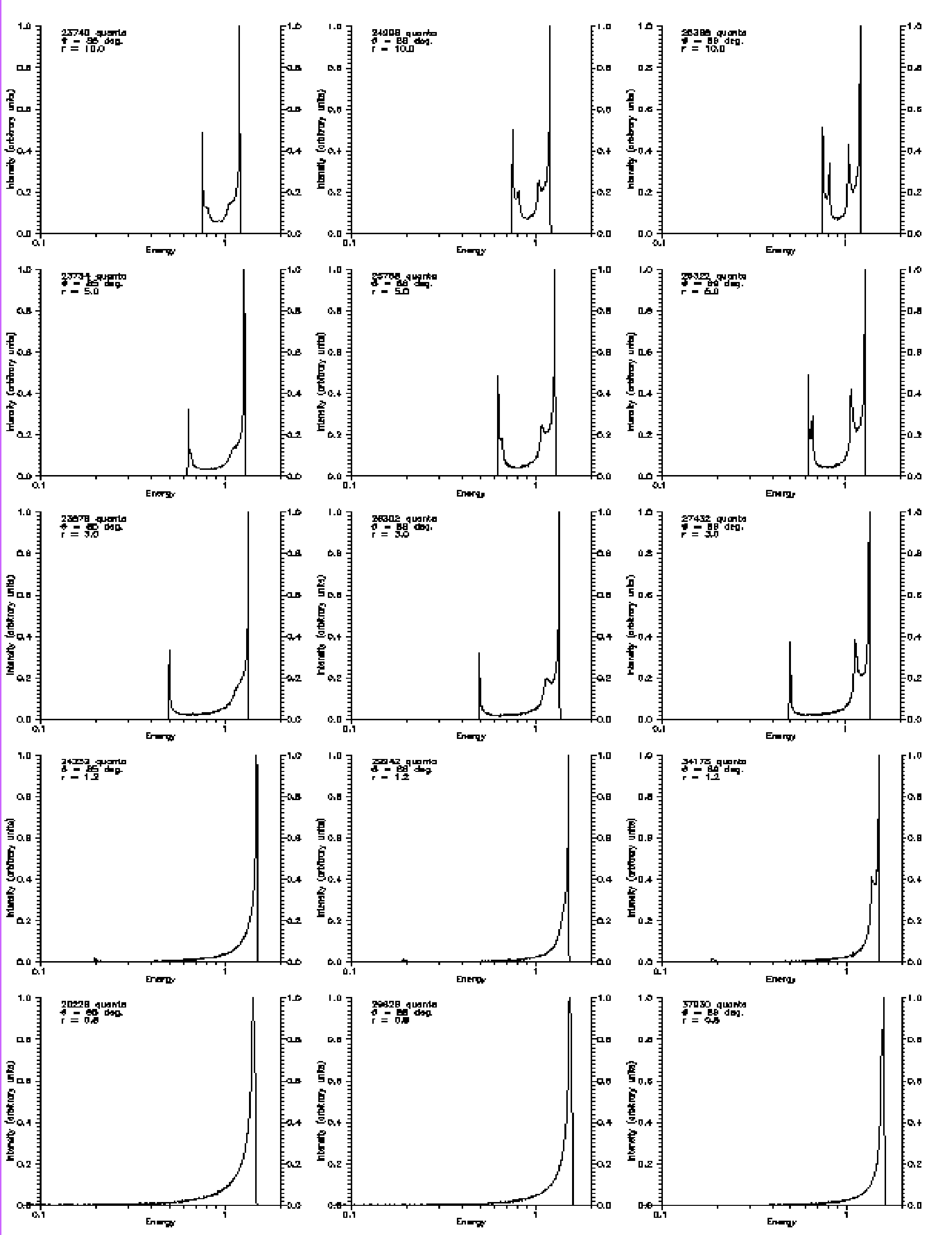

Overview of possible line profiles of a hot spot for different values of radial coordinate and inclination angle.

The radial coordinate decreases from 10 r_g on the top to 0.8 r_g on the bottom. The inclination angle increases from 85 degrees in the left column to 89 degrees in the right.

Zakharov A.F, Repin S.V. A&A, 2003, 406, 7.

Simulation result

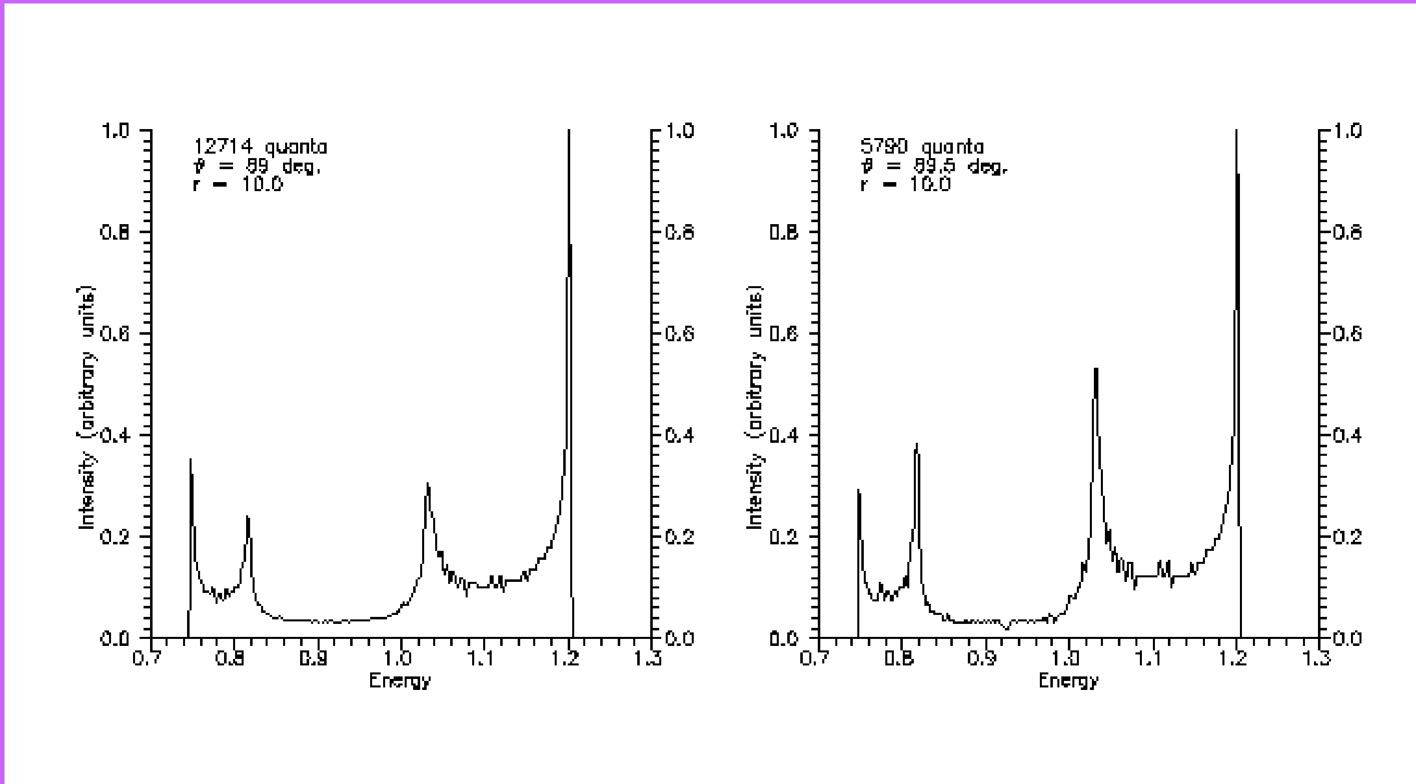

Spectrum of a hot spot rotating at the distance 10 r_g and observed at large inclination angles. Left panel includes all the quanta with $\theta > 89$ degrees. The right one includes the quanta with $\theta > 89.5$ degrees.

Simulation result

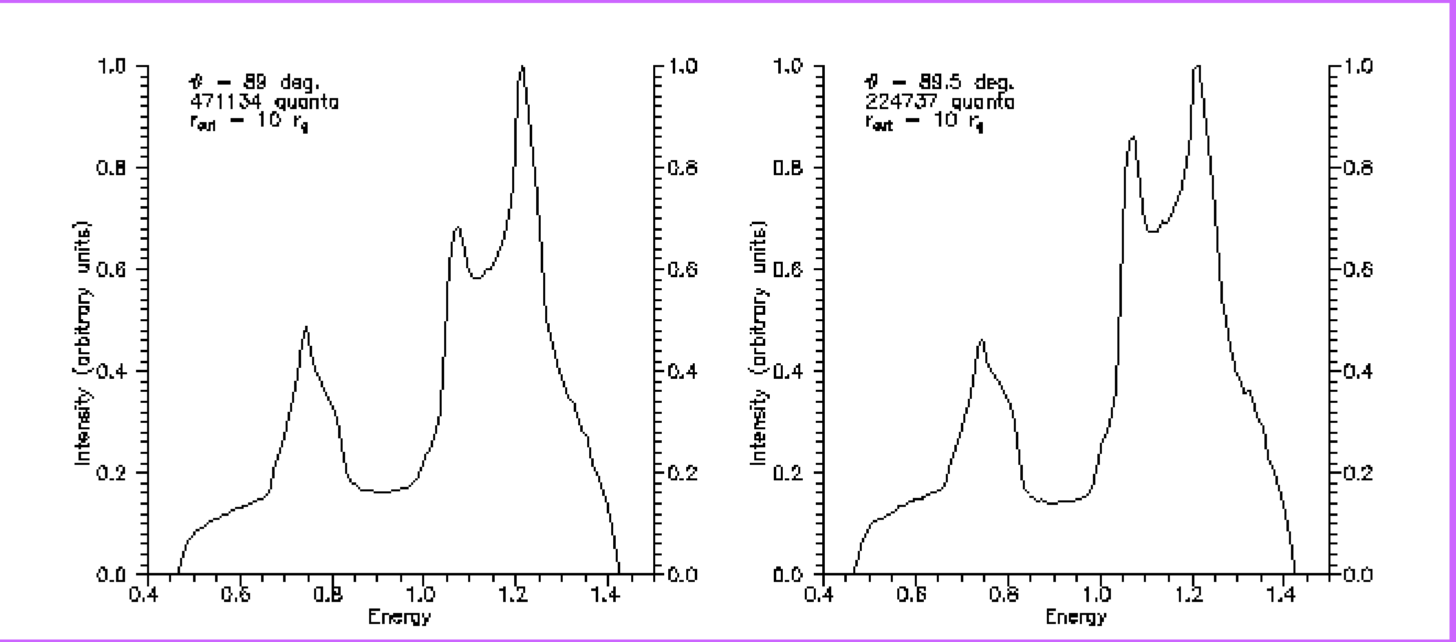

Spectrum of an entire α-disk observed at large inclination angles. Emitting region lies between 3 r_g and 10 r_g. Left panel includes all the quanta with $\theta > 89$ degrees. The right one includes the quanta with $\theta > 89.5$ degrees.

Magnetic field estimations near BH horizon in AGNs and GBHCs
(Zakharov, Kardashev, Lukash, Repin, MNRAS, 342,1325, (2003))

- Zeeman splitting $E_1=E_0-\mu_B H$, $E_2=E_0+\mu_B H$, $\mu_B=e\hbar/(2m_e c)$, $\mu_B=9.3*10^{-21}$ erg/G
- Figure1
- Figure2
- Figure3
- Figure4
- Figure5
- Figure6
- ASCAdata

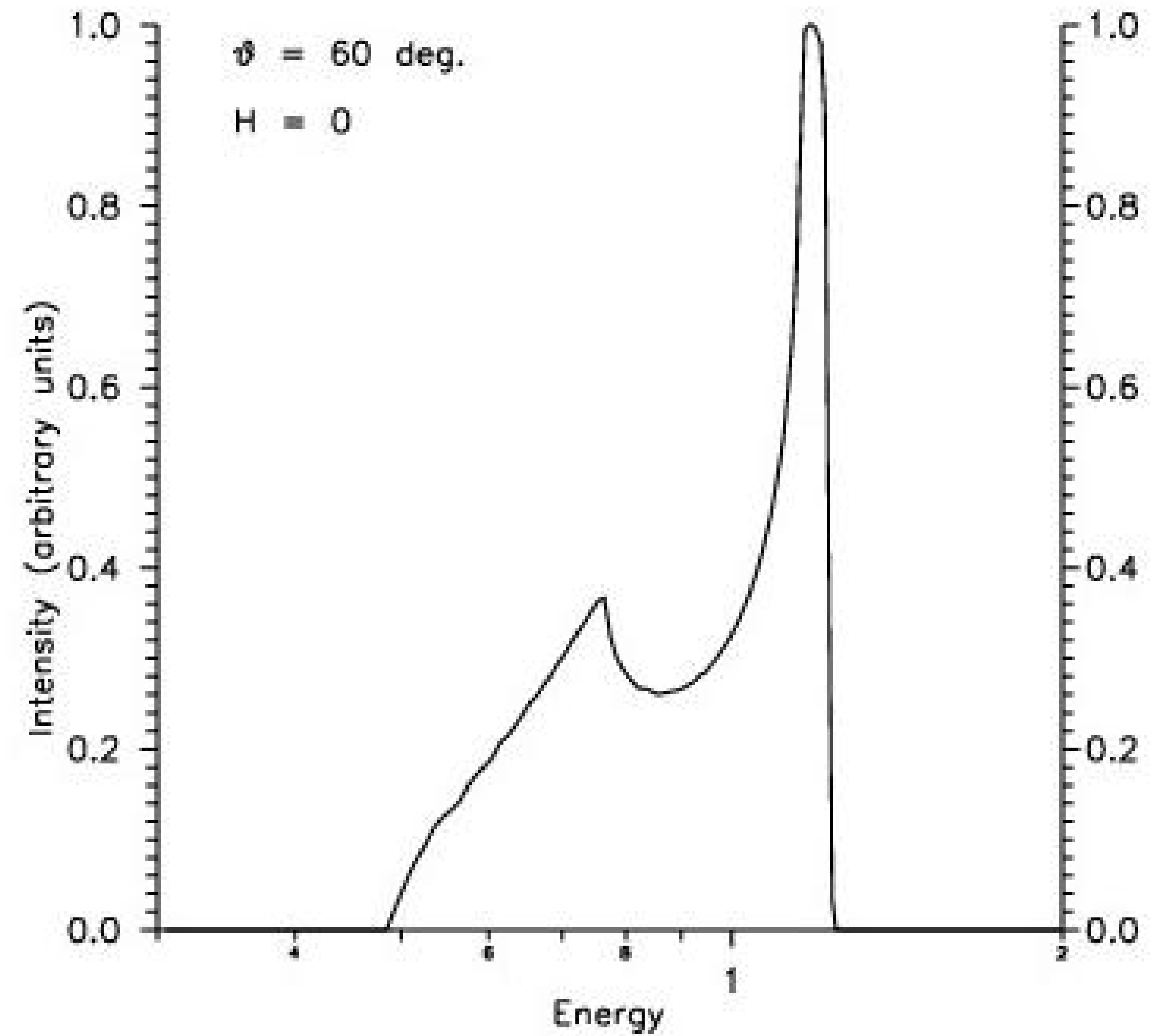
ϑ = 60 deg.
H = 0
Intensity (arbitrary units)
1.0
0.8
0.6
0.4
0.2
0.0
1
2
Energy

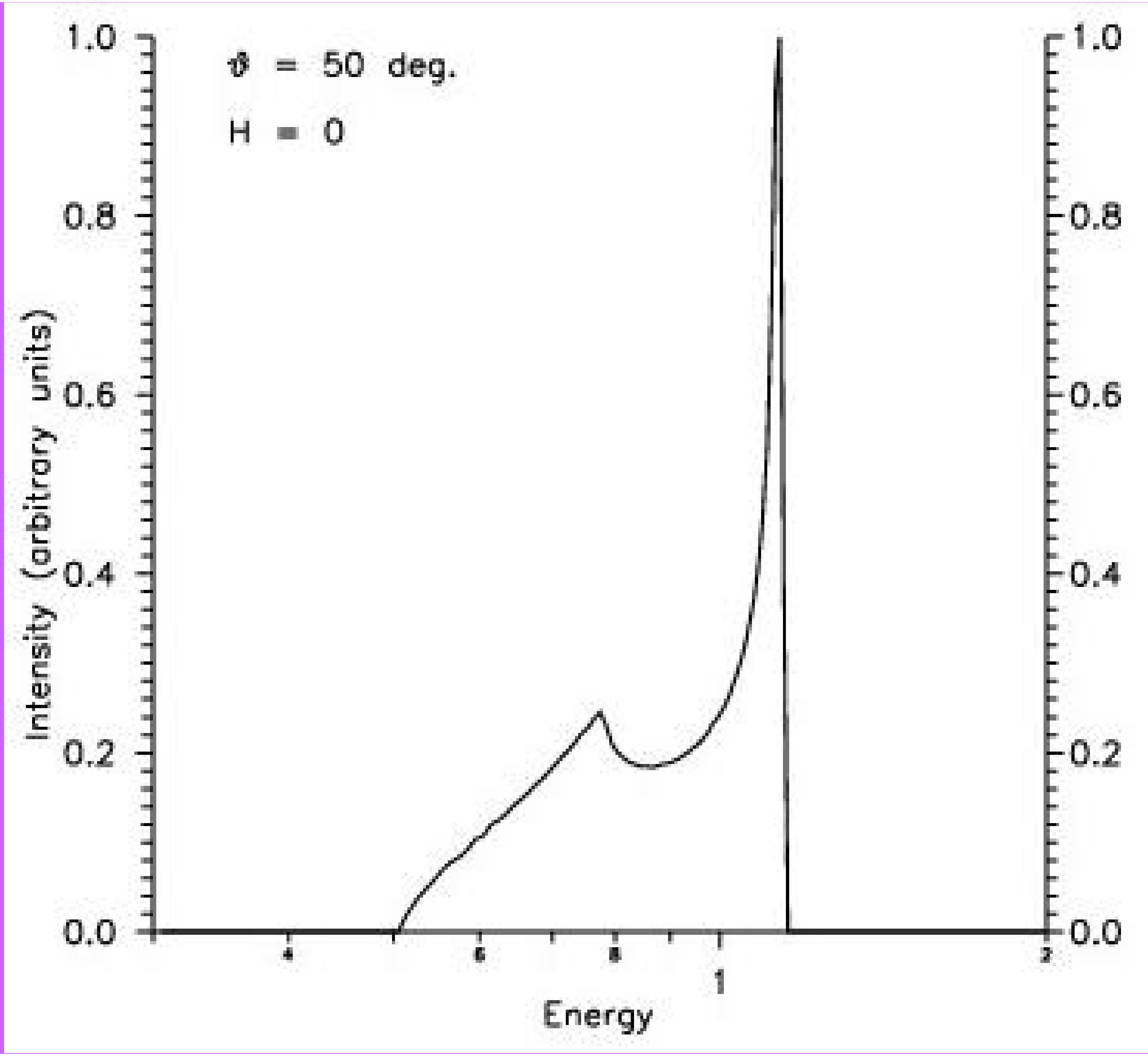

ϑ = 50 deg.
H = 0
Intensity (arbitrary units)
Energy
0.0
0.2
0.4
0.6
0.8
1.0
1

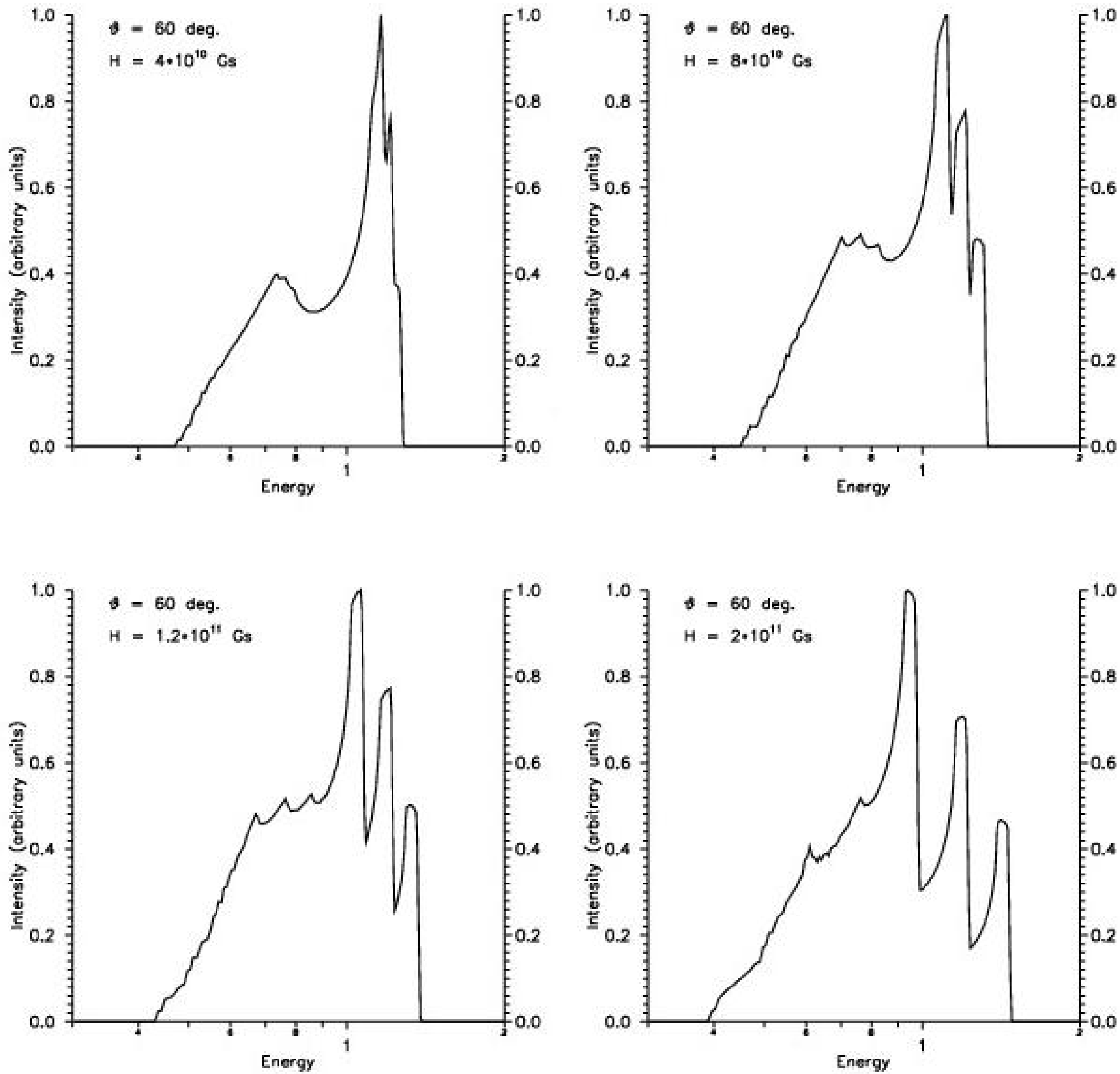

ϑ = 60 deg.
H = 4•10^10 Gs
ϑ = 60 deg.
H = 8•10^10 Gs
ϑ = 60 deg.
H = 1.2•10^11 Gs
ϑ = 60 deg.
H = 2•10^11 Gs
Intensity (arbitrary units)
Energy

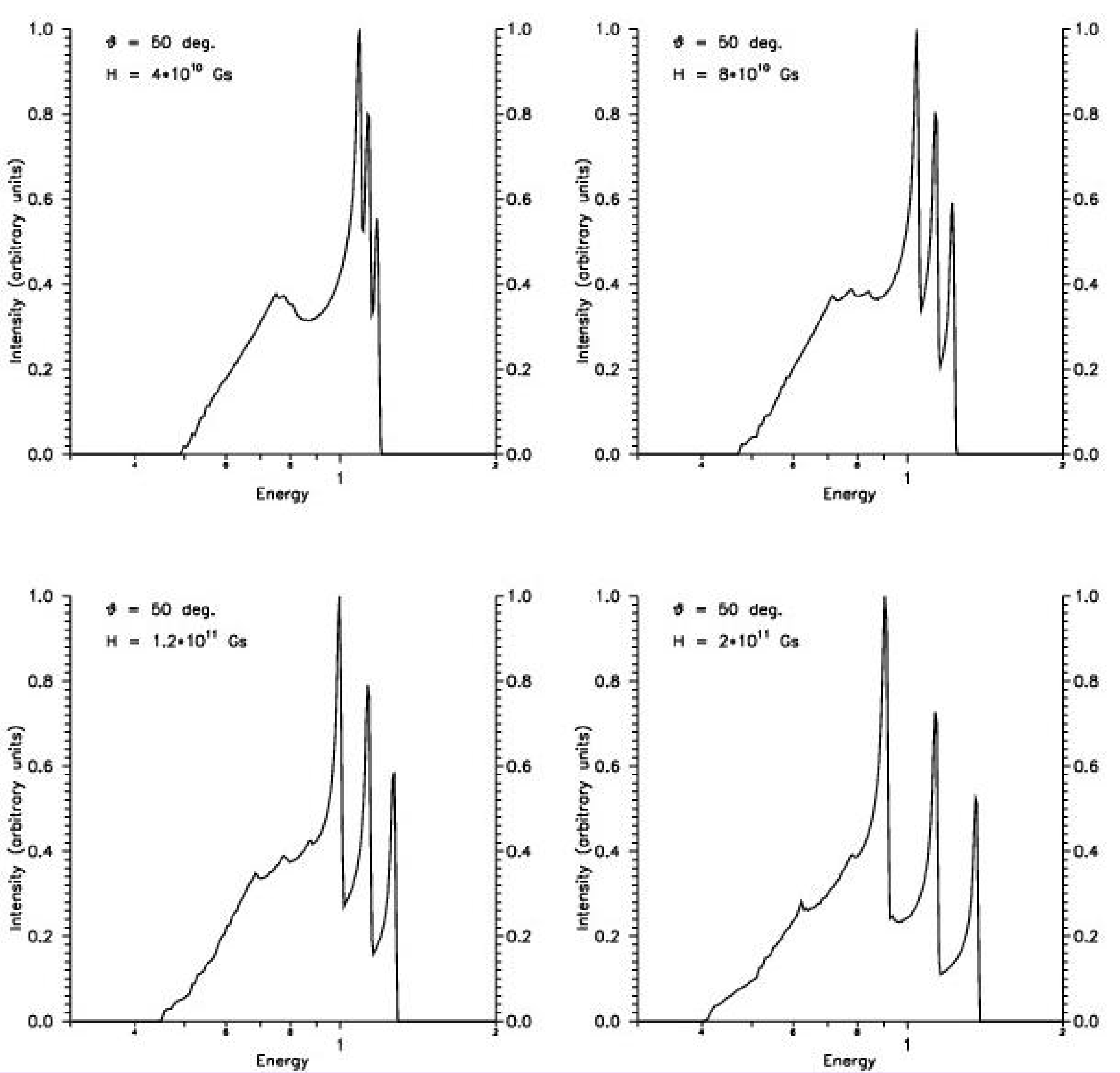

ϑ = 50 deg.
H = 4•10^10 Gs
ϑ = 50 deg.
H = 8•10^10 Gs
ϑ = 50 deg.
H = 1.2•10^11 Gs
ϑ = 50 deg.
H = 2•10^11 Gs
Intensity (arbitrary units)
Energy

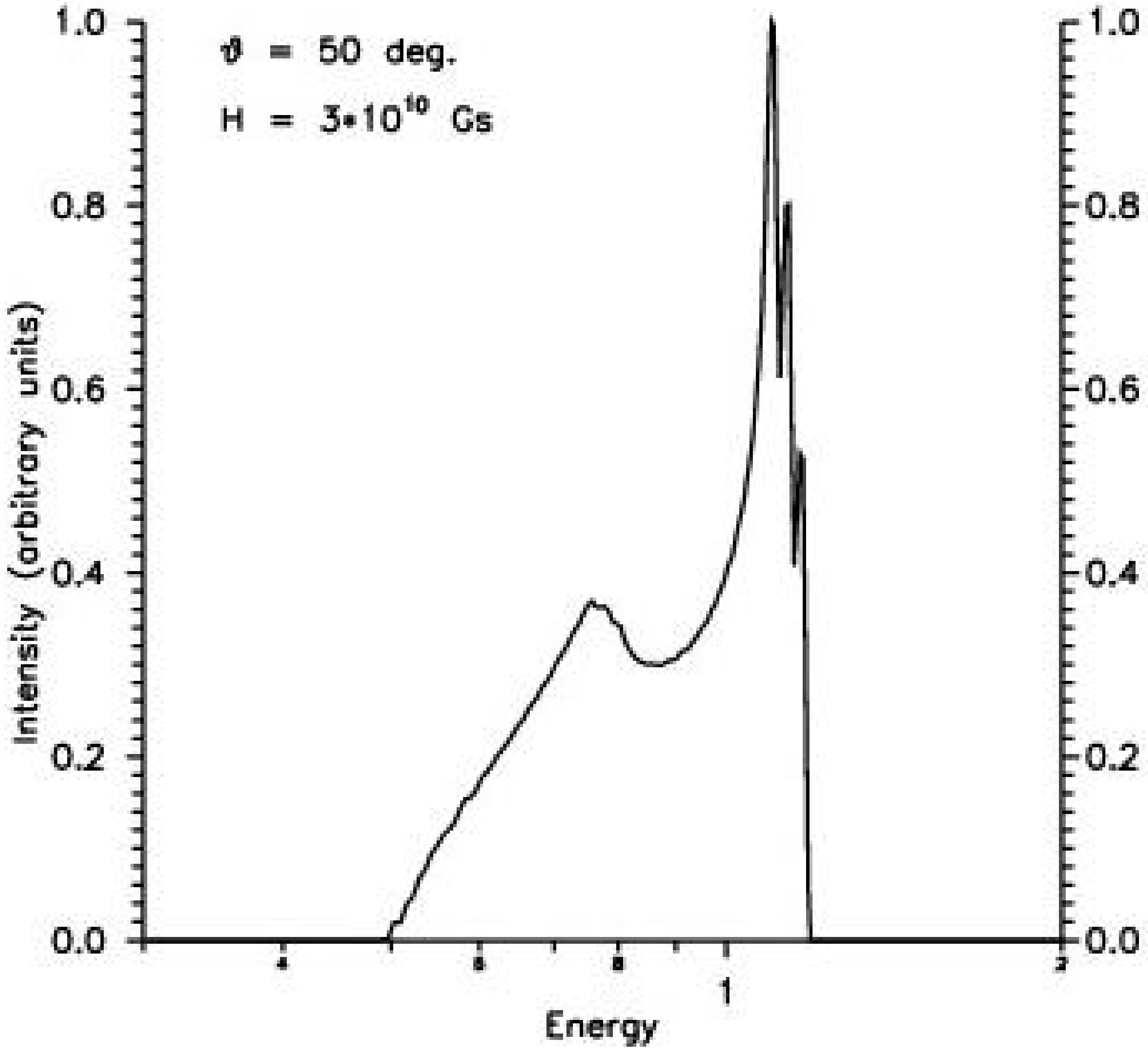

ϑ = 50 deg.
H = 3•10¹⁰ Gs
Intensity (arbitrary units)
1.0
0.8
0.6
0.4
0.2
0.0
1
Energy

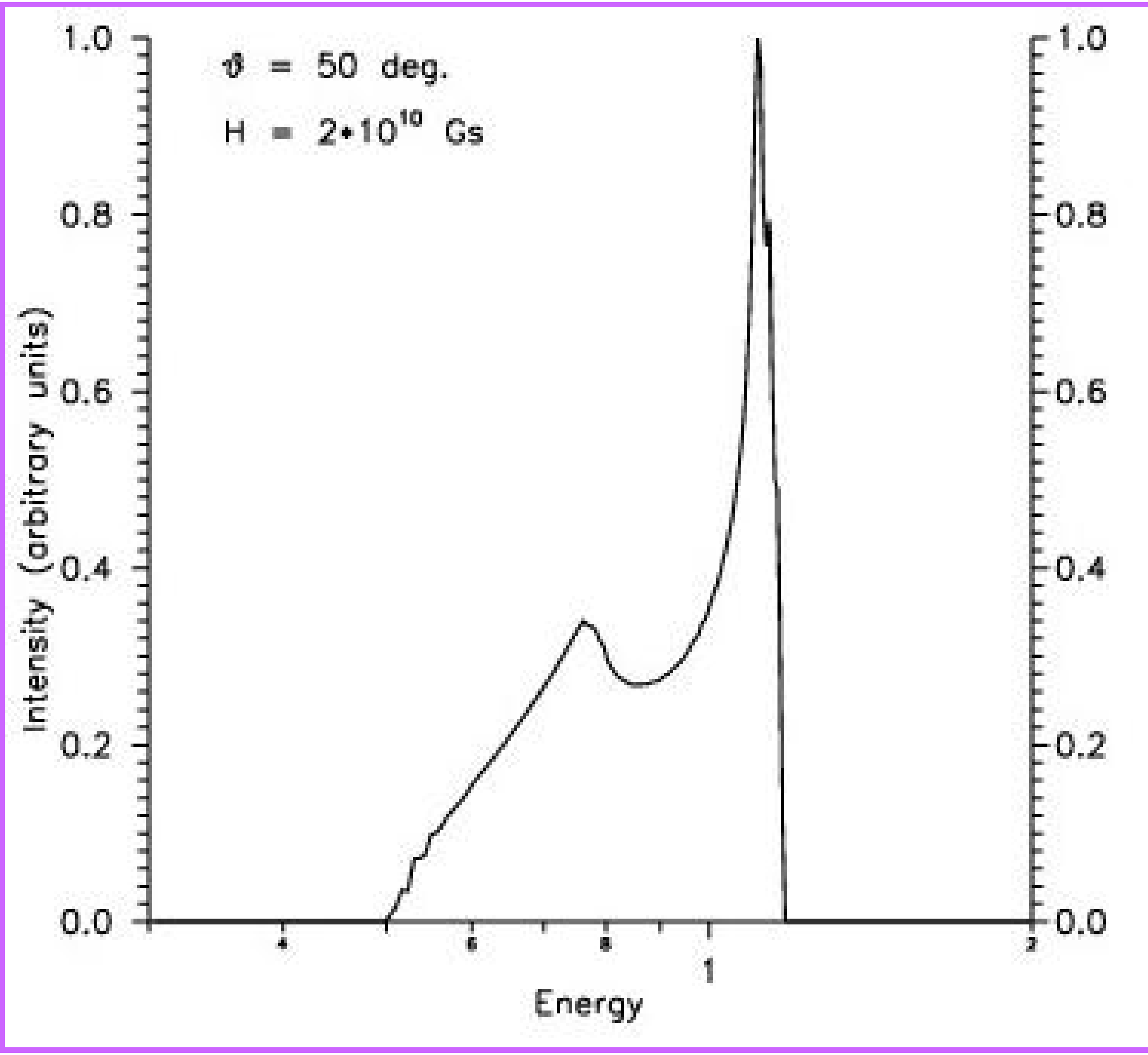

ϑ = 50 deg.
H = 2*10^10 Gs
Intensity (arbitrary units)
0.0
0.2
0.4
0.6
0.8
1.0
4
6
8
1
2
Energy

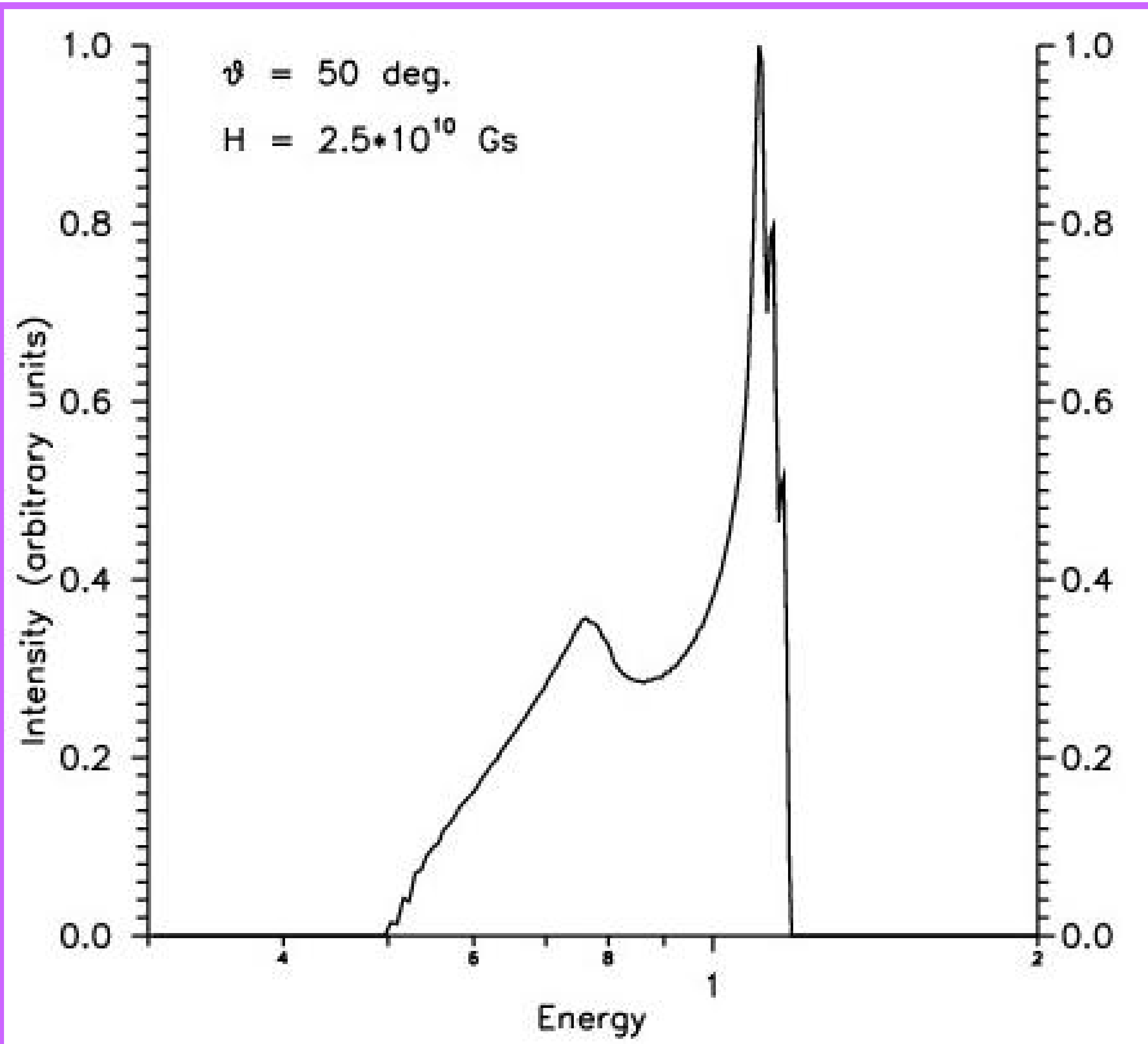
ϑ = 50 deg.
H = 2.5*10^10 Gs
Intensity (arbitrary units)
0.0
0.2
0.4
0.6
0.8
1.0
4
6
8
1
2
Energy

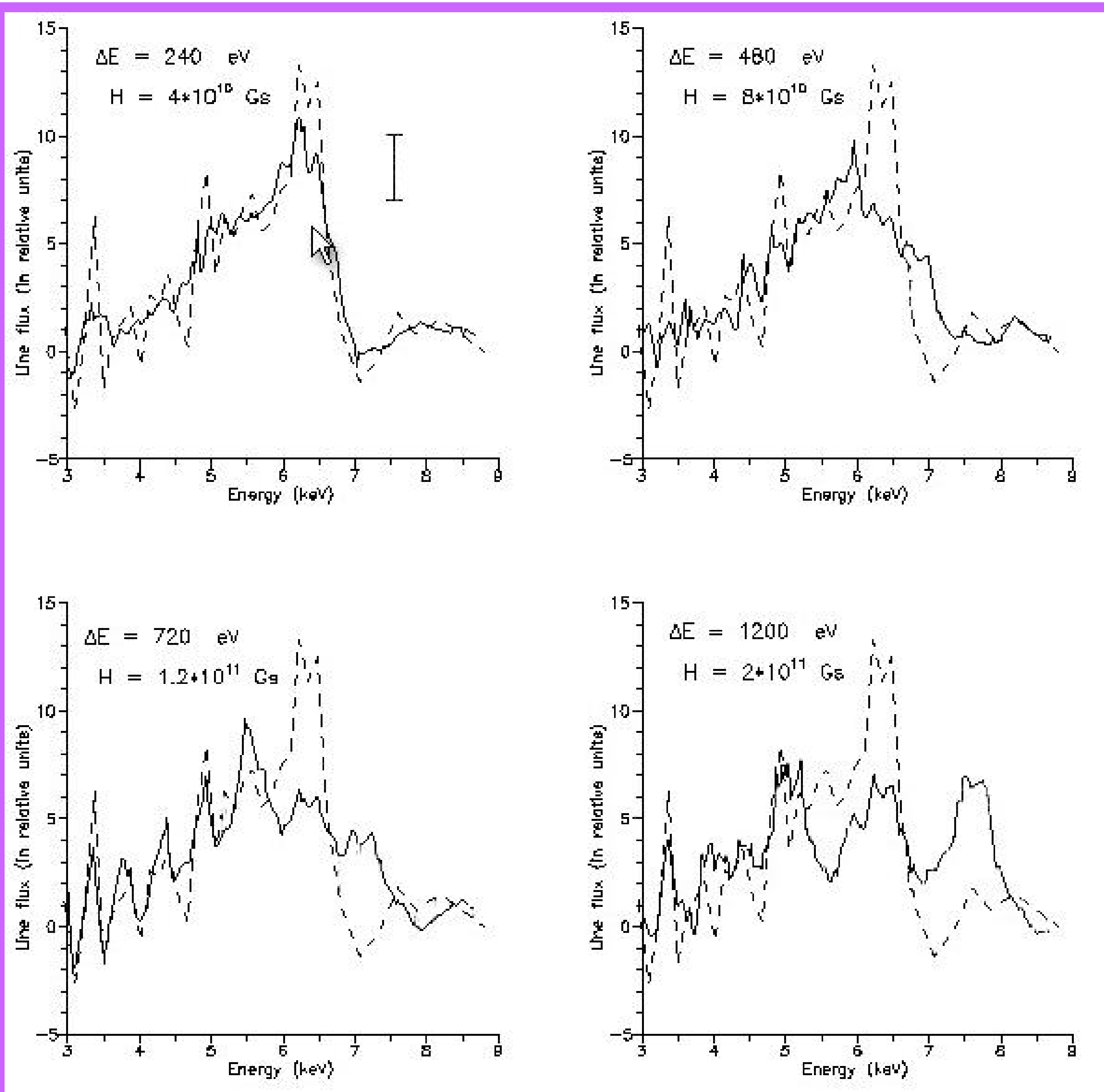

ΔE = 240 eV
H = 4*10^10 Gs
ΔE = 480 eV
H = 8*10^10 Gs
ΔE = 720 eV
H = 1.2*10^11 Gs
ΔE = 1200 eV
H = 2*10^11 Gs
Line flux (in relative units)
Energy (keV)

Magnetic field estimations near BH horizon in AGNs and GBHCs for non-flat accretion flows
(Zakharov, Ma, Bao, New Astronomy, **9**, 663 (2004))

- Figure1
- Figure2
- Figure3
- Figure4
- Figure5
- Figure6

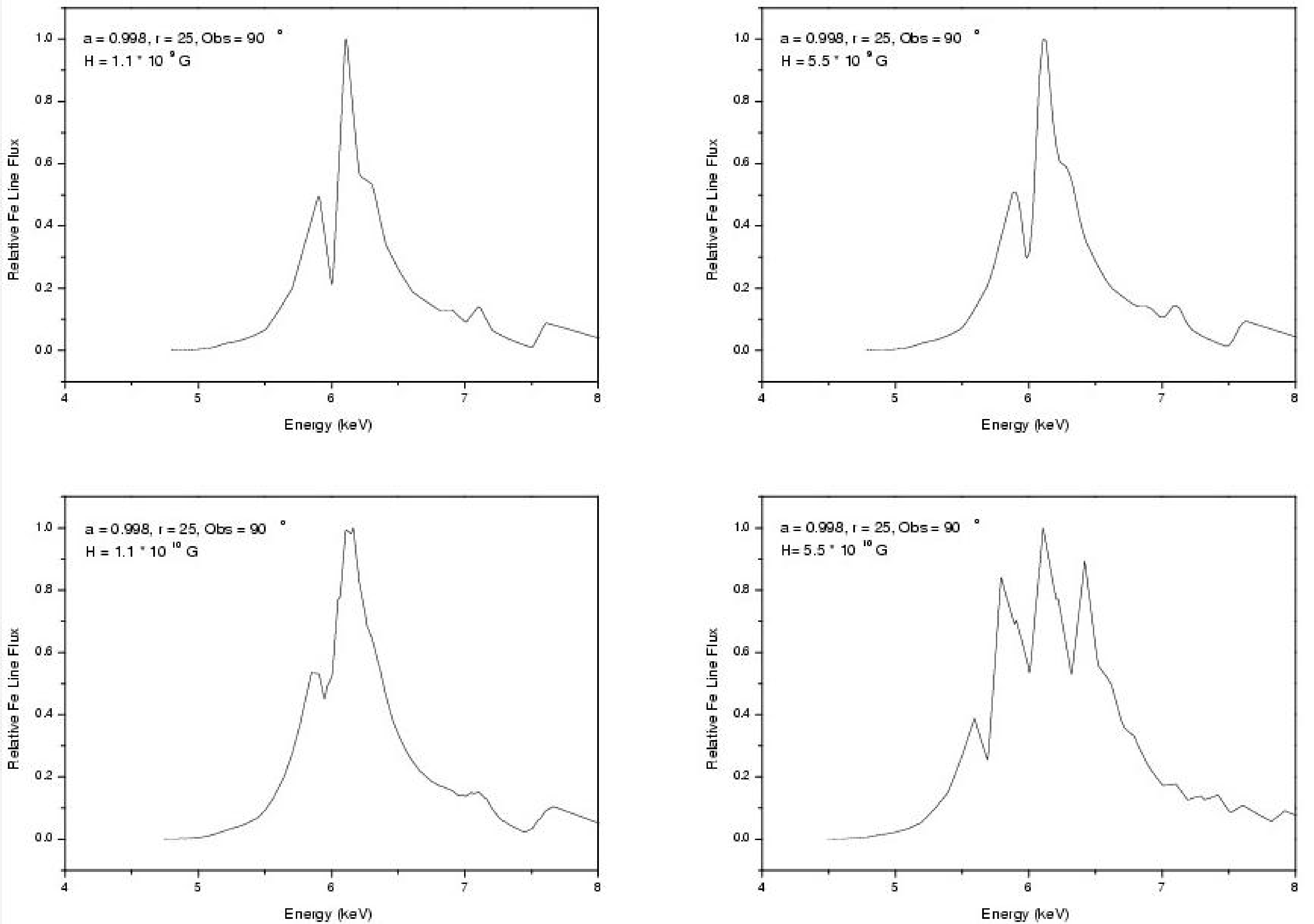
a = 0.998, r = 25, Obs = 90 °
H = 1.1 * 10 ⁹ G
a = 0.998, r = 25, Obs = 90 °
H = 5.5 * 10 ⁹ G
a = 0.998, r = 25, Obs = 90 °
H = 1.1 * 10 ¹⁰ G
a = 0.998, r = 25, Obs = 90 °
H= 5.5 * 10 ¹⁰ G
Relative Fe Line Flux
Energy (keV)

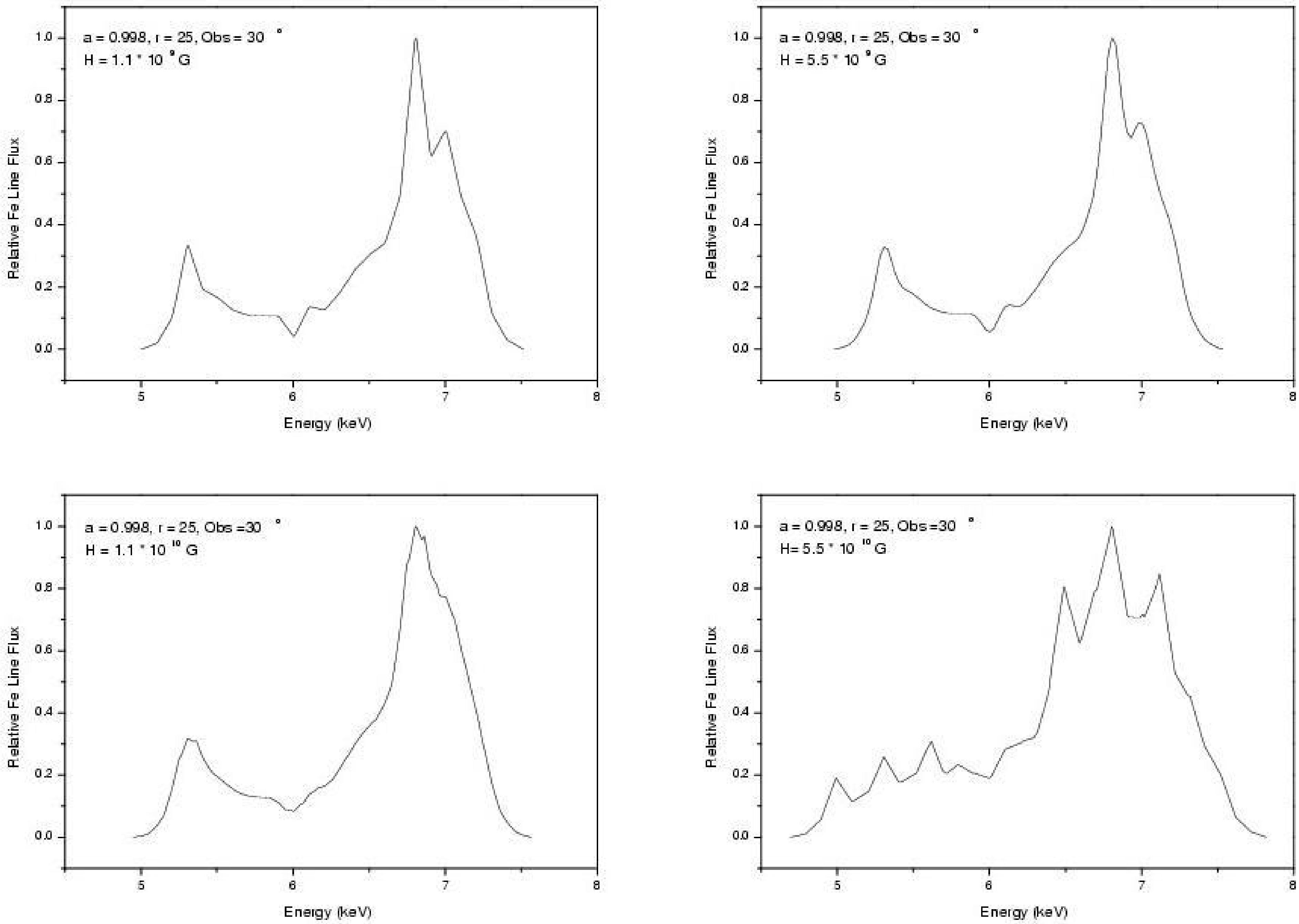

a = 0.998, r = 25, Obs = 30 °
H = 1.1 * 10 ⁹ G
Relative Fe Line Flux
Energy (keV)
a = 0.998, r = 25, Obs = 30 °
H = 5.5 * 10 ⁹ G
Relative Fe Line Flux
Energy (keV)
a = 0.998, r = 25, Obs =30 °
H = 1.1 * 10 ¹⁰ G
Relative Fe Line Flux
Energy (keV)
a = 0.998, r = 25, Obs =30 °
H= 5.5 * 10 ¹⁰ G
Relative Fe Line Flux
Energy (keV)

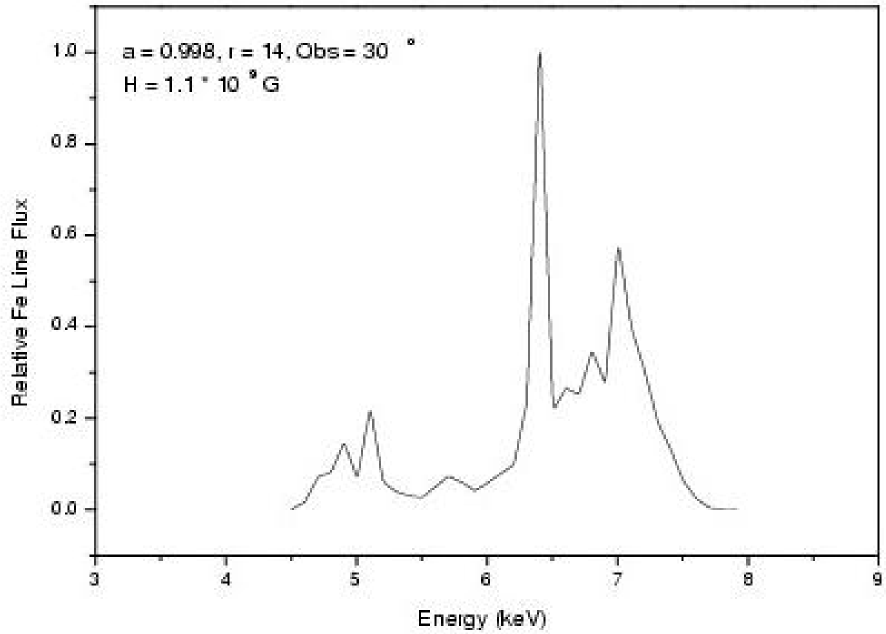

a = 0.998, r = 14, Obs = 30 °
H = 1.1 * 10 9 G
Relative Fe Line Flux
Energy (keV)

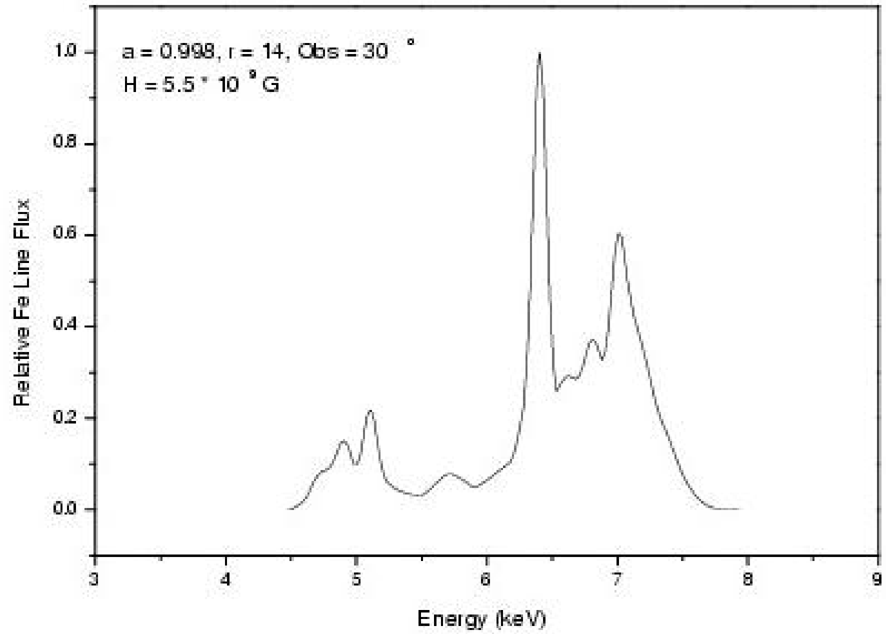

a = 0.998, r = 14, Obs = 30 °
H = 5.5 * 10 9 G
Relative Fe Line Flux
Energy (keV)

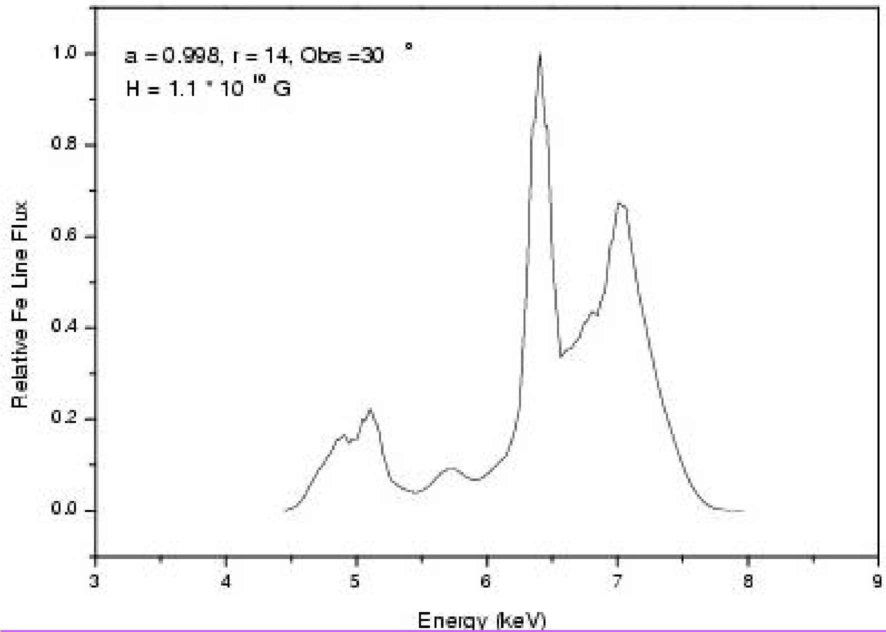

a = 0.998, r = 14, Obs =30 °
H = 1.1 * 10 10 G
Relative Fe Line Flux
Energy (keV)

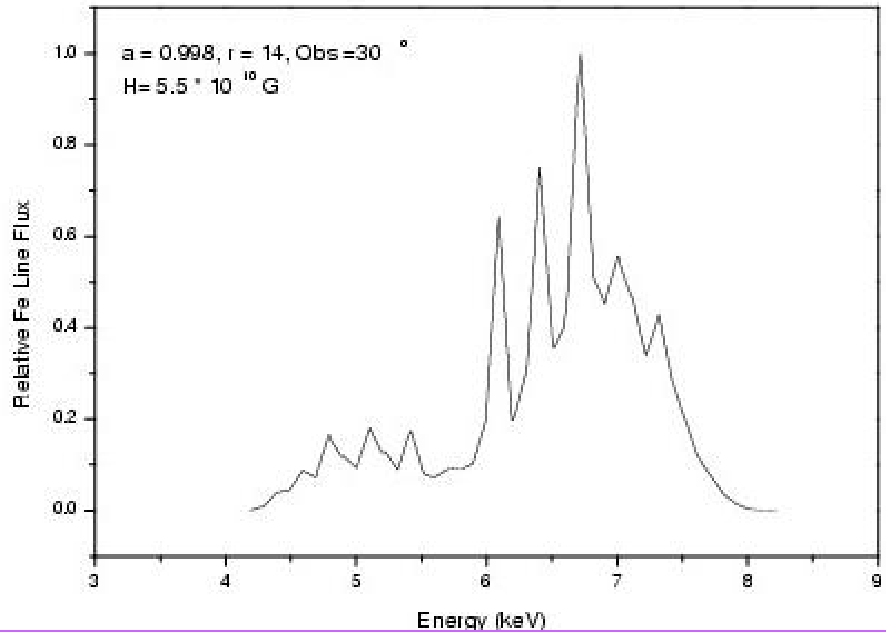

a = 0.998, r = 14, Obs =30 °
H= 5.5 * 10 10 G
Relative Fe Line Flux
Energy (keV)

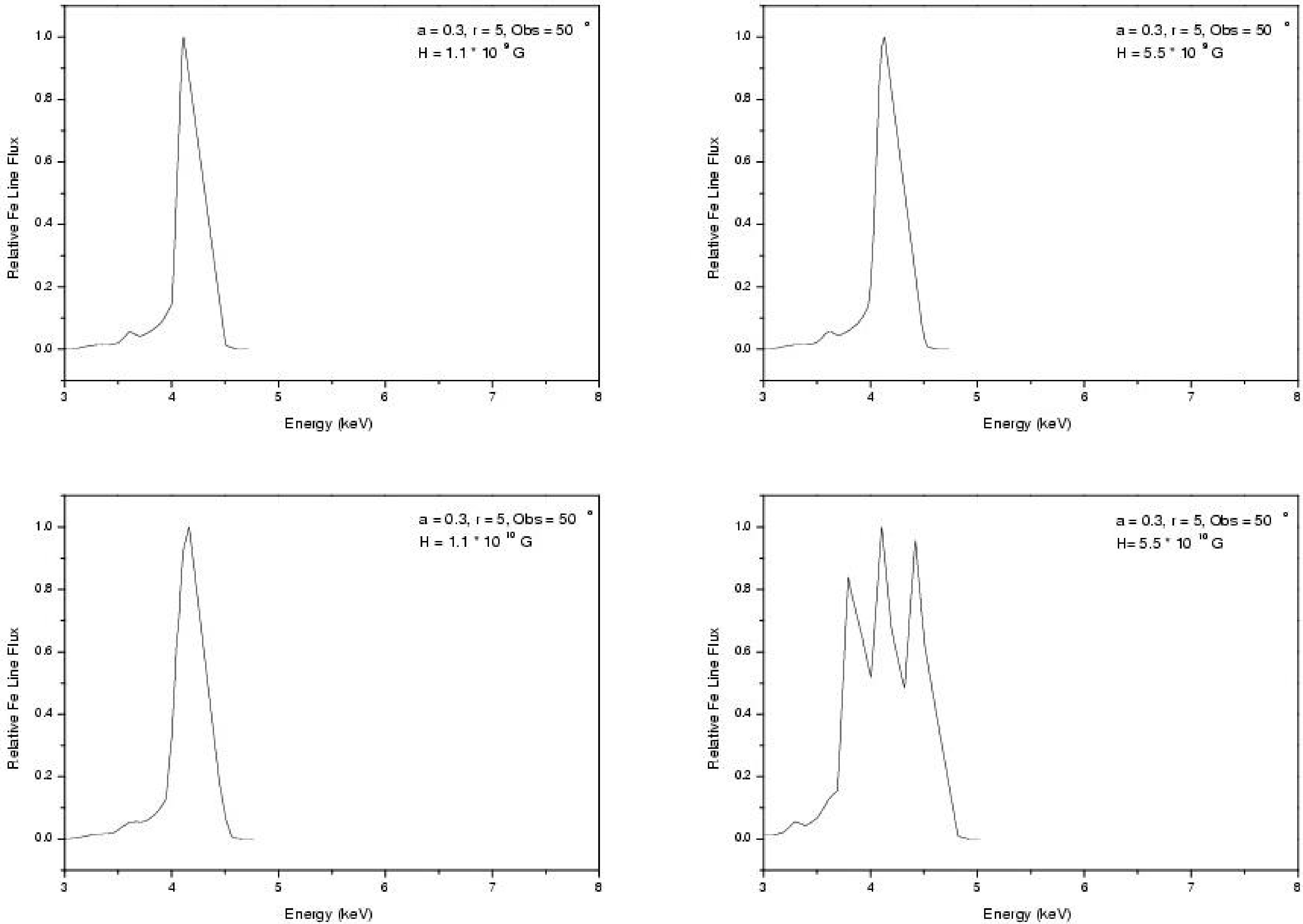

a = 0.3, r = 5, Obs = 50 °
H = 1.1 * 10 ^9 G
a = 0.3, r = 5, Obs = 50 °
H = 5.5 * 10 ^9 G
a = 0.3, r = 5, Obs = 50 °
H = 1.1 * 10 ^10 G
a = 0.3, r = 5, Obs = 50 °
H= 5.5 * 10 ^10 G
Relative Fe Line Flux
Energy (keV)

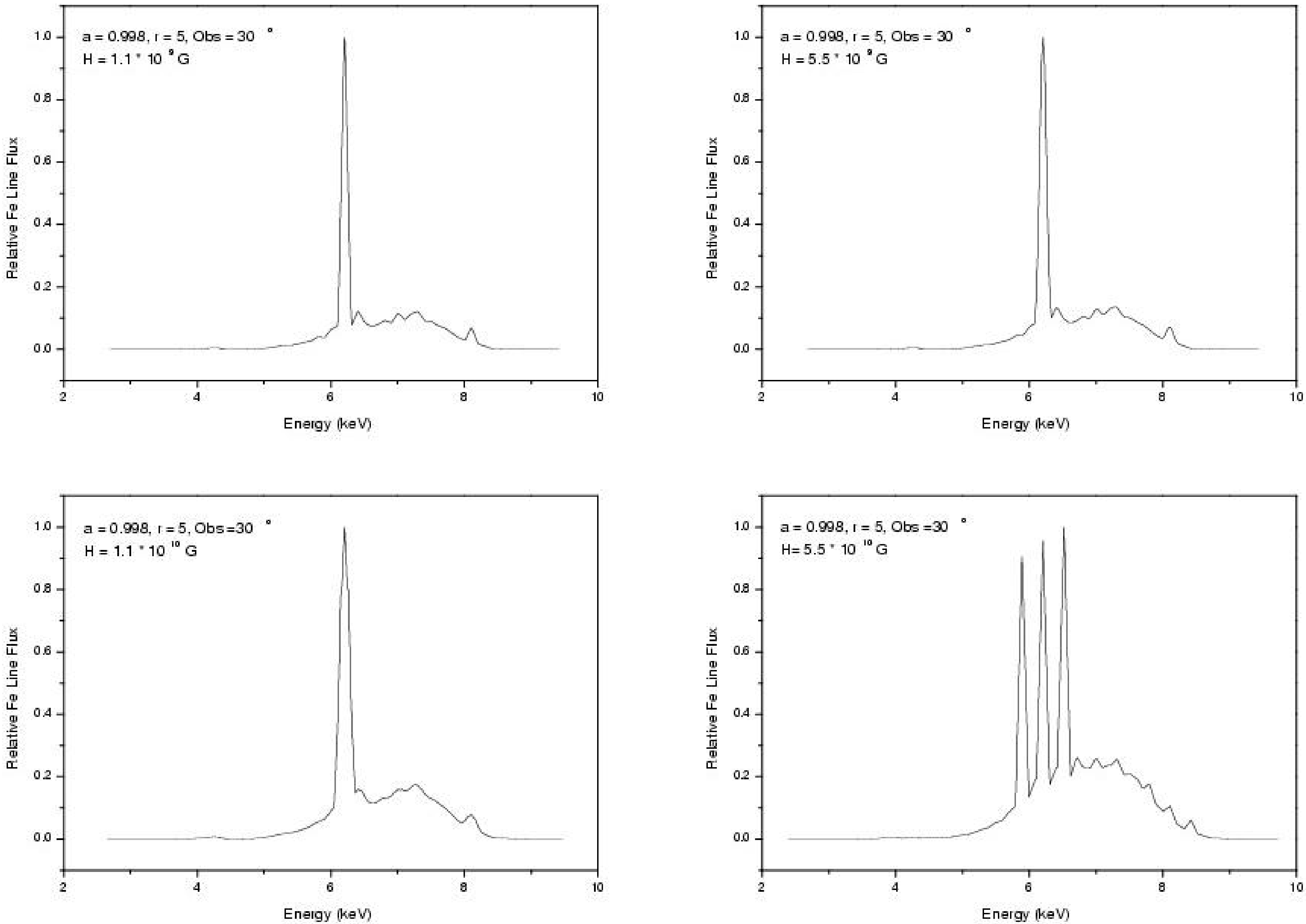
a = 0.998, r = 5, Obs = 30 °
H = 1.1 * 10 9 G
a = 0.998, r = 5, Obs = 30 °
H = 5.5 * 10 9 G
a = 0.998, r = 5, Obs =30 °
H = 1.1 * 10 10 G
a = 0.998, r = 5, Obs =30 °
H= 5.5 * 10 10 G
Relative Fe Line Flux
Energy (keV)

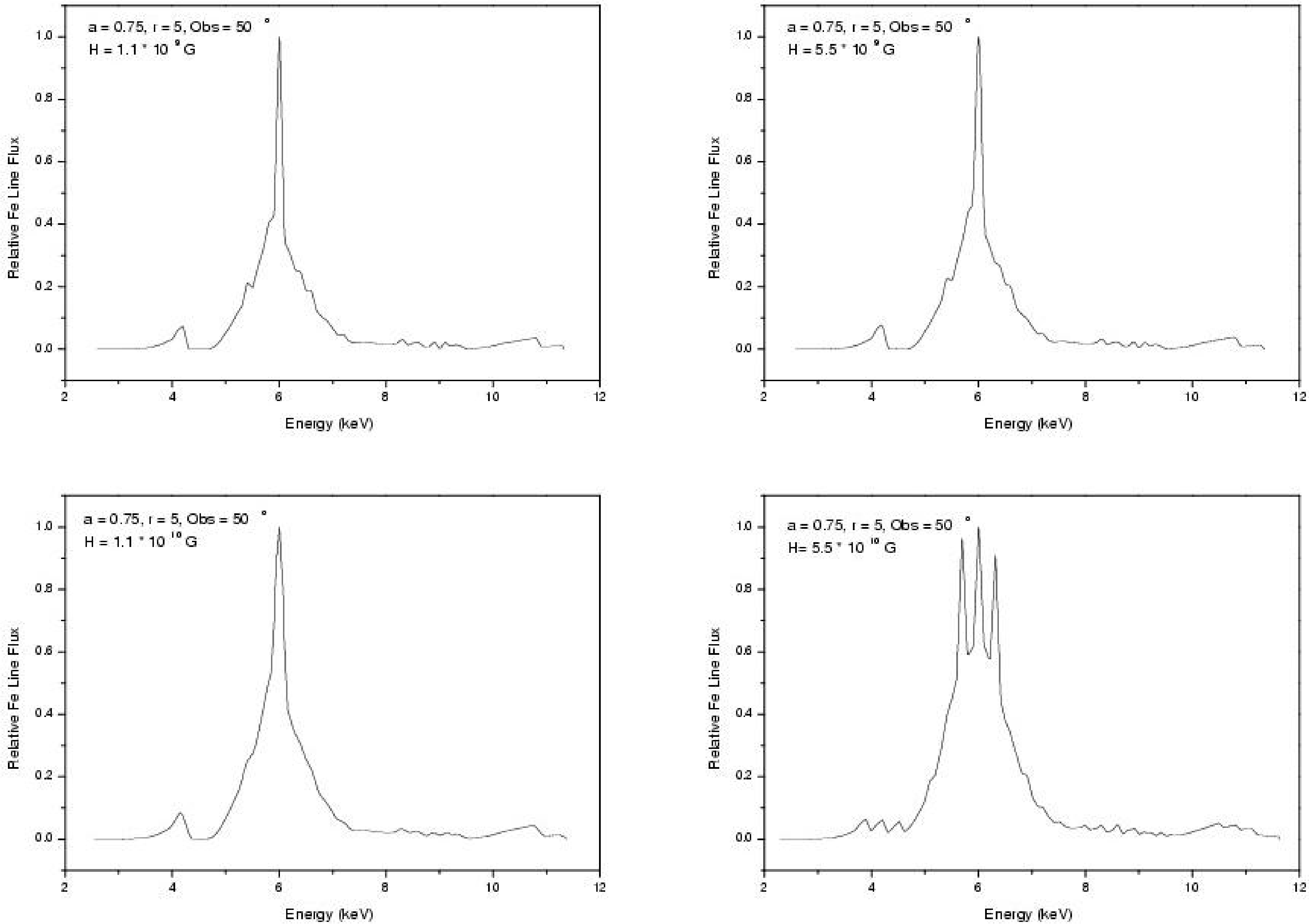
a = 0.75, r = 5, Obs = 50 °
H = 1.1 * 10 9 G
a = 0.75, r = 5, Obs = 50 °
H = 5.5 * 10 9 G
a = 0.75, r = 5, Obs = 50 °
H = 1.1 * 10 10 G
a = 0.75, r = 5, Obs = 50 °
H= 5.5 * 10 10 G
Relative Fe Line Flux
Energy (keV)

Mon. Not. R. Astron. Soc. **328,** L27–L31 (2001)

XMM-EPIC observation of MCG–6-30-15: direct evidence for the extraction of energy from a spinning black hole?

Jörn Wilms,[1★] Christopher S. Reynolds,[2,3†] Mitchell C. Begelman,[3,4] James Reeves,[5] Silvano Molendi,[6] Rüdiger Staubert[1] and Eckhard Kendziorra[1]

[1]*Institut für Astronomie und Astrophysik, Abt. Astronomie, Universität Tübingen, Sand 1, D-72076 Tübingen, Germany*
[2]*Department of Astronomy, University of Maryland, College Park, MD 20742, USA*
[3]*JILA, Campus Box 440, University of Colorado, Boulder, CO 80309, USA*
[4]*Department of Astrophysical and Planetary Sciences, University of Colorado, Boulder, CO 80309, USA*
[5]*X-Ray Astronomy Group, Department of Physics and Astronomy, Leicester University, Leicester LE1 7RH*
[6]*Istituto di Fisica Cosmica, CNR, via Bassini 15, I-20133 Milano, Italy*

Accepted 2001 October 22. Received 2001 October 22; in original form 2001 August 24

ABSTRACT

We present *XMM-Newton* European Photon Imaging Camera (EPIC) observations of the bright Seyfert 1 galaxy MCG–6-30-15, focusing on the broad Fe Kα line at $\sim$6 keV and the associated reflection continuum, which is believed to originate from the inner accretion disc. We find these reflection features to be *extremely* broad and redshifted, indicating an origin in the very central regions of the accretion disc. It seems likely that we have caught this source in the 'deep minimum' state first observed by Iwasawa et al. The implied central concentration of X-ray illumination is difficult to understand in any pure accretion disc model. We suggest that we are witnessing the extraction and dissipation of rotational energy from a spinning black hole by magnetic fields connecting the black hole or plunging region to the disc.

Key words: accretion, accretion discs – black hole physics – galaxies: individual: MCG–6-30-15 – galaxies: Seyfert – X-rays: galaxies.

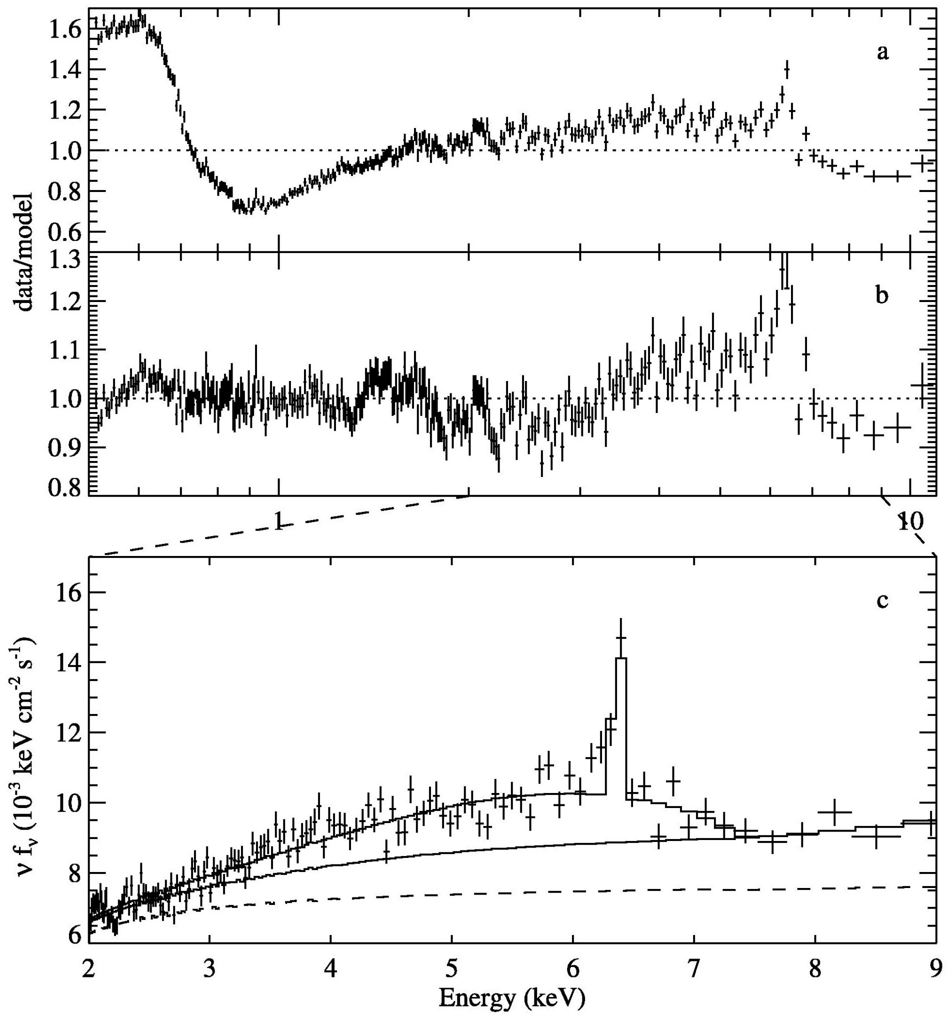

Figure 1. (a) Ratio between data and model from fitting a power law to the 0.5–11 keV data. (b) Ratio from fitting a power law and the empirical warm absorber model (see text). (c) Deconvolved spectrum of the Fe Kα band, showing the total LAOR model and the continuum with and without (dashed) the reflection component for a model with reflection from an ionized disc. For clarity, the data have been rebinned and only the single-event data points are shown.

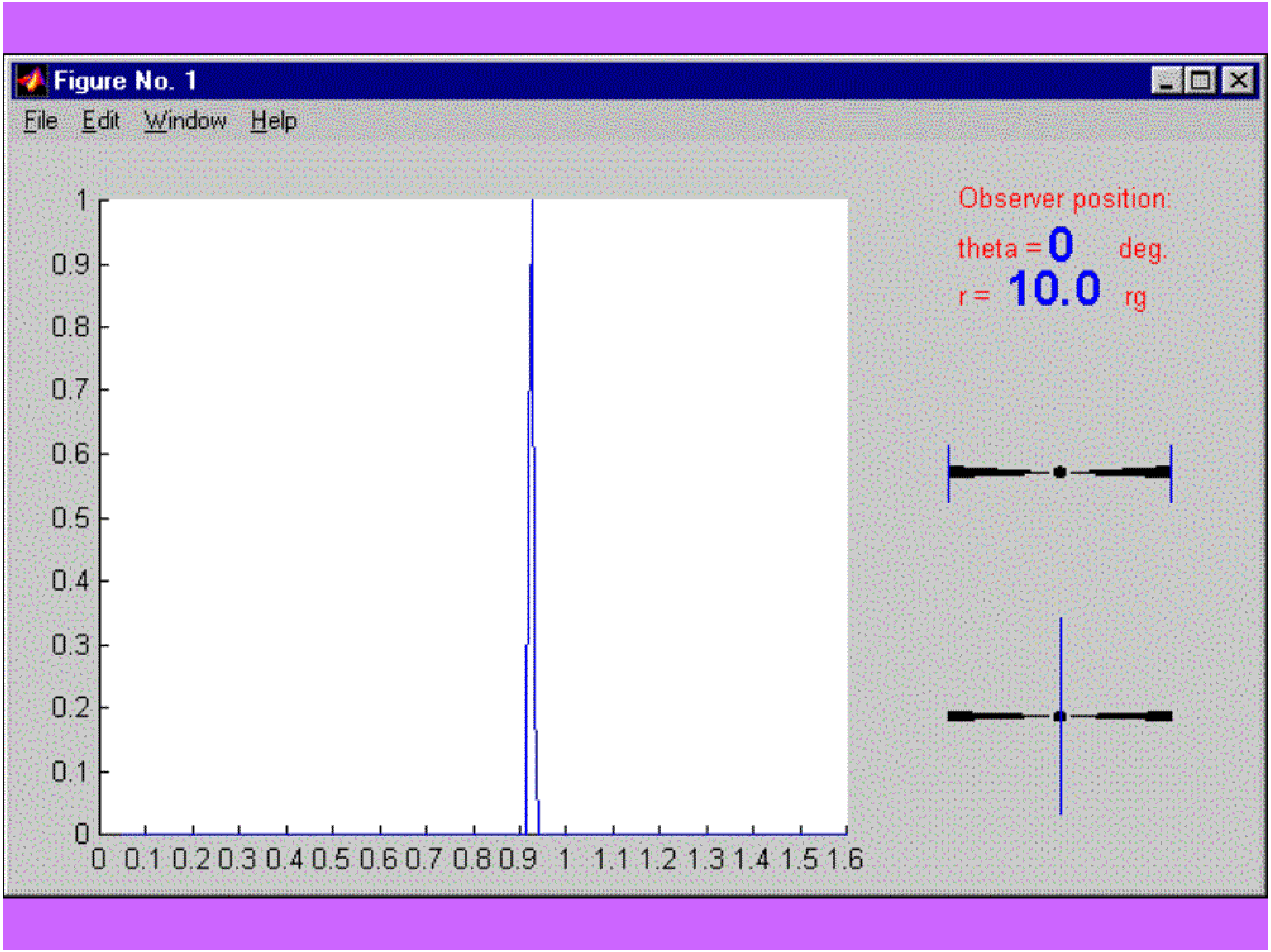
Figure No. 1
File Edit Window Help
Observer position:
theta = 0 deg.
r = 10.0 rg
0 0.1 0.2 0.3 0.4 0.5 0.6 0.7 0.8 0.9 1
0 0.1 0.2 0.3 0.4 0.5 0.6 0.7 0.8 0.9 1 1.1 1.2 1.3 1.4 1.5 1.6

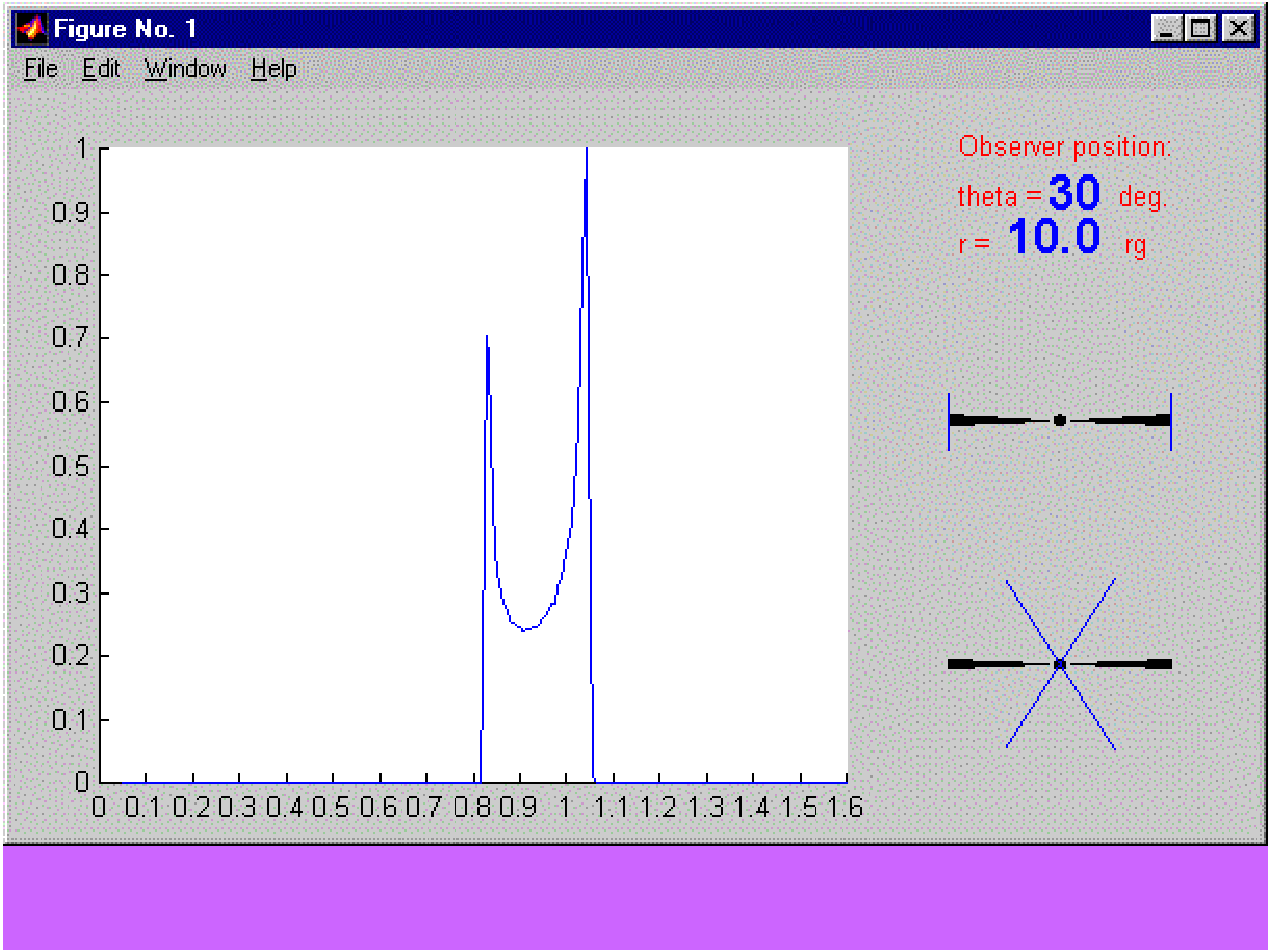
Figure No. 1
File Edit Window Help
1
0.9
0.8
0.7
0.6
0.5
0.4
0.3
0.2
0.1
0
0 0.1 0.2 0.3 0.4 0.5 0.6 0.7 0.8 0.9 1 1.1 1.2 1.3 1.4 1.5 1.6
Observer position:
theta = 30 deg.
r = 10.0 rg

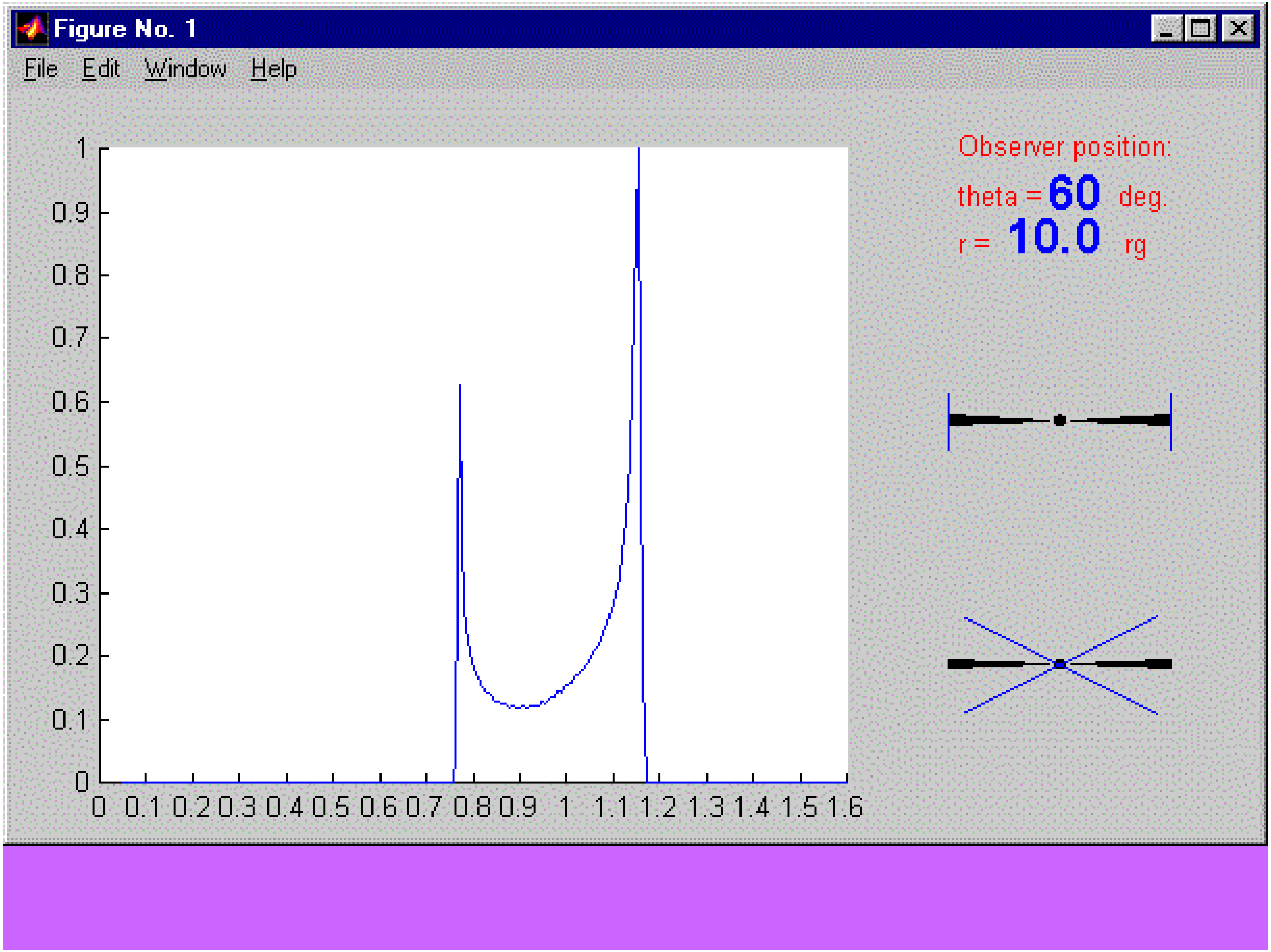
Figure No. 1
File Edit Window Help
Observer position:
theta = 60 deg.
r = 10.0 rg
0 0.1 0.2 0.3 0.4 0.5 0.6 0.7 0.8 0.9 1 1.1 1.2 1.3 1.4 1.5 1.6
0 0.1 0.2 0.3 0.4 0.5 0.6 0.7 0.8 0.9 1

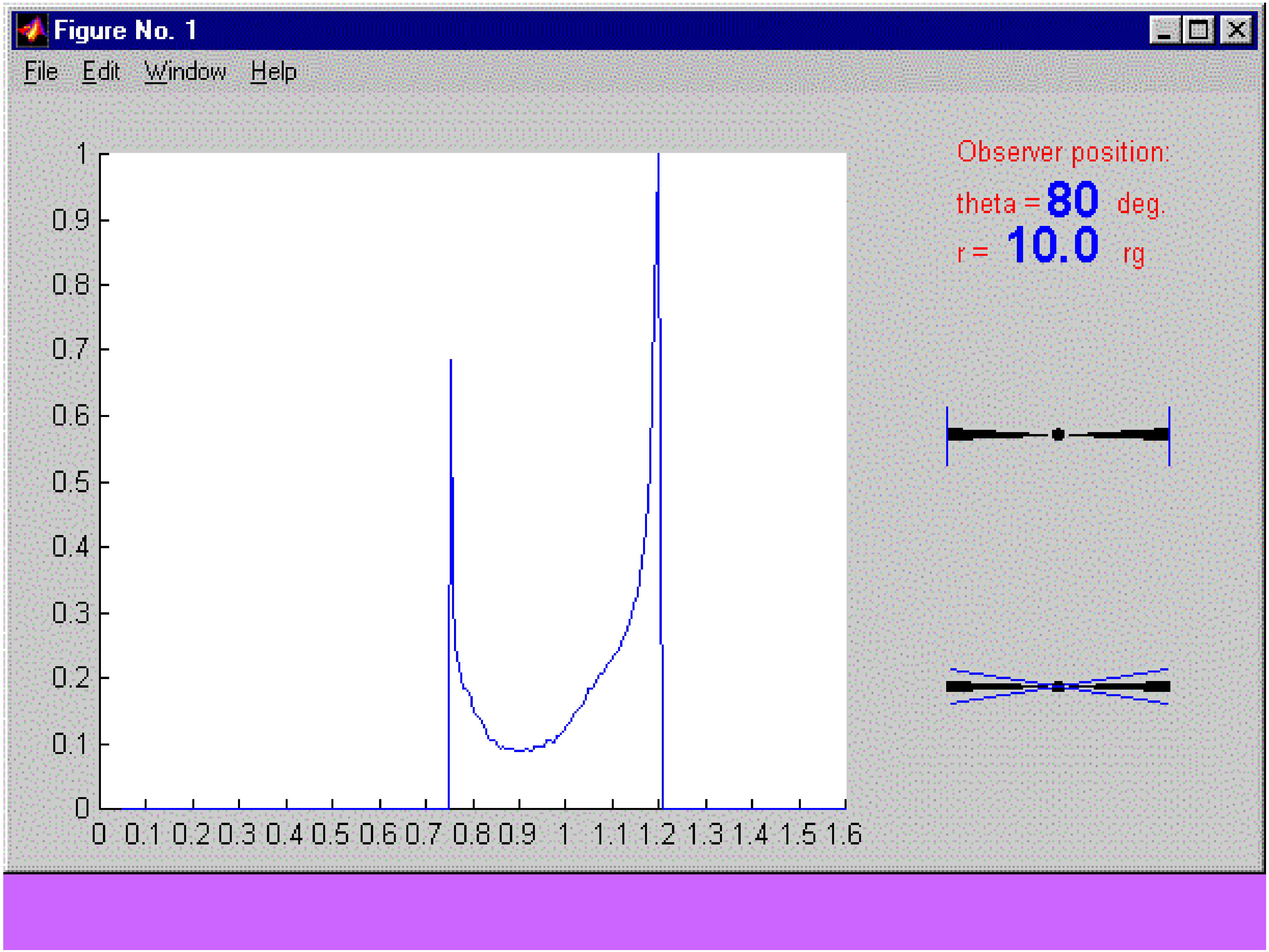
Figure No. 1
File Edit Window Help
1
0.9
0.8
0.7
0.6
0.5
0.4
0.3
0.2
0.1
0
0 0.1 0.2 0.3 0.4 0.5 0.6 0.7 0.8 0.9 1 1.1 1.2 1.3 1.4 1.5 1.6
Observer position:
theta = 80 deg.
r = 10.0 rg

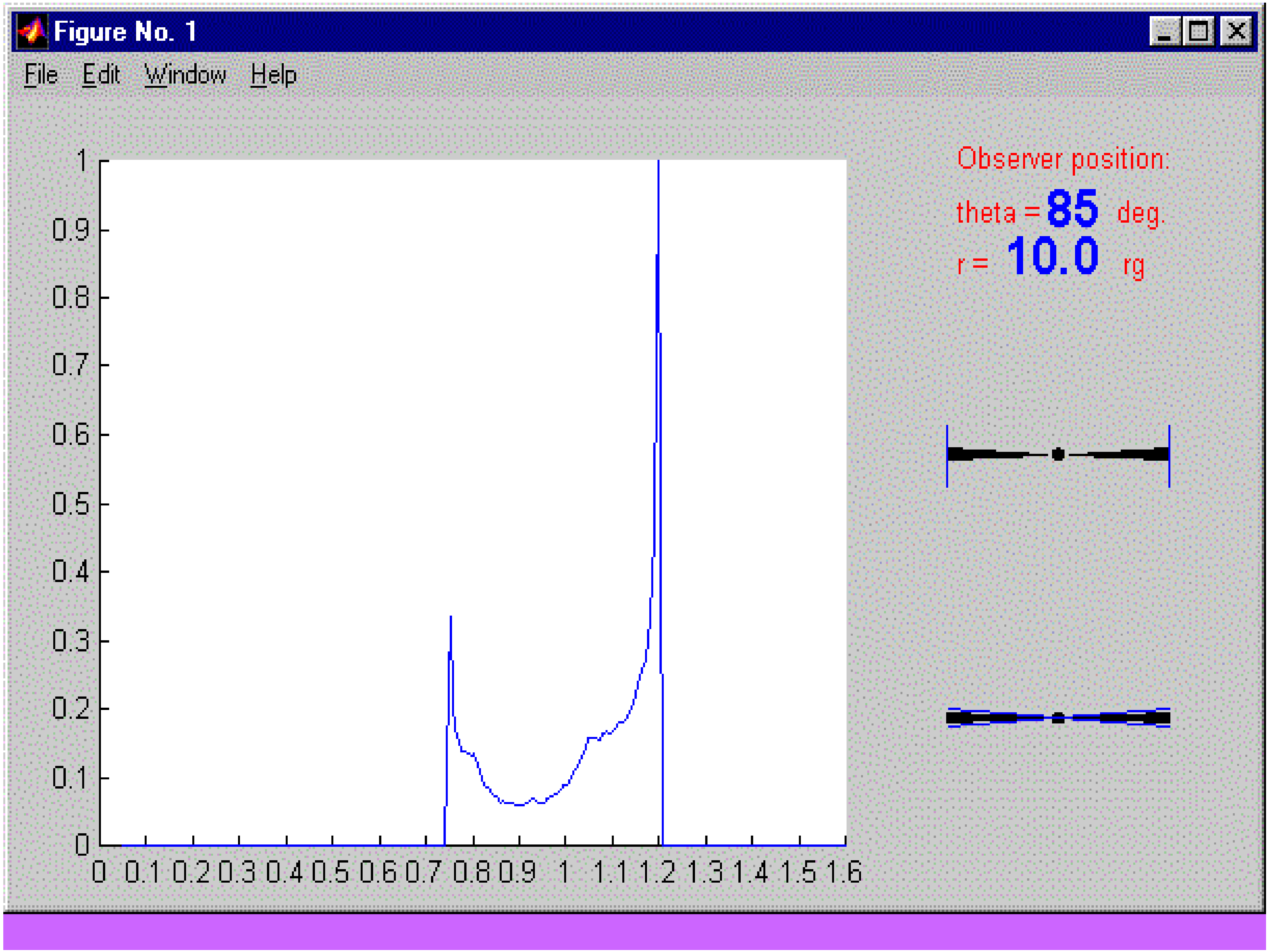

Figure No. 1
File Edit Window Help
Observer position:
theta = 85 deg.
r = 10.0 rg
0 0.1 0.2 0.3 0.4 0.5 0.6 0.7 0.8 0.9 1
0 0.1 0.2 0.3 0.4 0.5 0.6 0.7 0.8 0.9 1 1.1 1.2 1.3 1.4 1.5 1.6

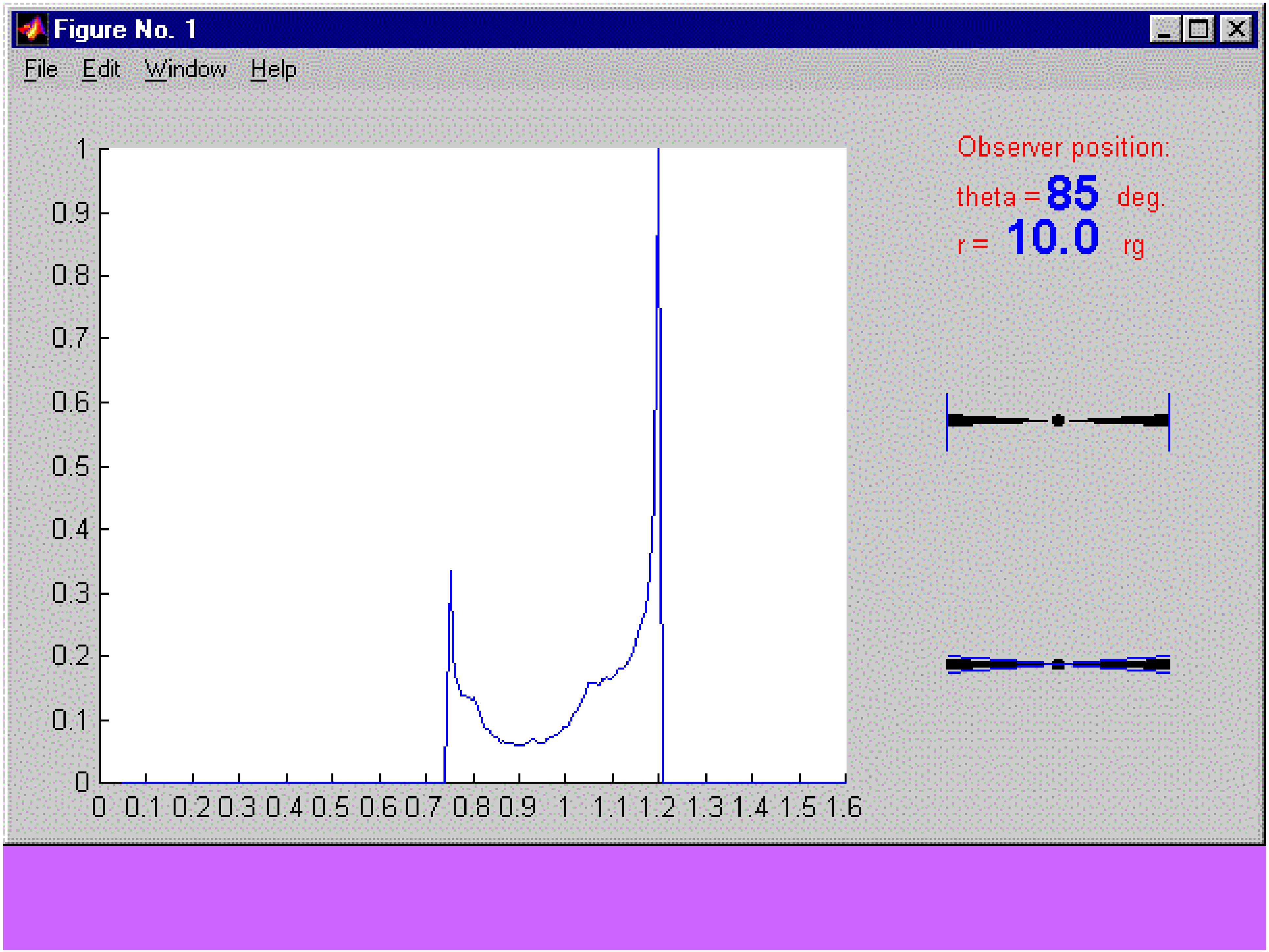

Figure No. 1
File
Edit
Window
Help
1
0.9
0.8
0.7
0.6
0.5
0.4
0.3
0.2
0.1
0
0 0.1 0.2 0.3 0.4 0.5 0.6 0.7 0.8 0.9 1 1.1 1.2 1.3 1.4 1.5 1.6
Observer position:
theta = 85 deg.
r = 10.0 rg

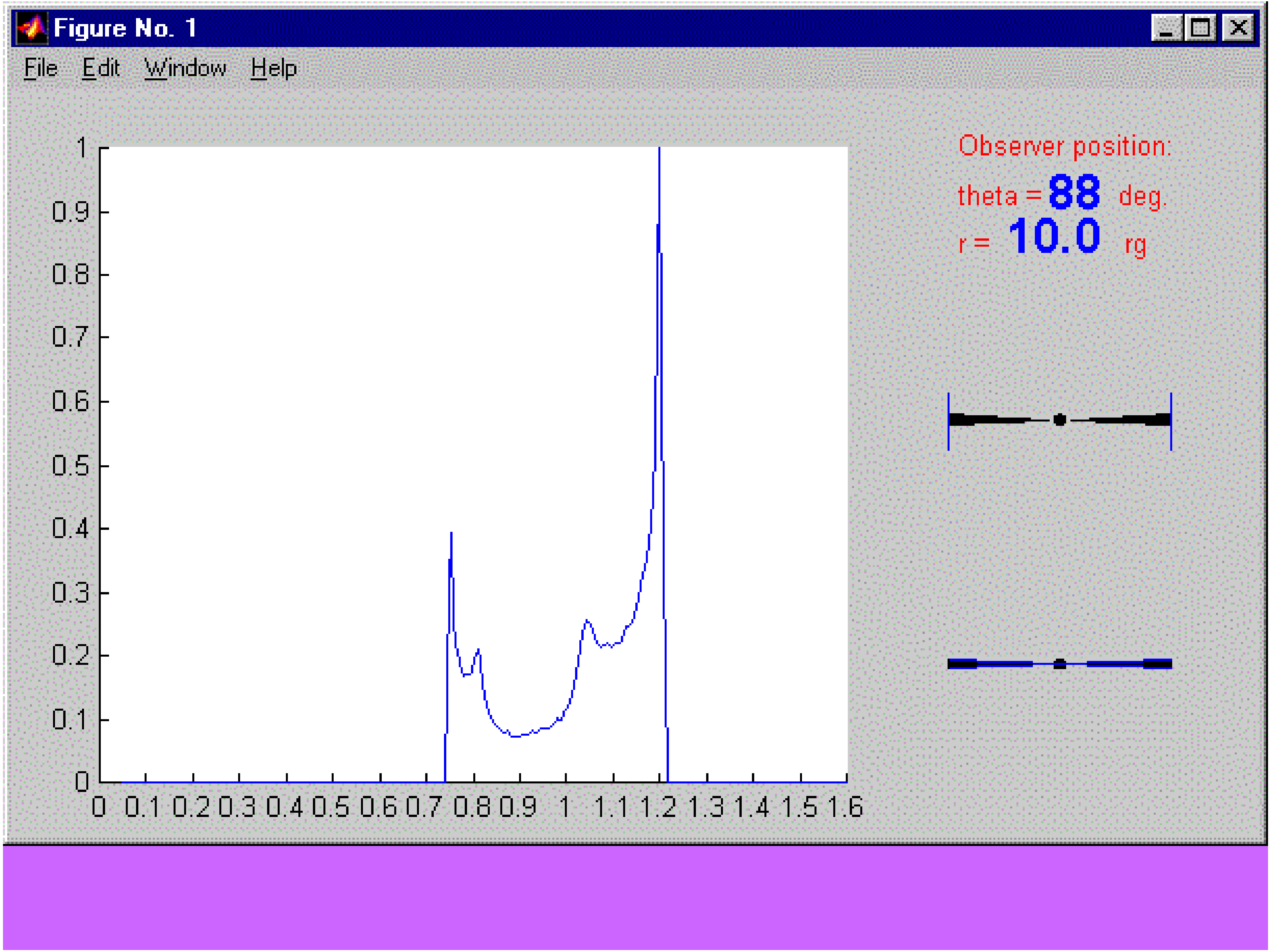
Figure No. 1
File Edit Window Help
1
0.9
0.8
0.7
0.6
0.5
0.4
0.3
0.2
0.1
0
0 0.1 0.2 0.3 0.4 0.5 0.6 0.7 0.8 0.9 1 1.1 1.2 1.3 1.4 1.5 1.6
Observer position:
theta = 88 deg.
r = 10.0 rg

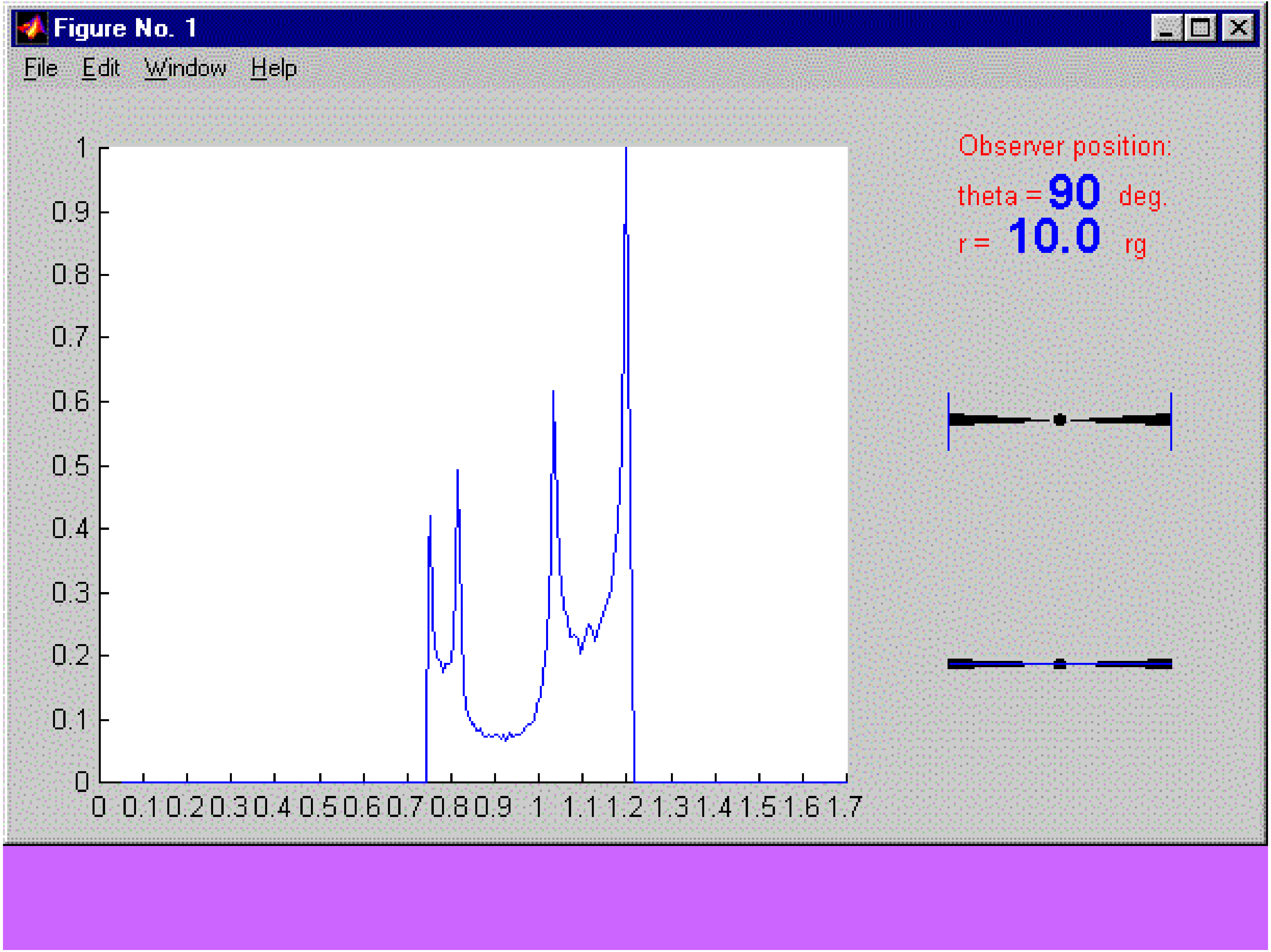
Figure No. 1
File Edit Window Help
1
0.9
0.8
0.7
0.6
0.5
0.4
0.3
0.2
0.1
0
0 0.1 0.2 0.3 0.4 0.5 0.6 0.7 0.8 0.9 1 1.1 1.2 1.3 1.4 1.5 1.6 1.7
Observer position:
theta = 90 deg.
r = 10.0 rg

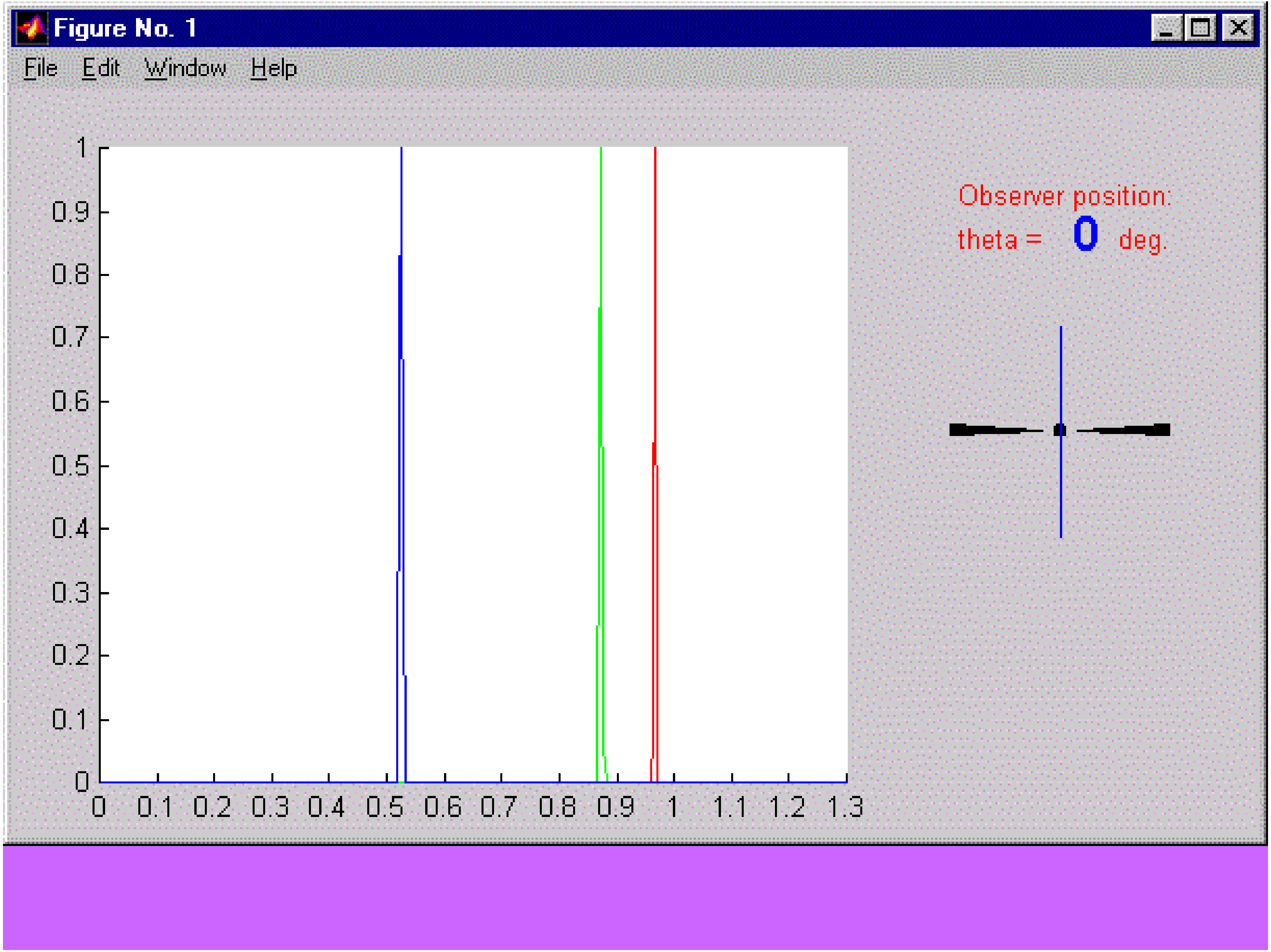
Figure No. 1
File Edit Window Help
1
0.9
0.8
0.7
0.6
0.5
0.4
0.3
0.2
0.1
0
0 0.1 0.2 0.3 0.4 0.5 0.6 0.7 0.8 0.9 1 1.1 1.2 1.3
Observer position:
theta = 0 deg.

- http://www.gsfc.nasa.gov/gsfc/spacesci/pictures/blackhole/BH1m.jpg

What is a black hole?

Everyone already seems to know!

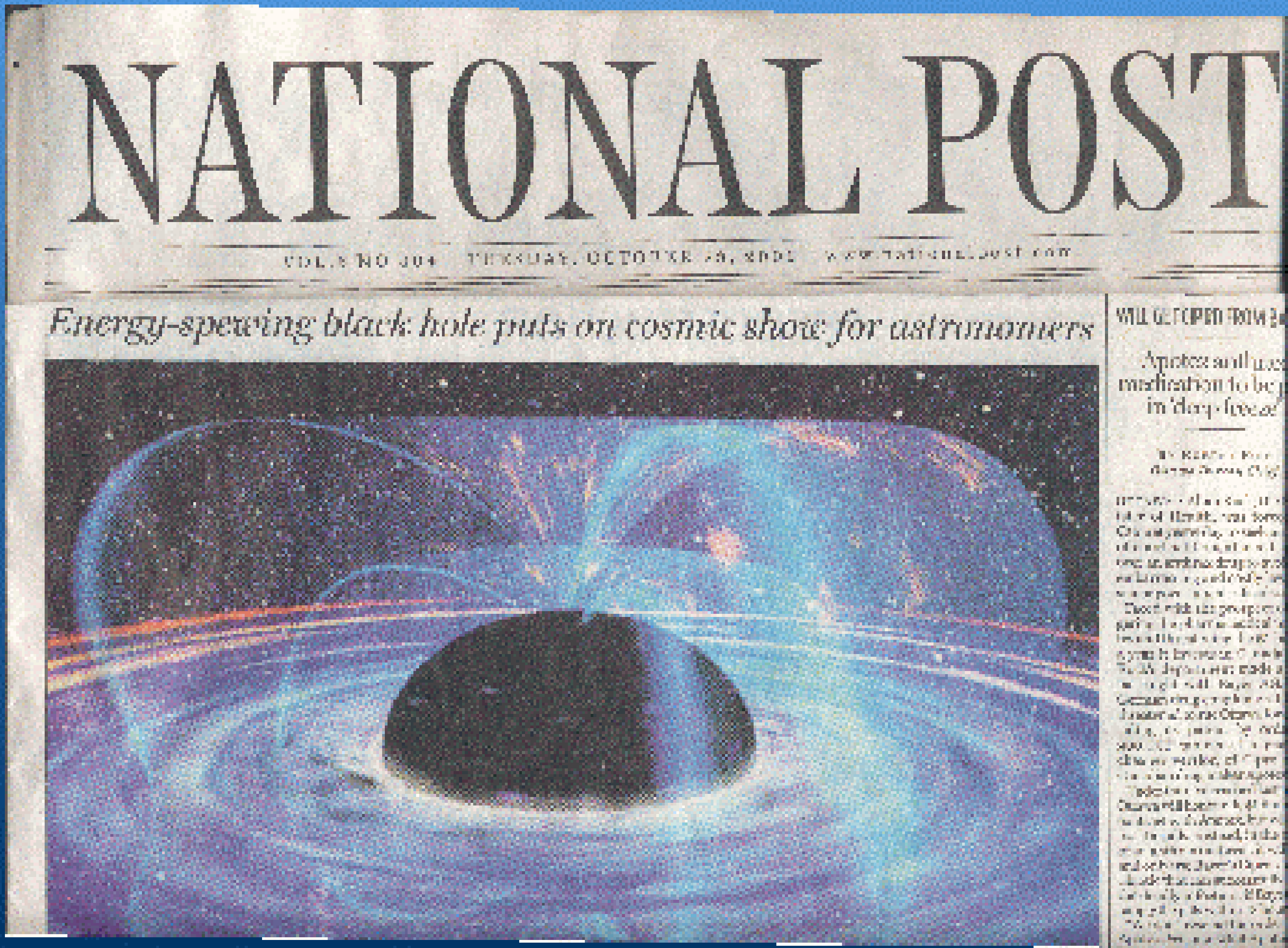

Mirages around Kerr black holes and retro-gravitational lenses

- Let us consider an illumination of black holes. Then retro-photons form caustics around black holes or mirages around black holes or boundaries around shadows.
- (Zakharov, Nucita, DePaolis, Ingrosso,
- New Astronomy (accepted); astro-ph/0411511)

RETRO-MACHOS: π IN THE SKY?

DANIEL E. HOLZ
Institute for Theoretical Physics, University of California, Santa Barbara, CA 93106

AND

JOHN A. WHEELER
Department of Physics, Princeton University, Princeton, NJ 08544

Draft version September 20, 2004

ABSTRACT

Shine a flashlight on a black hole, and one is greeted with the return of a series of concentric rings of light. For a point source of light, and for perfect alignment of the lens, source, and observer, the rings are of infinite brightness (in the limit of geometric optics). In this manner, distant black holes can be revealed through their reflection of light from the Sun. Such retro-MACHO events involve photons leaving the Sun, making a π rotation about the black hole, and then returning to be detected at the Earth. Our calculations show that, although the light return is quite small, it may nonetheless be detectable for stellar-mass black holes at the edge of our solar system. For example, all (unobscured) black holes of mass M or greater will be observable to a limiting magnitude $\bar{m}$, at a distance given by: $0.02\,\mathrm{pc} \times \sqrt[3]{10^{(\bar{m}-30)/2.5}\,(M/10\,M_{\odot})^2}$. Discovery of a Retro-MACHO offers a way to *directly* image the presence of a black hole, and would be a stunning confirmation of strong-field general relativity.

Subject headings: gravitational lensing—black hole physics—relativity

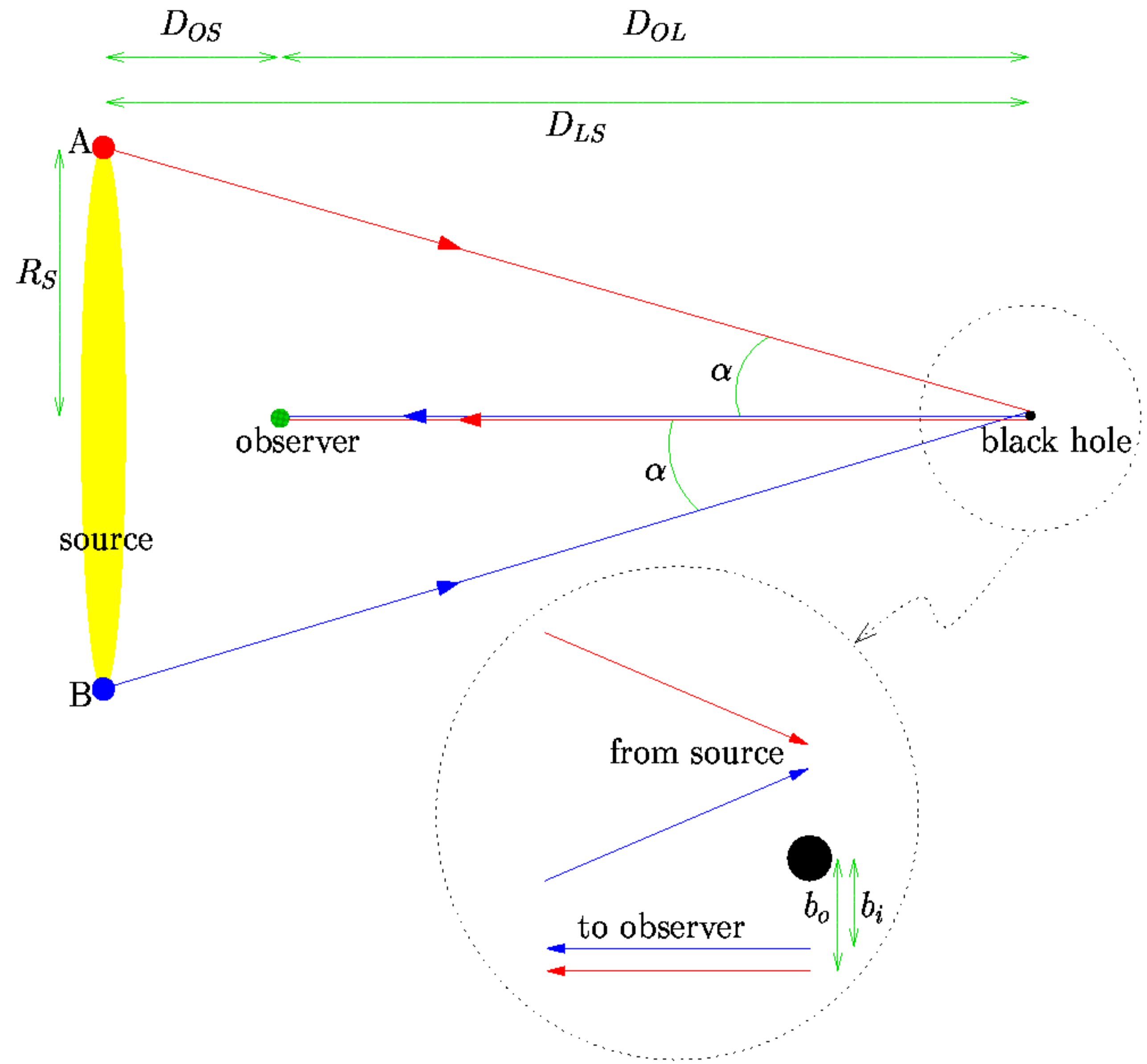

FIG. 1.— Perfect alignment: the (extended) source, observer, and lens are colinear. The resulting image of the source, as lensed by the black hole, is a ring. (The angles in this figure are greatly exaggerated.)

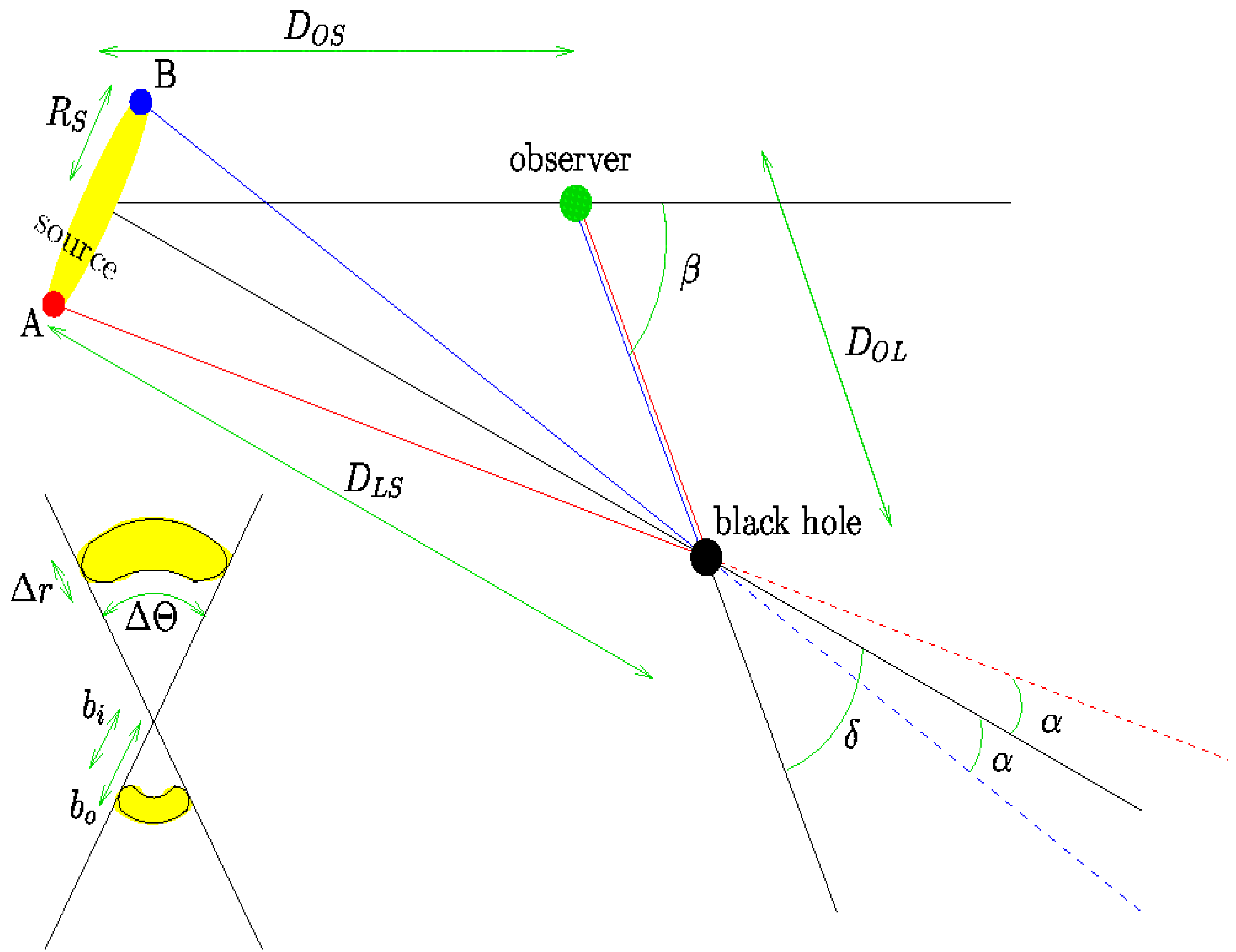

FIG. 2.— Imperfect alignment: the source, observer, and lens are not colinear. Pairs of images are produced, centered on the source–observer–lens plane, on opposite sides of the lens (see inset).

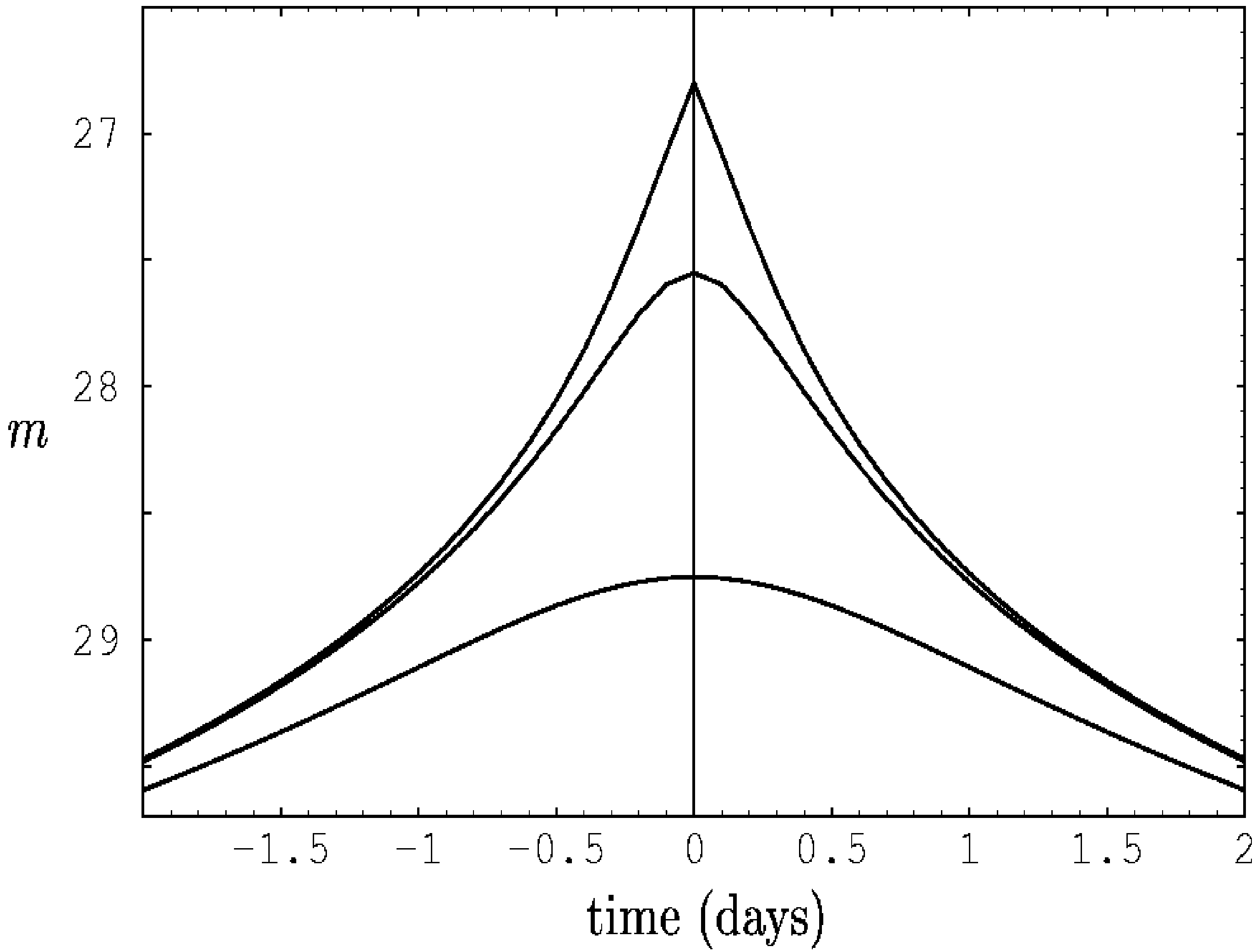

FIG. 3.— Solar retro-MACHO lightcurves: The apparent visual magnitude, m, of the Sun, imaged in a $10\,M_\odot$ black hole at a distance of 0.01 pc. The different curves are for the black hole at angular displacements from the ecliptic plane of 0, $R_\odot/1\,\mathrm{AU}$, and 1° respectively (top to bottom).

TABLE 1

RETRO-MACHO BRIGHTNESSES OF THE SUN

BH mass ($M_\odot$)	BH distance (pc)	$\beta = 0$ (perfect alignment)	$\beta = R_\odot/1\,\mathrm{AU}$ (edge alignment)	$\beta = 1^\circ$	$\beta = \pi/4$	$\beta = \pi/2$ (max misalignment)
1	10^{-2}	31.0	32.6	34	38	38
1	10^{-1}	38.6	40.1	41	45	46
10	10^{-2}	26.1	27.6	29	33	33
10	10^{-1}	33.6	35.1	36	40	41
10	1	41.1	42.6	44	48	48

The full classification of geodesic types for Kerr metric is given by Zakharov (1986). As it was shown in this paper, there are three photon geodesic types: capture, scattering and critical curve which separates the first two sets. This classification fully depends only on two parameters $\xi = L_z/E$ and $\eta = Q/E^2$, which are known as Chandrasekhar's constants (Chandrasekhar 1983). Here the Carter constant Q is given by Carter (1968)

$$Q = p_\theta^2 + \cos^2\theta \left[a^2\left(m^2 - E^2\right) + L_z^2/\sin^2\theta\right], \tag{1}$$

where $E = p_t$ is the particle energy at infinity, $L_z = p_\phi$ is z-component of its angular momentum, $m = p_i p^i$ is the particle mass. Therefore, since photons have $m = 0$

$$\eta = p_\theta^2/E^2 + \cos^2\theta \left[-a^2 + \xi^2/\sin^2\theta\right]. \tag{2}$$

The first integral for the equation of photon motion (isotropic geodesics) for a radial coordinate in the Kerr metric is described by the following equation (Carter 1968; Chandrasekhar 1983; Zakharov 1986, 1991a)

$$\rho^4 (dr/d\lambda)^2 = R(r),$$

where

$$R(r) = r^4 + (a^2 - \xi^2 - \eta) r^2 + 2[\eta + (\xi - a)^2] r - a^2 \eta, \tag{3}$$

and $\rho^2 = r^2 + a^2\cos^2\theta, \Delta = r^2 - 2r + a^2, a = S/M^2$. The constants M and S are the black hole mass and angular momentum, respectively. Eq. (3) is written in dimensionless variables (all lengths are expressed in black hole mass units M).

If we fix a black hole spin parameter a and consider a plane (ξ, η) and different types of photon trajectories corresponding to (ξ, η), namely, a capture region, a scatter region and the critical curve $\eta_{\rm crit}(\xi)$ separating the scatter and capture regions. The critical curve is a set of (ξ, η) where the polynomial $R(r)$ has a multiple root (a double root for this case). Thus, the critical curve $\eta_{\rm crit}(\xi)$ could be determined from the system (Zakharov 1986, 1991a)

$$\begin{aligned} R(r) &= 0, \\ \frac{\partial R}{\partial r}(r) &= 0, \end{aligned} \tag{4}$$

for $\eta \geq 0, r \geq r_+ = 1 + \sqrt{1-a^2}$, because by analysing of trajectories along the θ coordinate we know that for $\eta < 0$ we have $M = \{(\xi, \eta) | \eta \geq -a^2 + 2a|\xi| - \xi^2, -a \leq \xi \leq a\}$ and for each point $(\xi, \eta) \in M$ photons will be captured. If instead $\eta < 0$ and $(\xi, \eta) \bar{\in} M$, photons cannot have such constants of motion, corresponding to the forbidden region (see, (Chandrasekhar 1983; Zakharov 1986) for details).

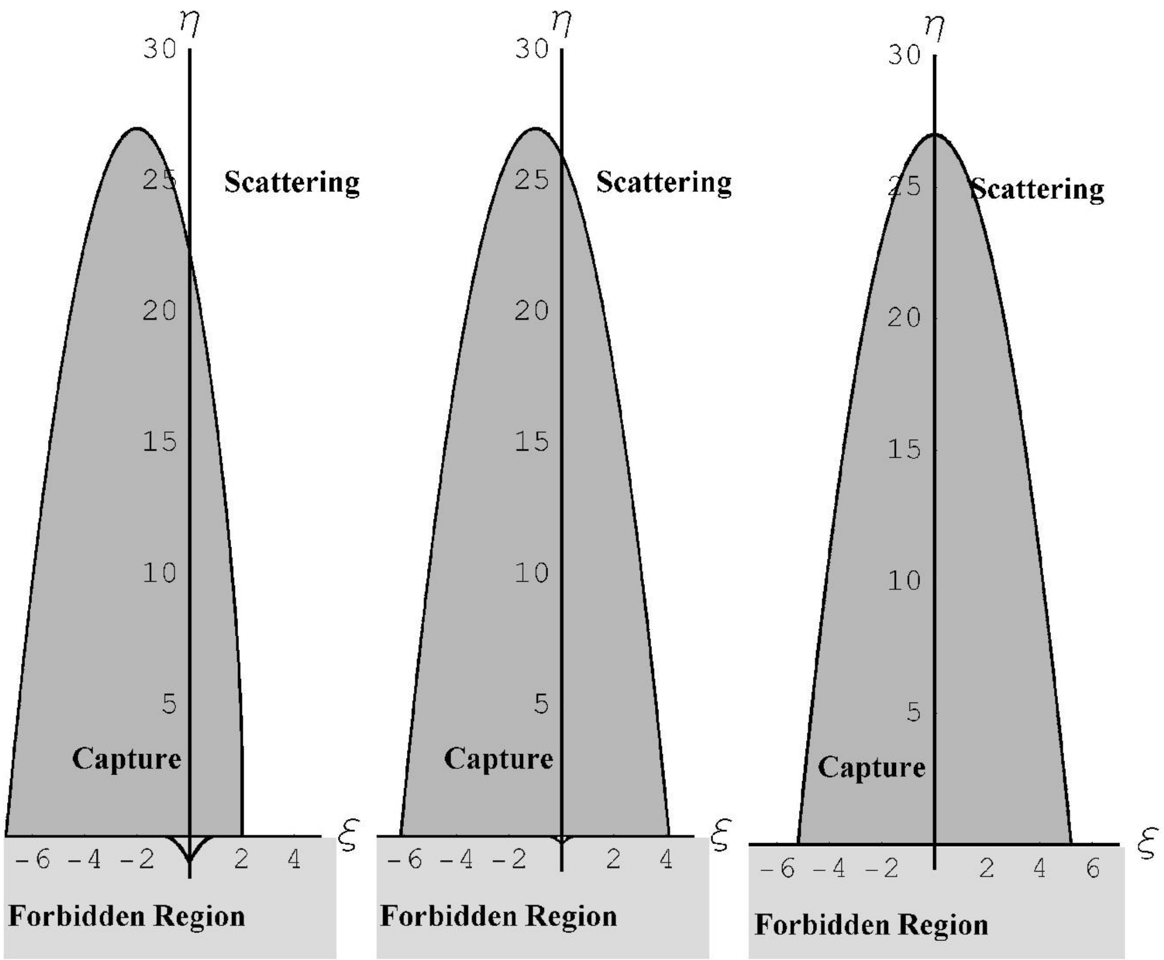

Fig. 1. Different types for photon trajectories and spin parameters ($a = 1., a = 0.5, a = 0.$). Critical curves separate capture and scatter regions. Here we show also the forbidden region corresponding to constants of motion $\eta < 0$ and $(\xi, \eta) \bar{\in} M$ as it was discussed in the text.

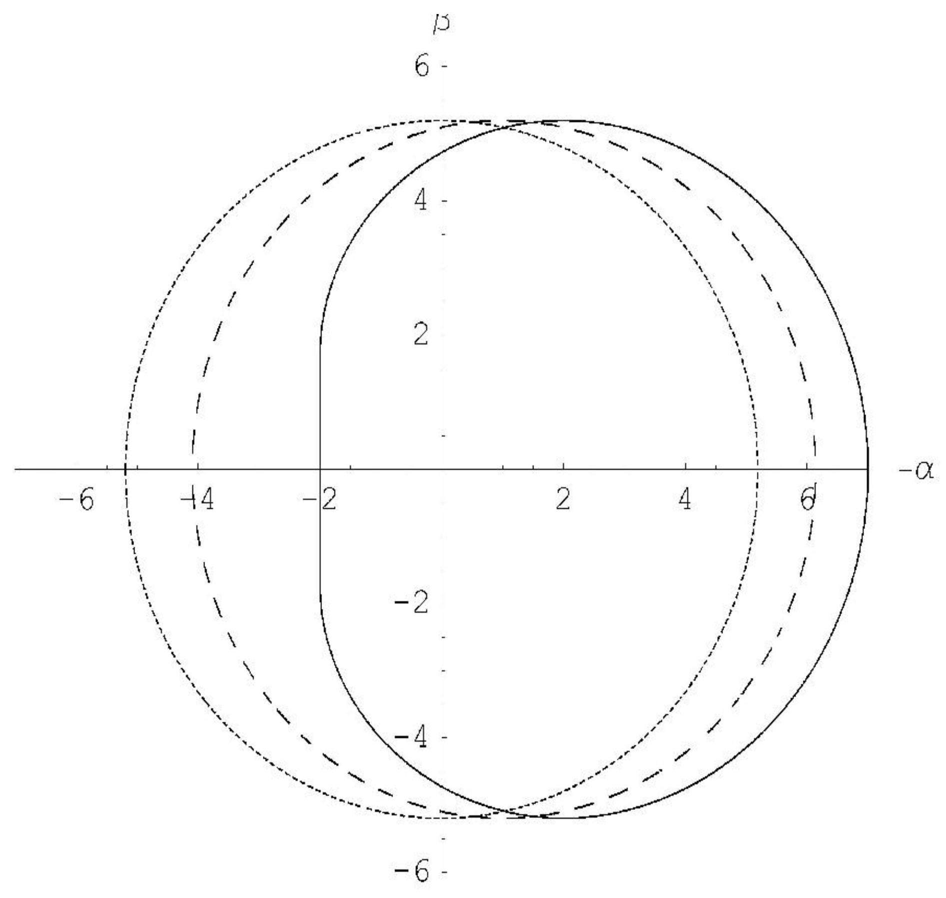

Fig. 2. Mirages around black hole for equatorial position of distant observer and different spin parameters. The solid line, the dashed line and the dotted line correspond to $a = 1, a = 0.5, a = 0$ correspondingly

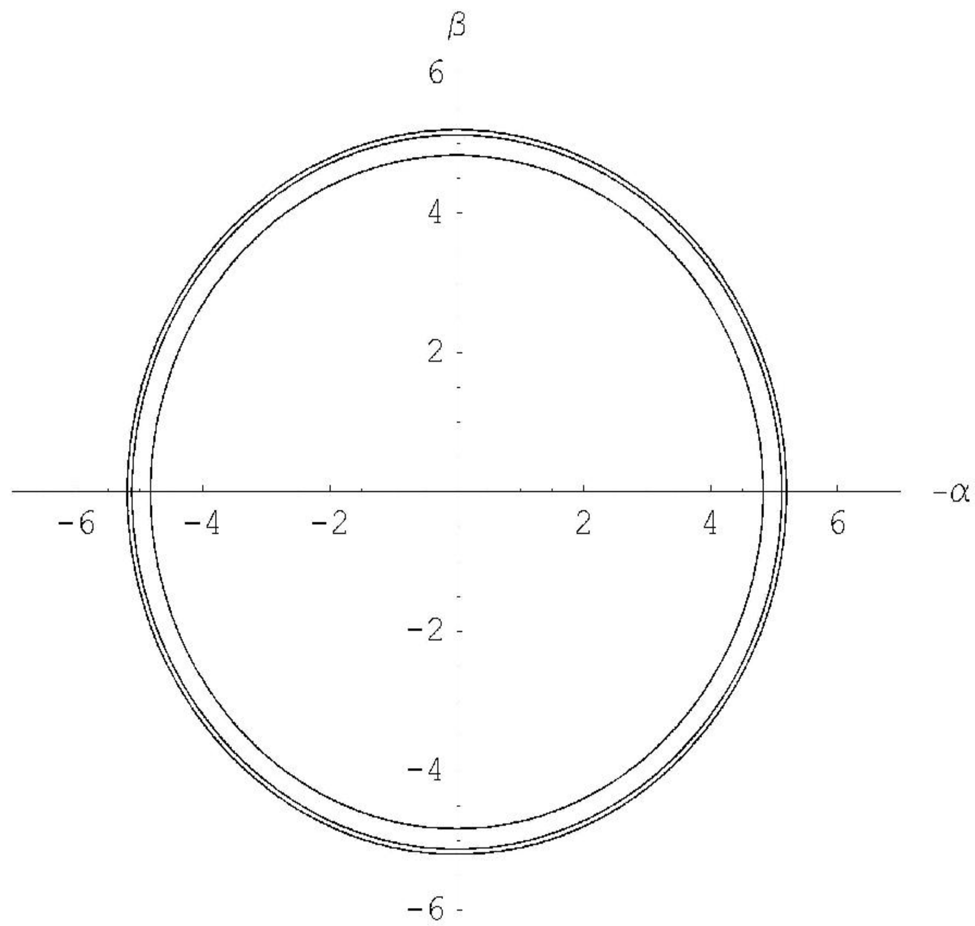

Fig. 3. Mirages around a black hole for the polar axis position of distant observer and different spin parameters ($a = 0, a = 0.5, a = 1$). Smaller radii correspond to greater spin parameters.

Table 1. Dependence of $\eta(0)$ and mirage radii $R_{\rm circ} = (\eta(0) + a^2)^{1/2}$ on spins.

a	0	0.2	0.4	0.5	0.6	0.8	1.
$\eta(0)$	27	26.839	26.348	25.970	25.495	24.210	22.314
$R_{\rm circ}$	5.196	5.185	5.14 9	5.121	5.085	4.985	4.828

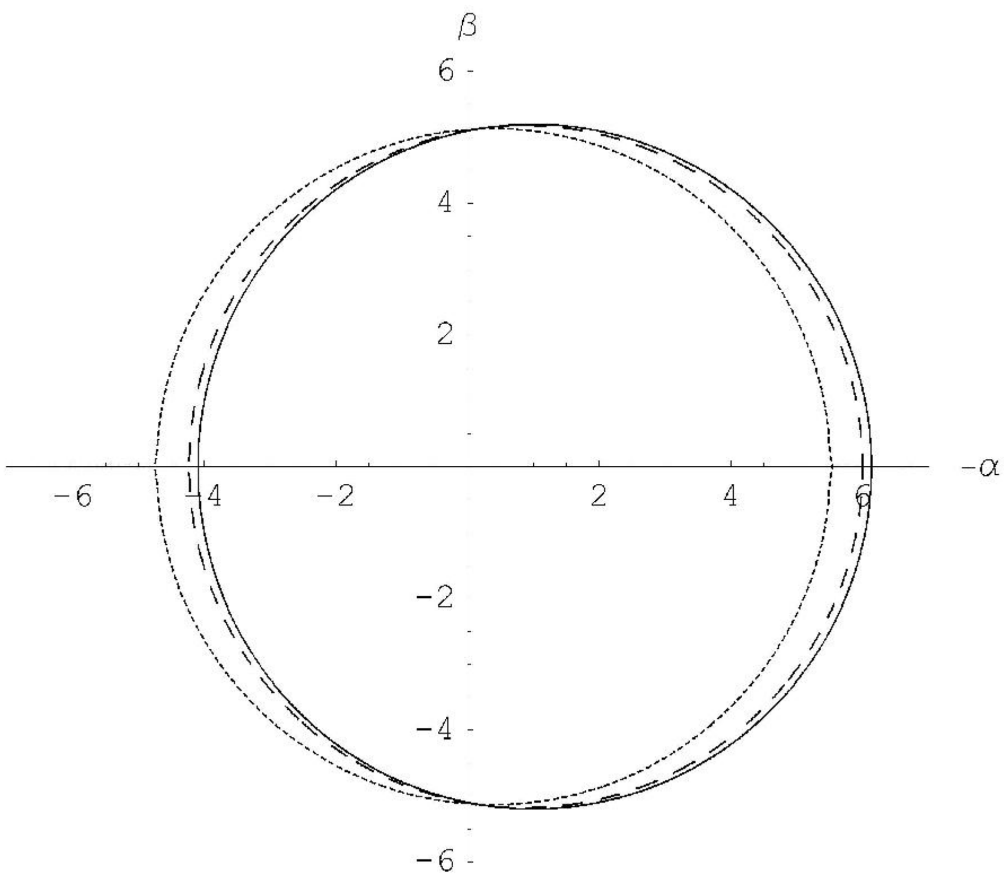

Fig. 4. Mirages around black hole for different angular positions of a distant observer and the spin $a = 0.5$. Solid, dashed and dotted lines correspond to $\theta_0 = \pi/2, \pi/3$ and $\pi/8$, respectively.

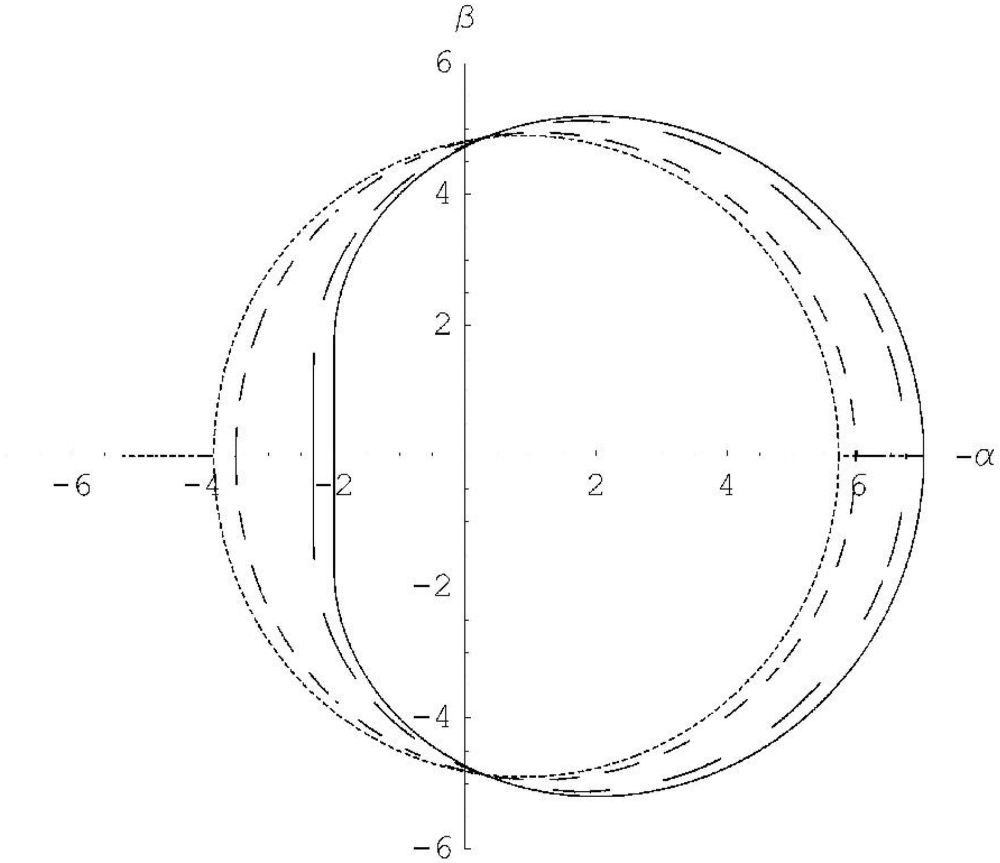

Fig. 5. Mirages around black hole for different angular positions of a distant observer and the spin $a = 1$. Solid, long dashed, short dashed and dotted lines correspond to $\theta_0 = \pi/2, \pi/3, \pi/6$ and $\pi/8$, respectively.

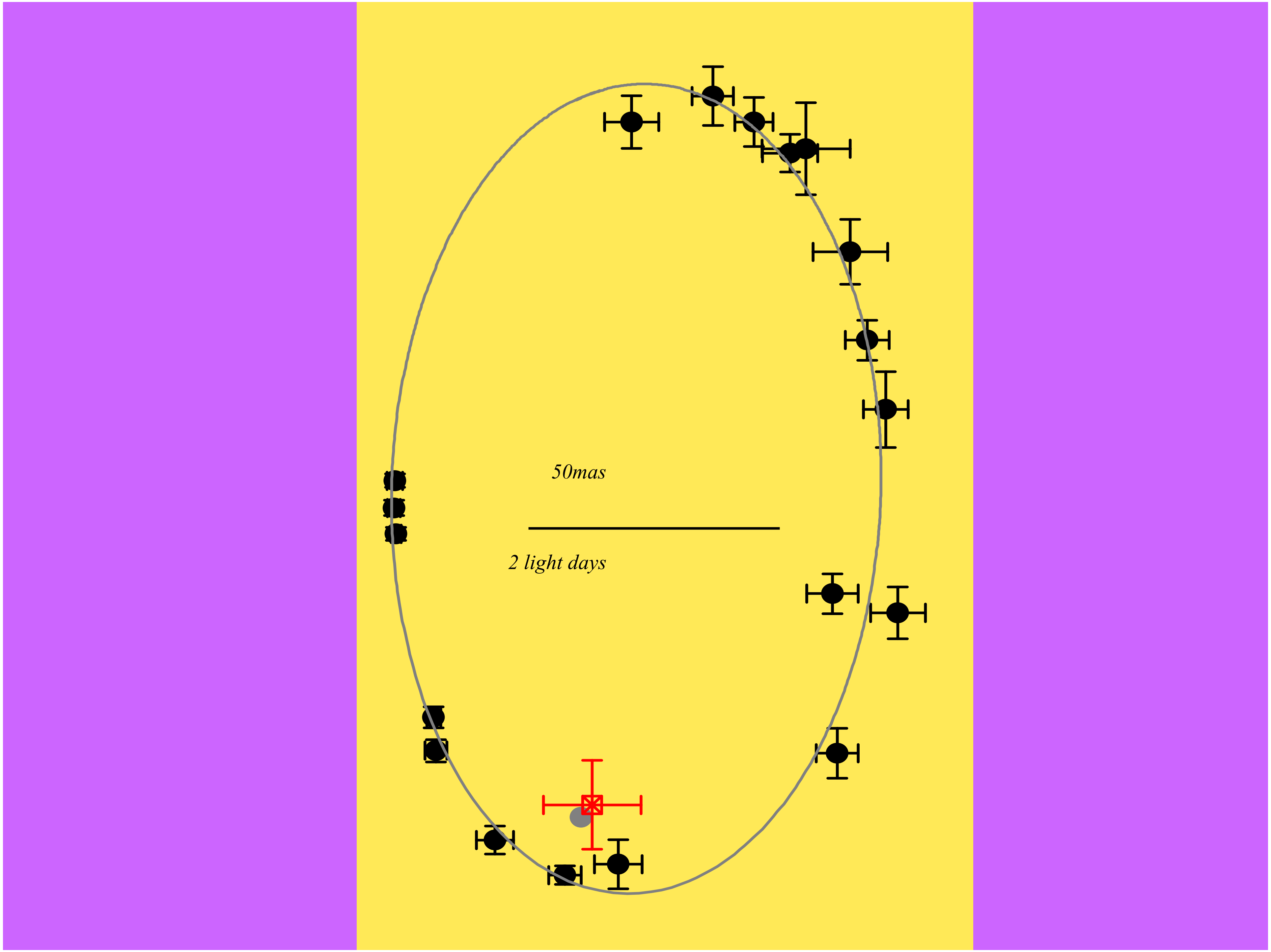
50mas
2 light days

Similarly to Falcke, Melia & Agol (2000) we propose to use VLBI technique to observe the discussed mirages around black holes. They used ray-tracing calculations to evaluate the shapes of shadows. The boundaries of the shadows are black hole mirages (glories or "faces") analyzed earlier. We use the length parameter $r_g = \frac{GM}{c^2} = 6 \times 10^{11}$ cm to calculate all values in these units as it was explained in the text. If we take into account the distance towards the Galactic Center $D_{\rm GC} = 8$ kpc then the length r_g corresponds to angular sizes $\sim 5\mu$as. Since the minimum arc size for the considered mirages are about $2r_g$, the standard RADIOASTRON resolution of about 8 μas is comparable with the required precision. The resolution in the case of the higher orbit and shortest wavelength is $\sim 1\mu$as (Table 2) good enough to reconstruct the shapes. Therefore, in principle it will be possible to evaluate a and θ parameters after mirage shape reconstructions from observational data even if we will observe only the bright part of the image (the bright arc) corresponding to positive parameters α. However, Gammie, Shapiro & McKinney (2004)

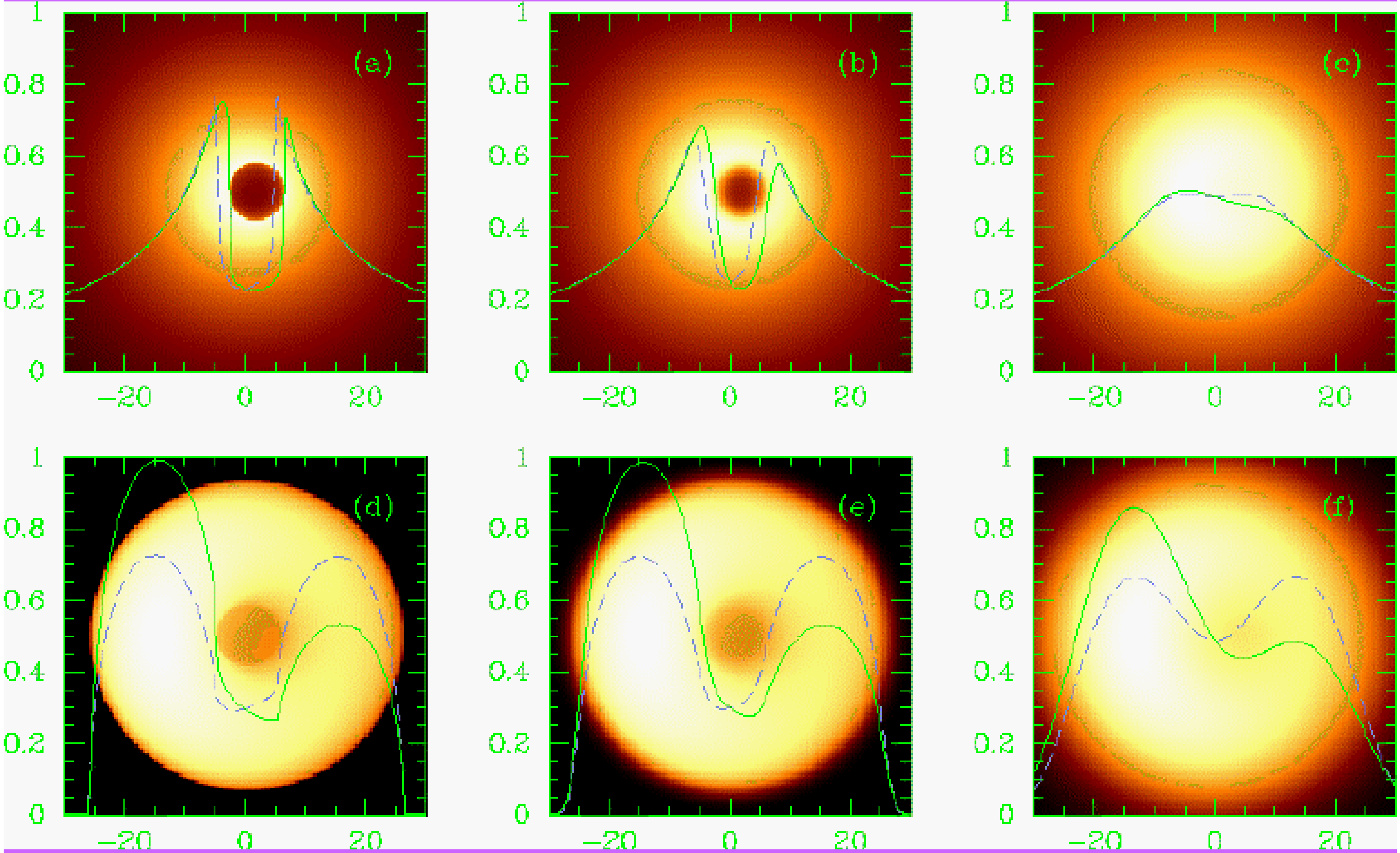
(a)
(b)
(c)
(d)
(e)
(f)
0
0.2
0.4
0.6
0.8
1
−20
0
20

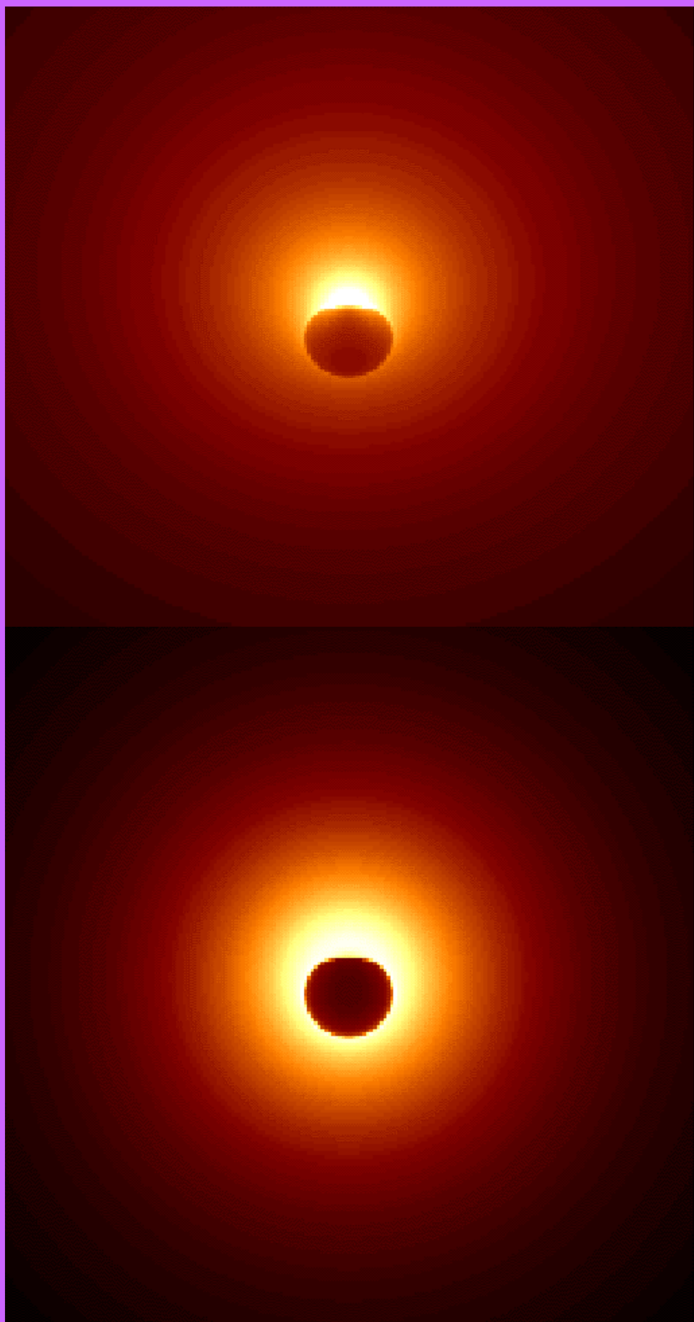

Table 2. The fringe sizes (in micro arc seconds) for the standard and advanced apogees B_{max} (350 000 and 3 200 000 km correspondingly).

B_{max}(km)\\λ(cm)	92	18	6.2	1.35
3.5×10^5	540	106	37	8
3.2×10^6	59	12	4	0.9

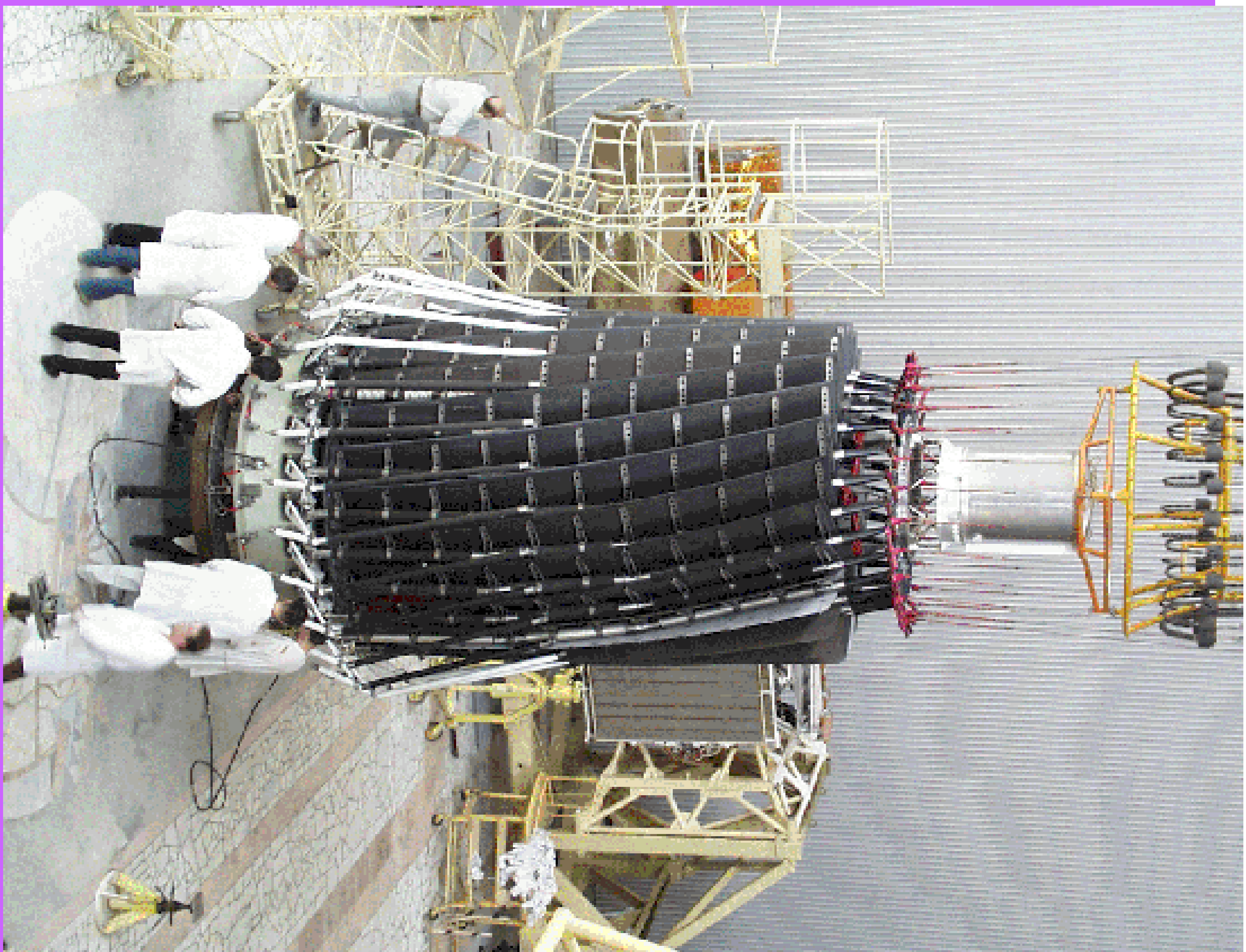

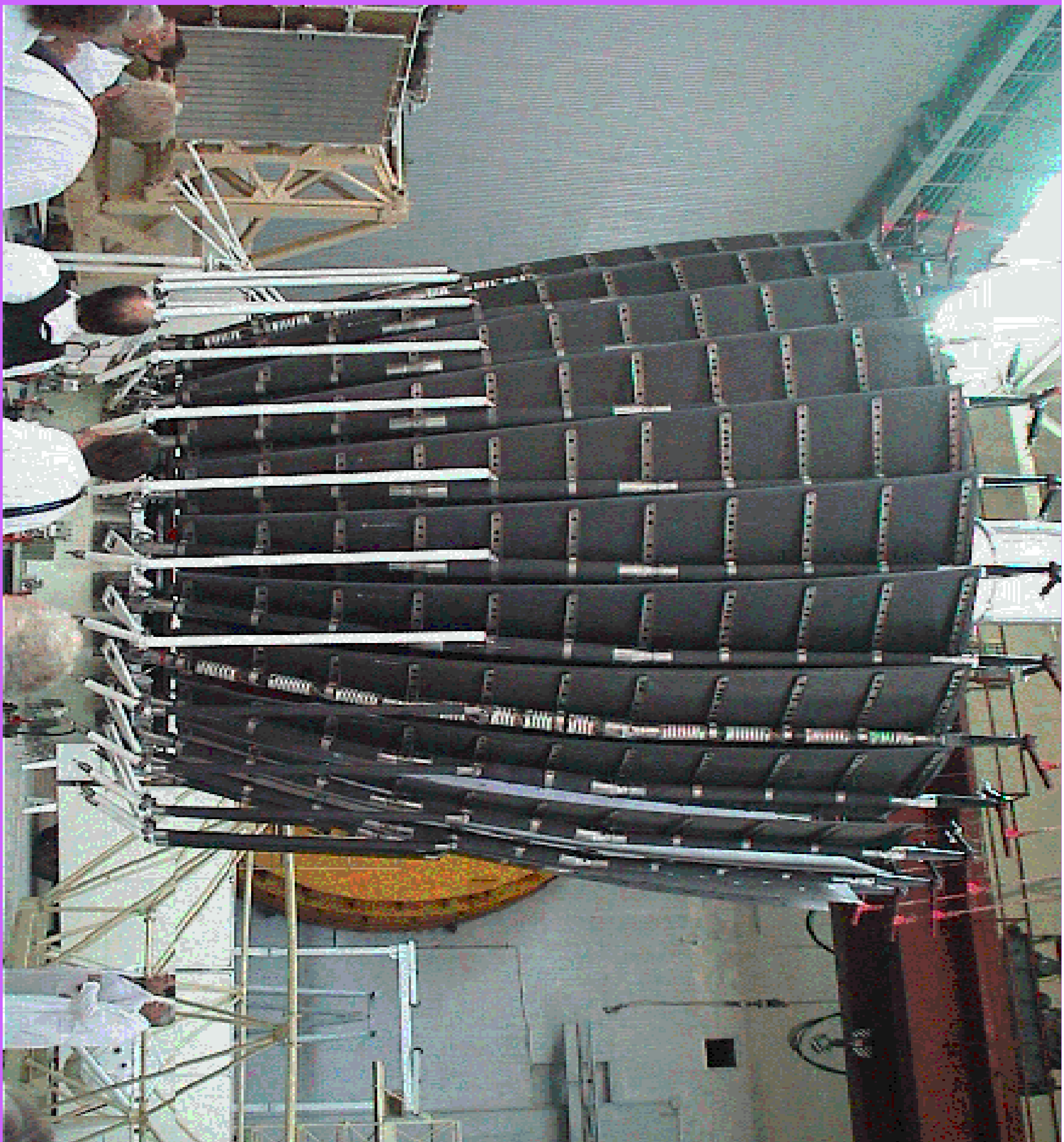

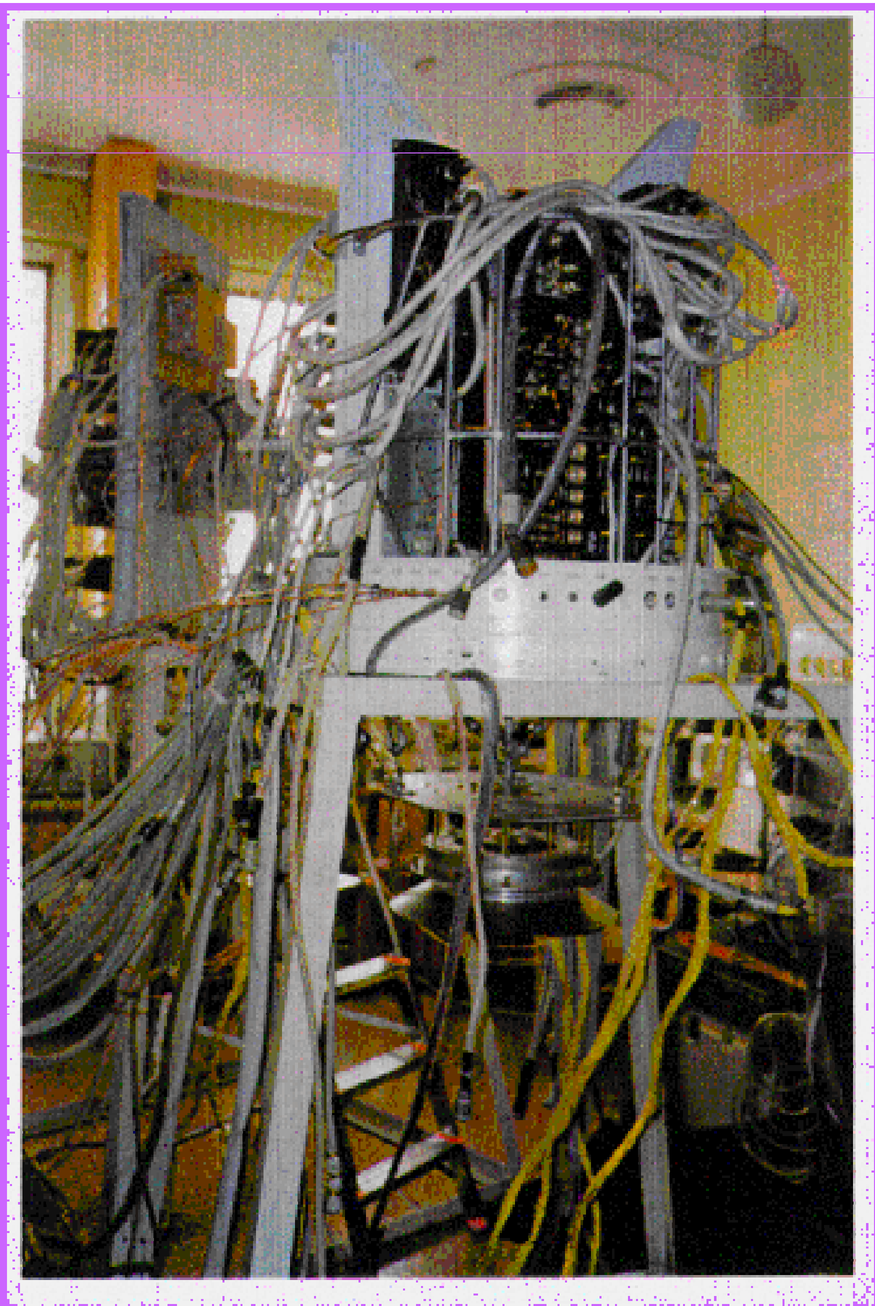

SRT electronics - under testing in ASC

Schwarzschild black hole images (with P. Jovanovic, L. Popovic in preparation)

θ=15 deg

- Redshift map

Intensity map

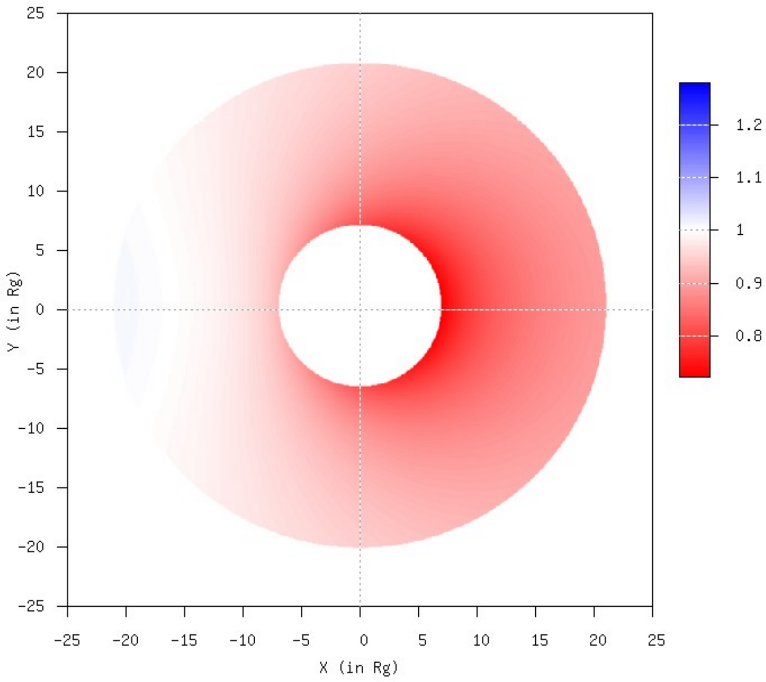

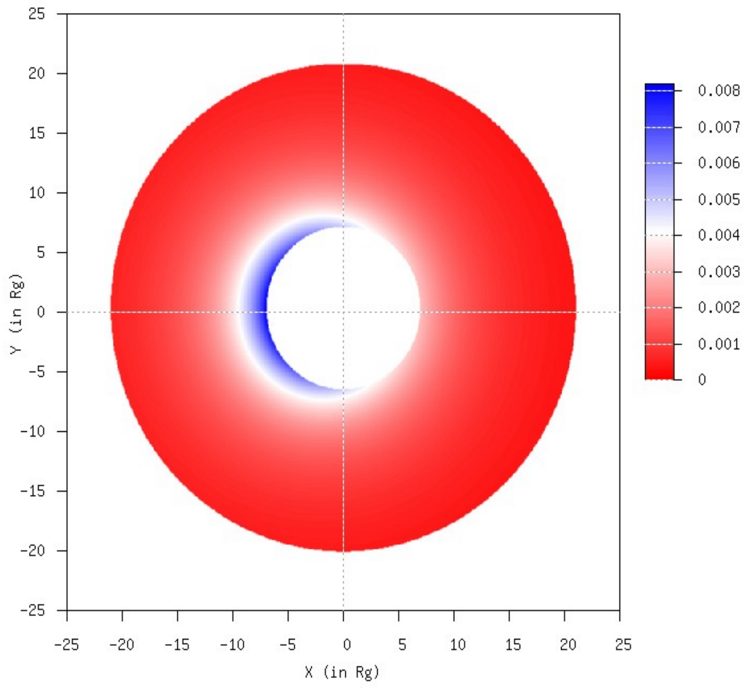

Schwarzschild black hole images

θ=30 deg

- Redshift map

Intensity map

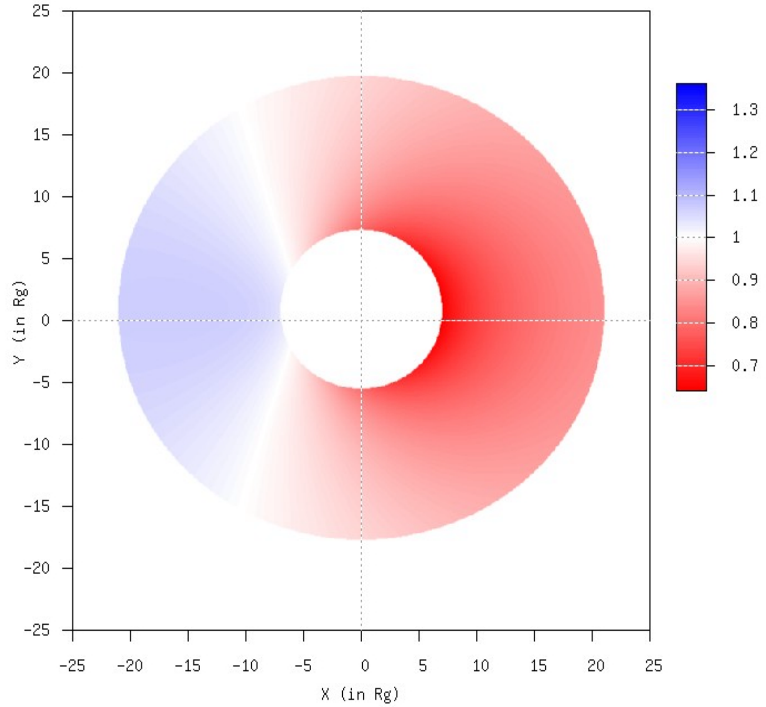

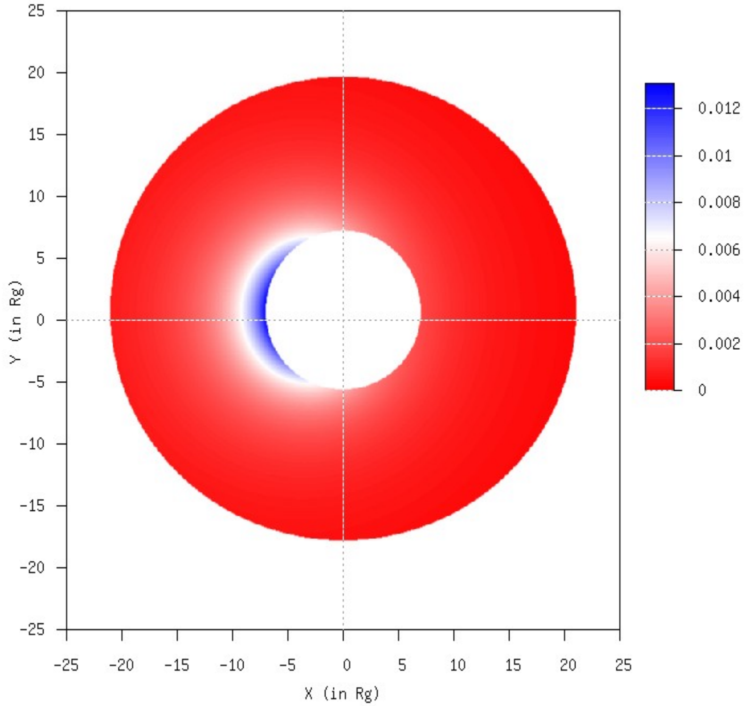

Schwarzschild black hole images: **θ=45 deg**

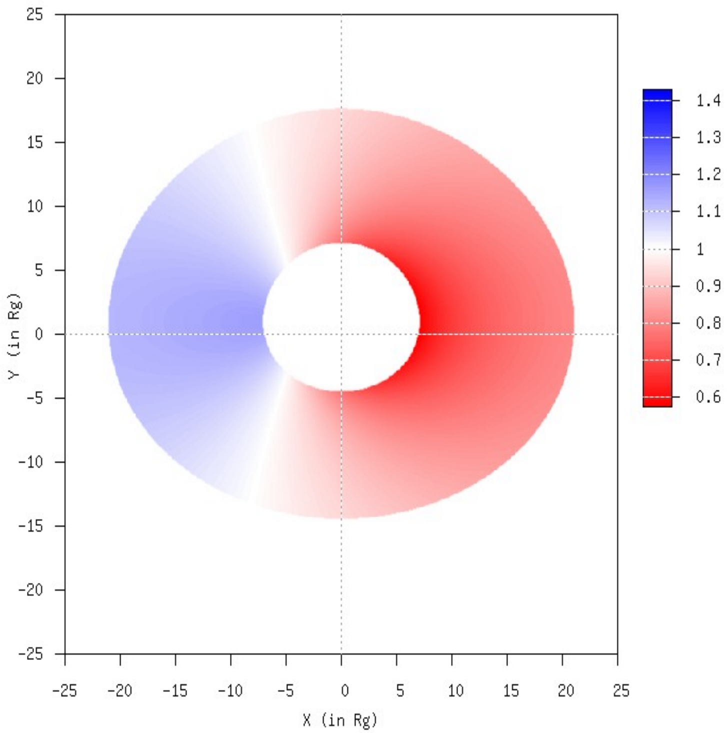

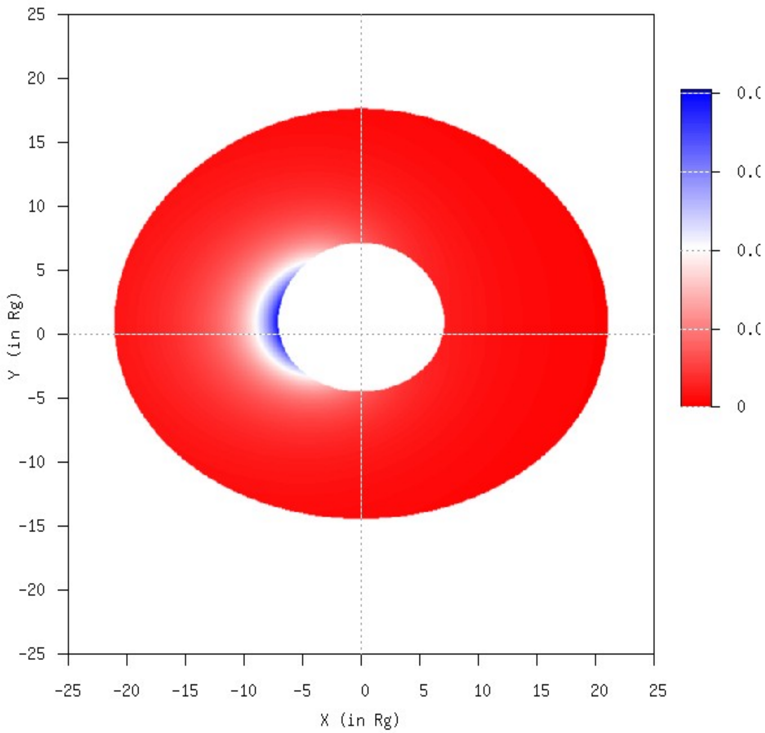

Schwarzschild black hole images: **θ=60 deg**

- Redshift map
- Intensity map

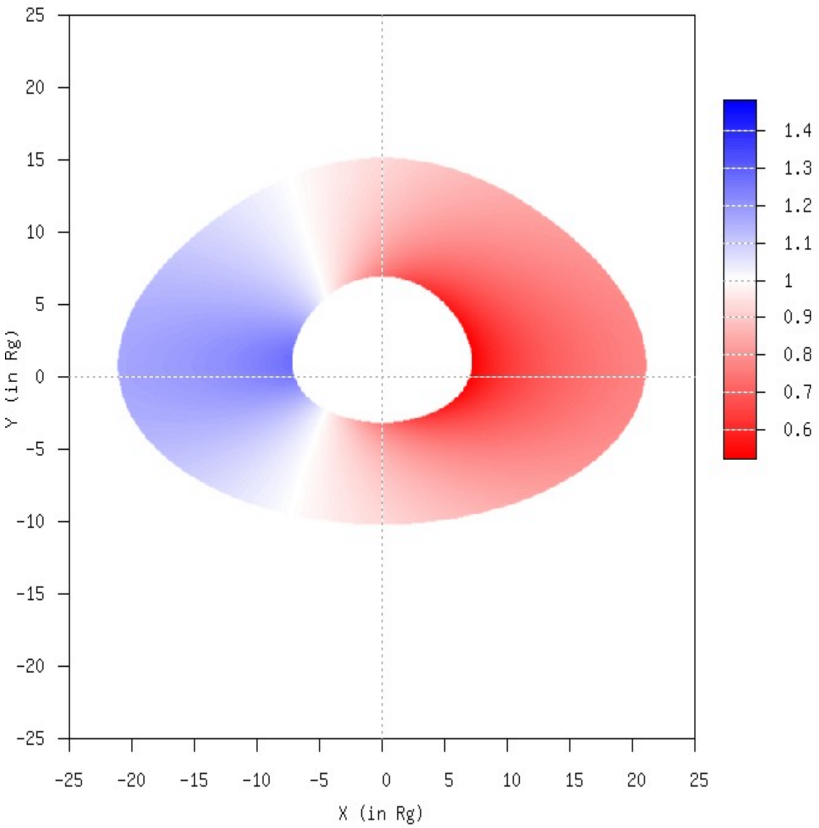

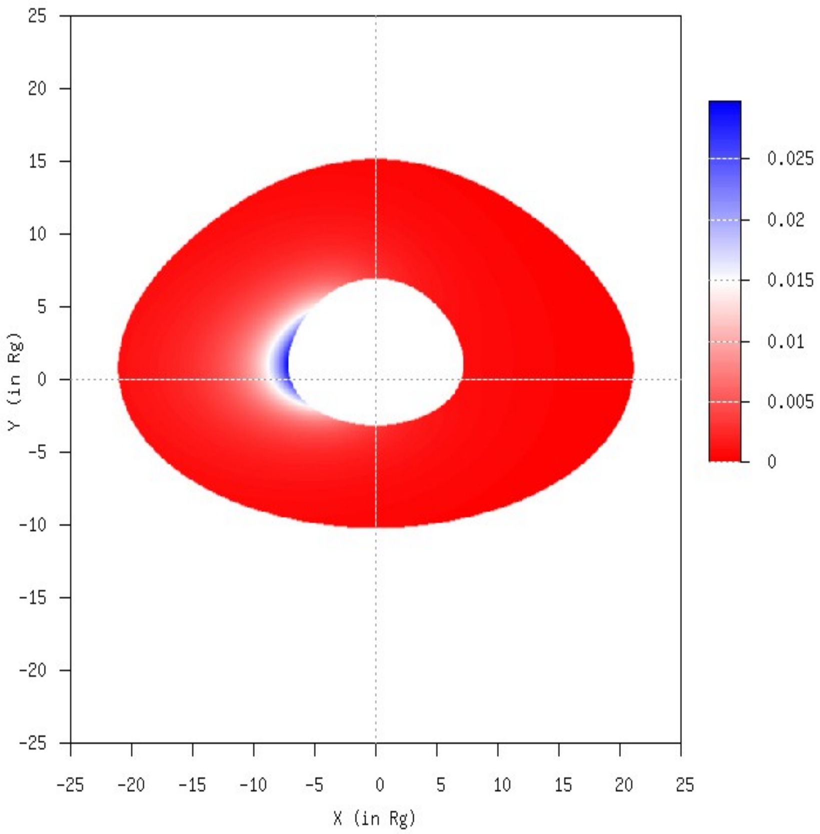

Schwarzschild black hole images: **θ=75 deg**

- Redshift map
- Intensity map

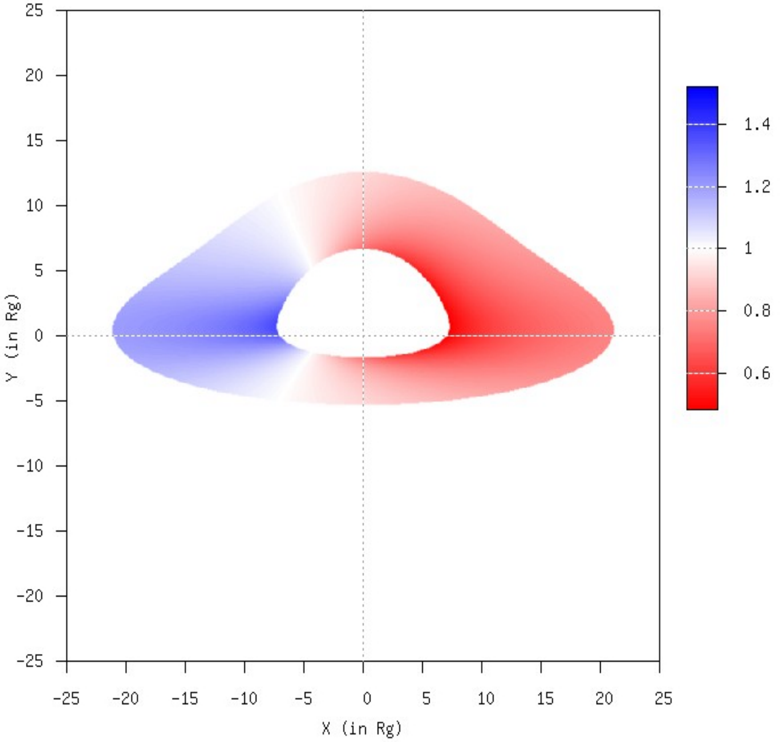

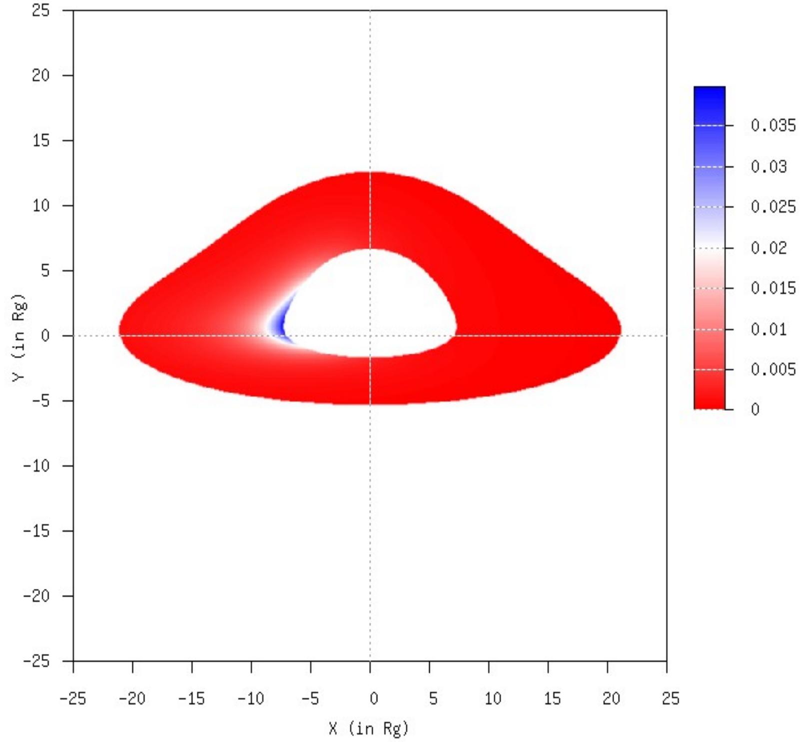

Schwarzschild black hole images: **θ=85 deg**

- Redshift map
- Intensity map

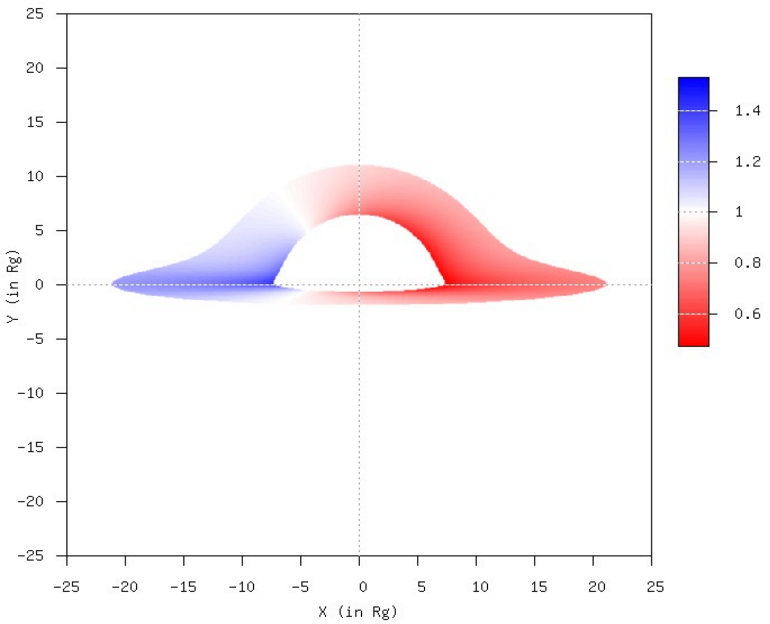

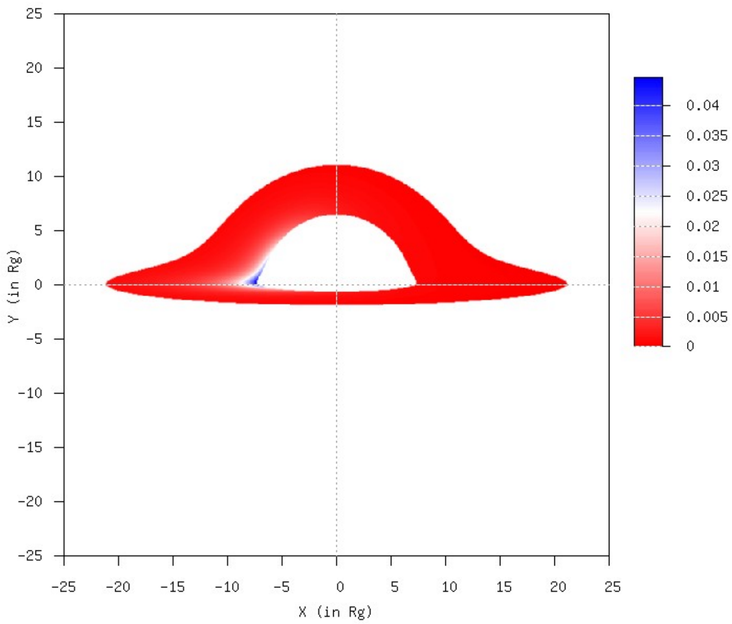

Schwarzschild black hole images: **θ=89 deg**

- Redshift map

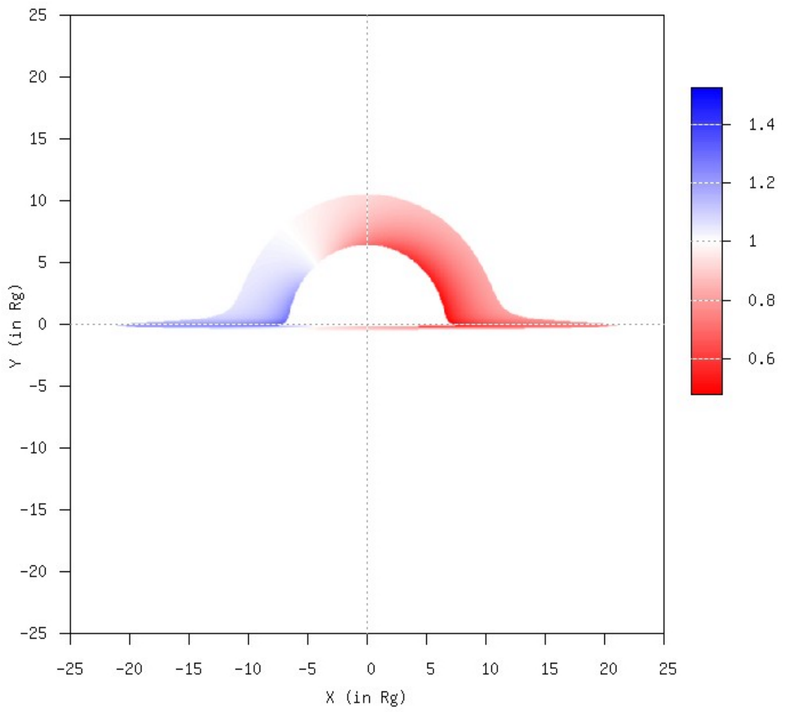

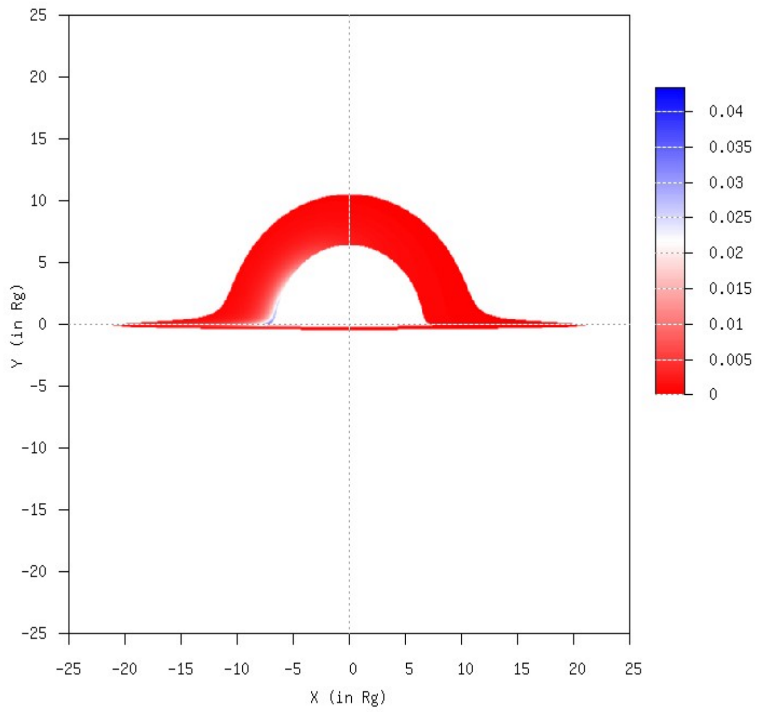

Kerr black hole images (a=0.5): **θ=15 deg**

- Redshift map
- Intensity map

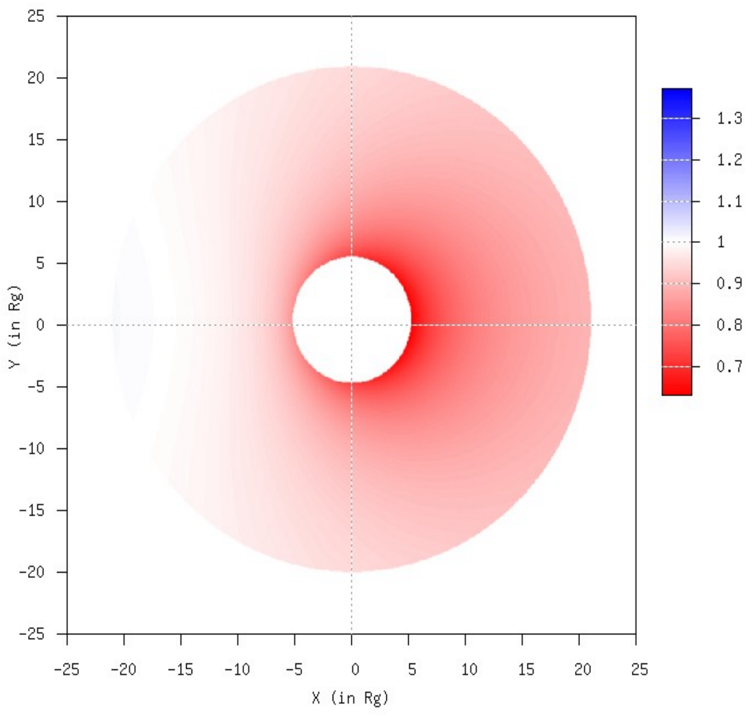

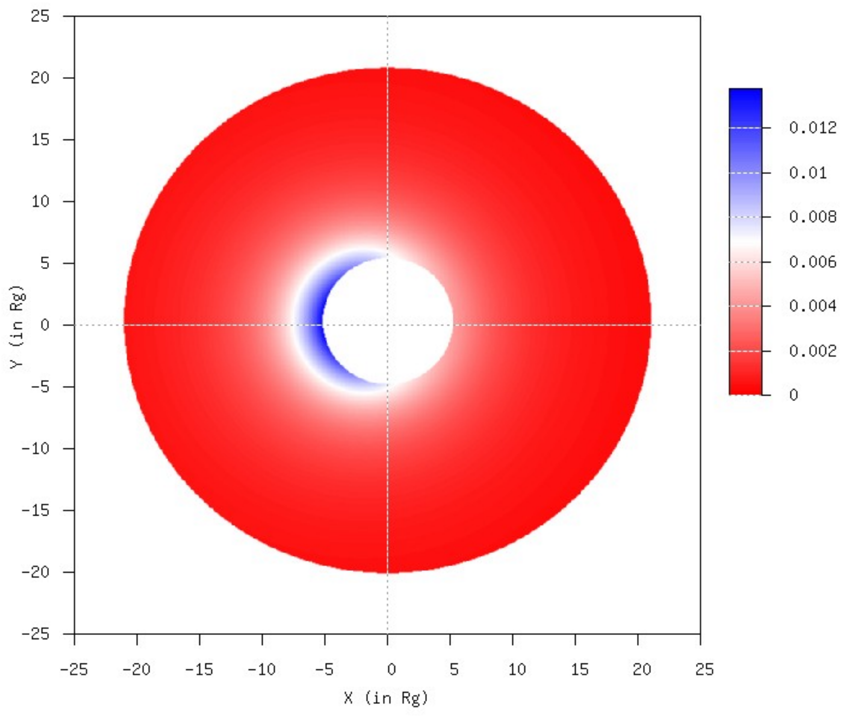

Kerr black hole images (*a*=0.5): **θ=30 deg**

- Redshift map
- Intensity map

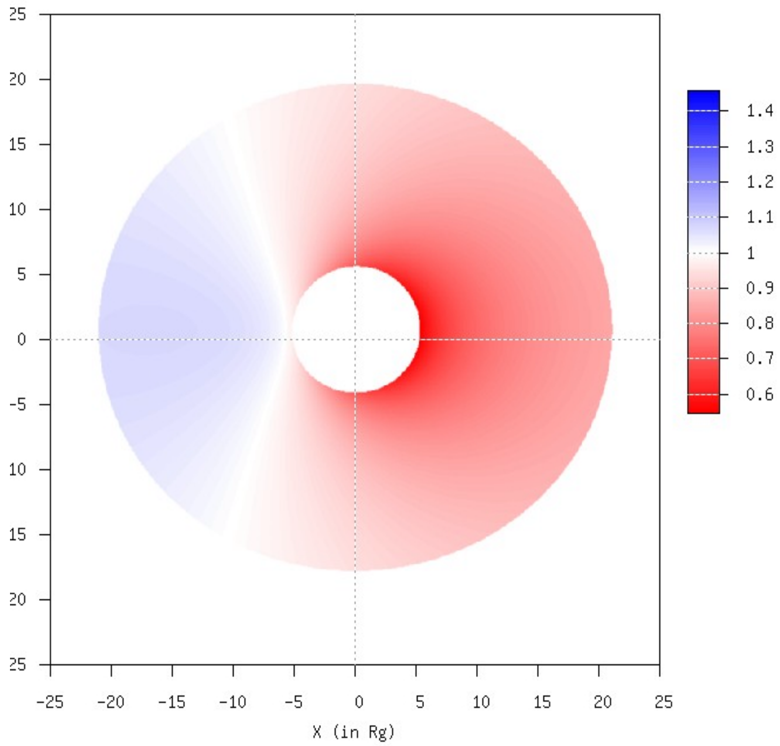

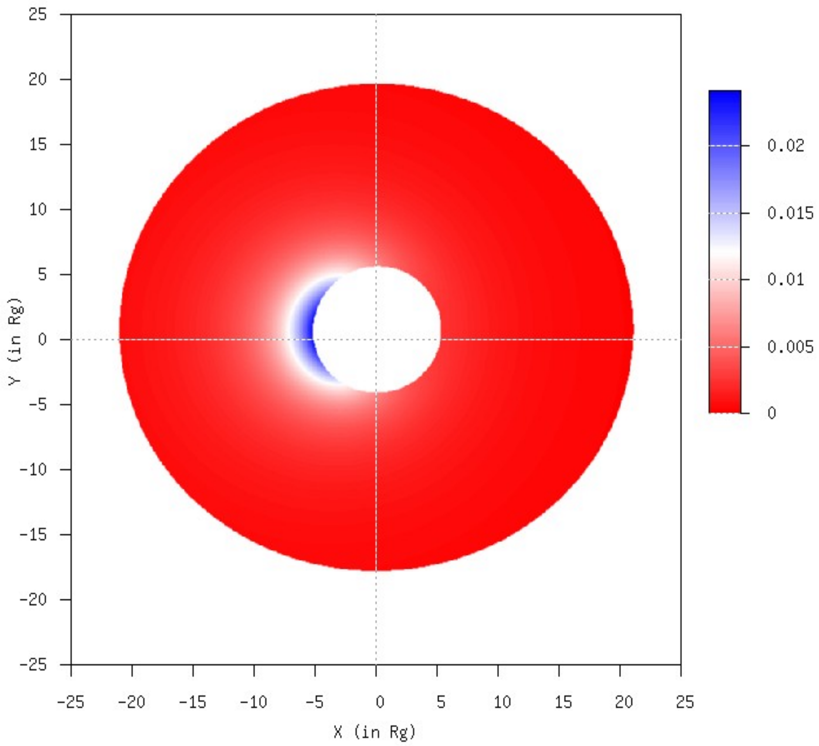

Kerr black hole images (a=0.5): **θ=45 deg**

- Redshift map
- Intensity map

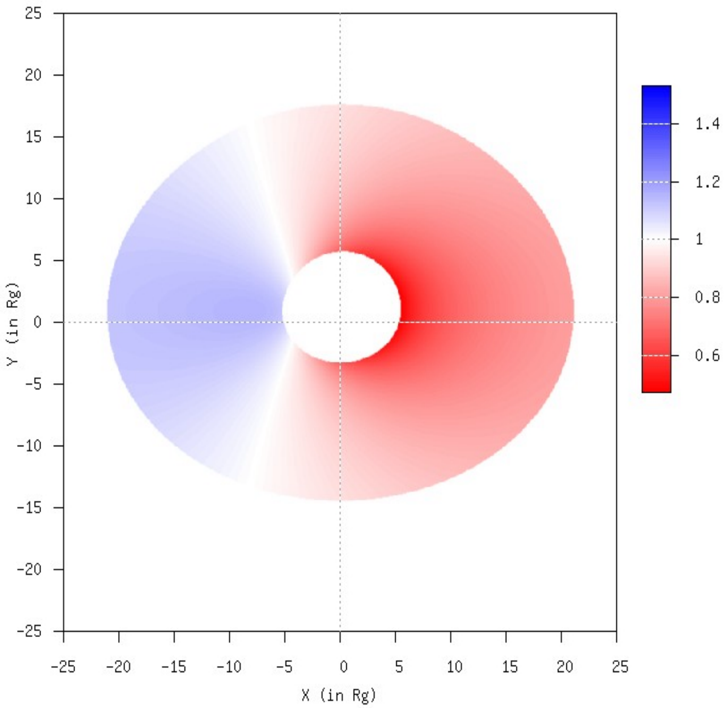

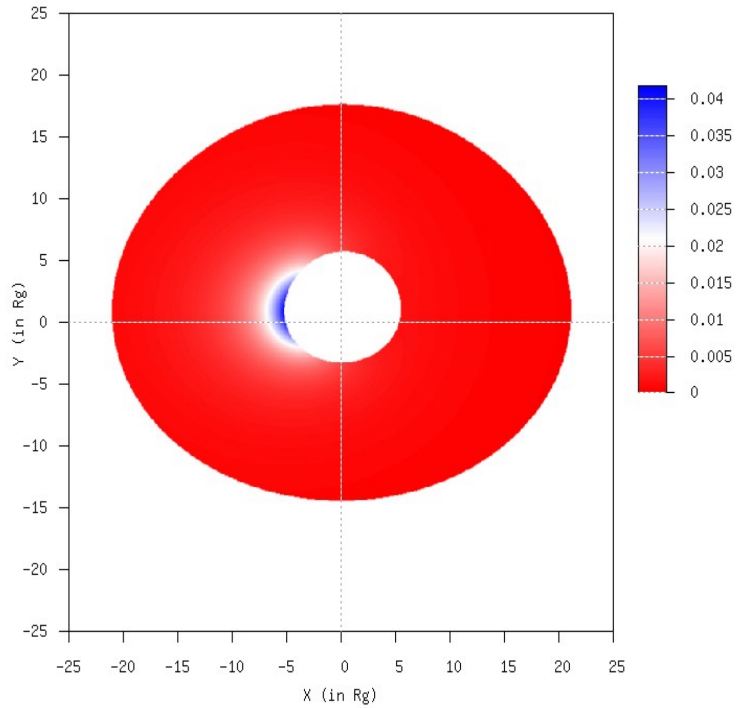

Kerr black hole images (a=0.5): θ=60 deg

- Redshift map
- Intensity map

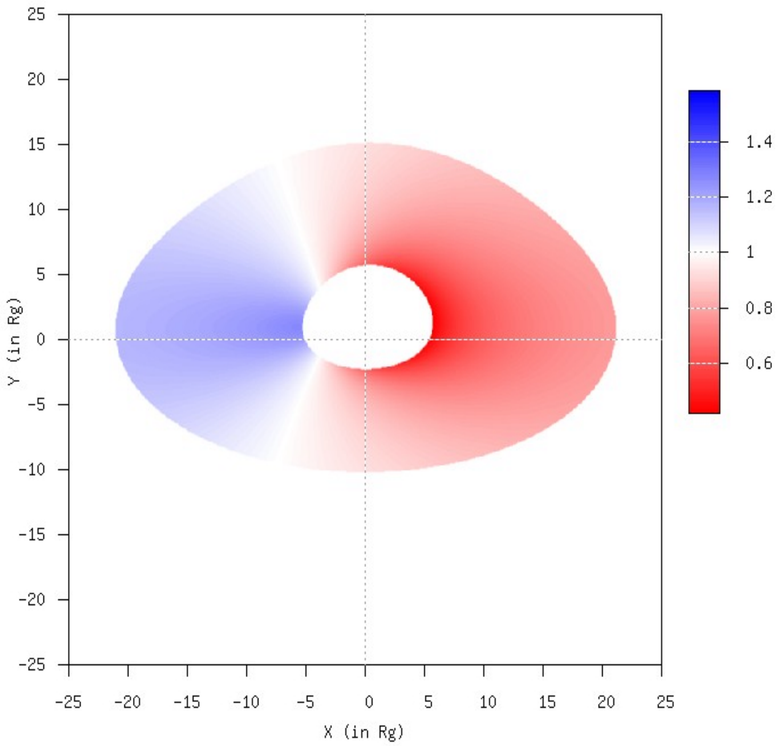

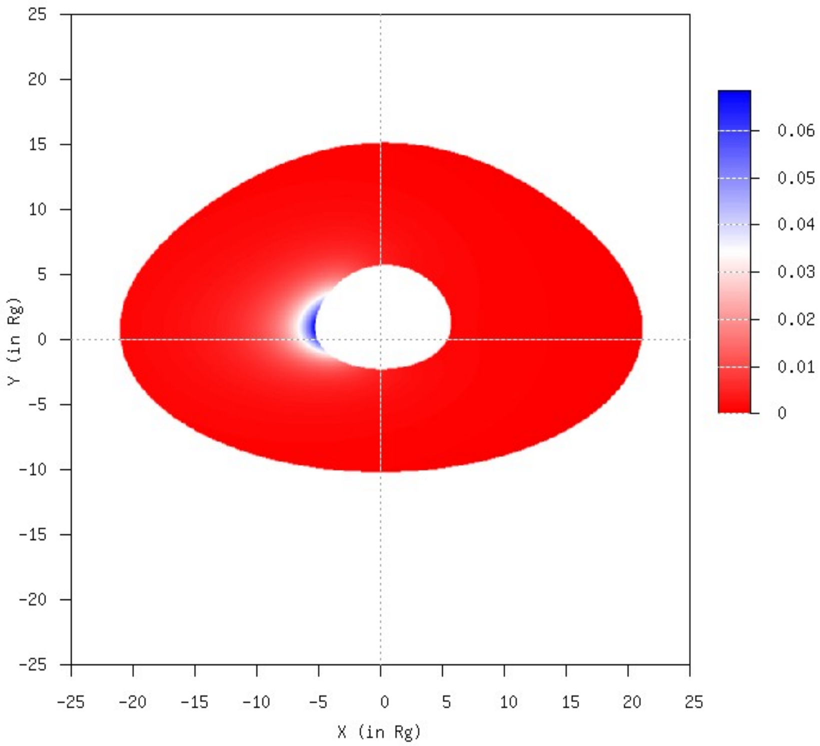

Kerr black hole images (a=0.5): **θ=75 deg**

- Redshift map
- Intensity map

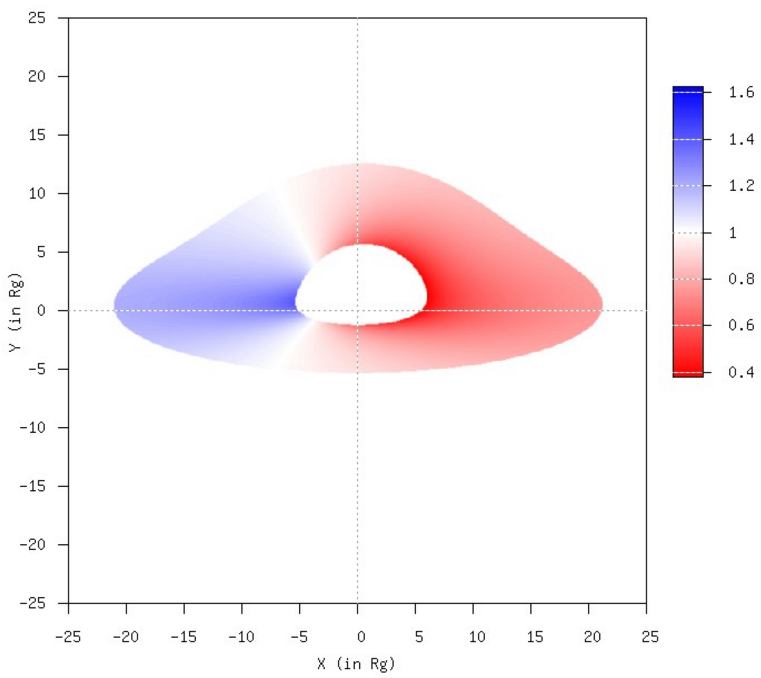

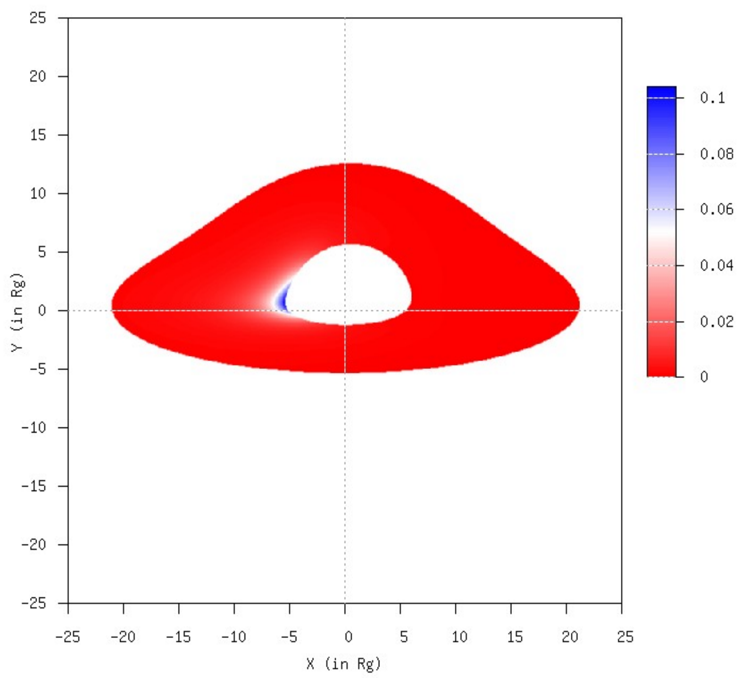

Kerr black hole images (a=0.5): **θ=85 deg**

- Redshift map
- Intensity map

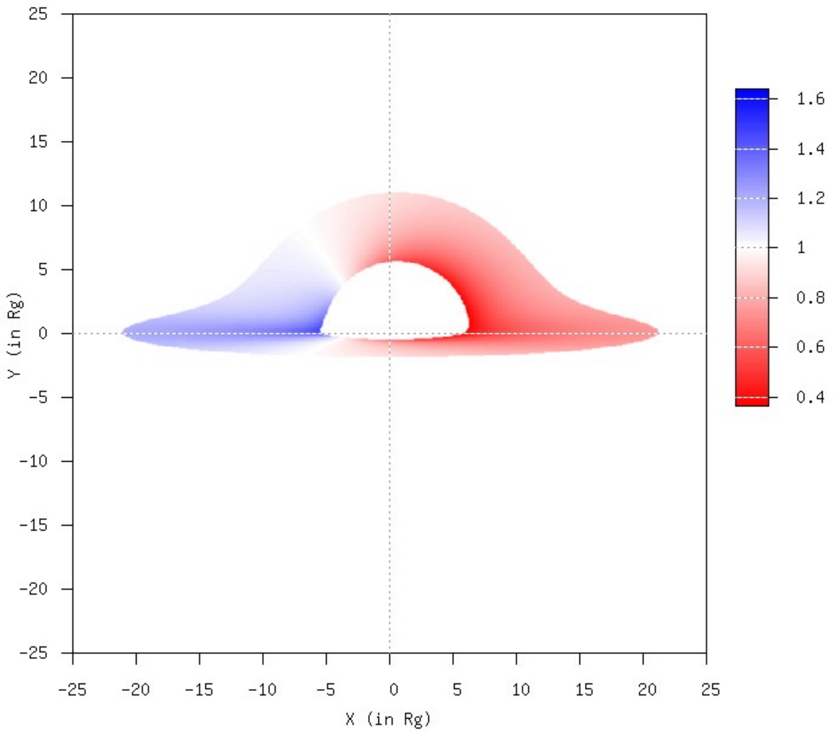

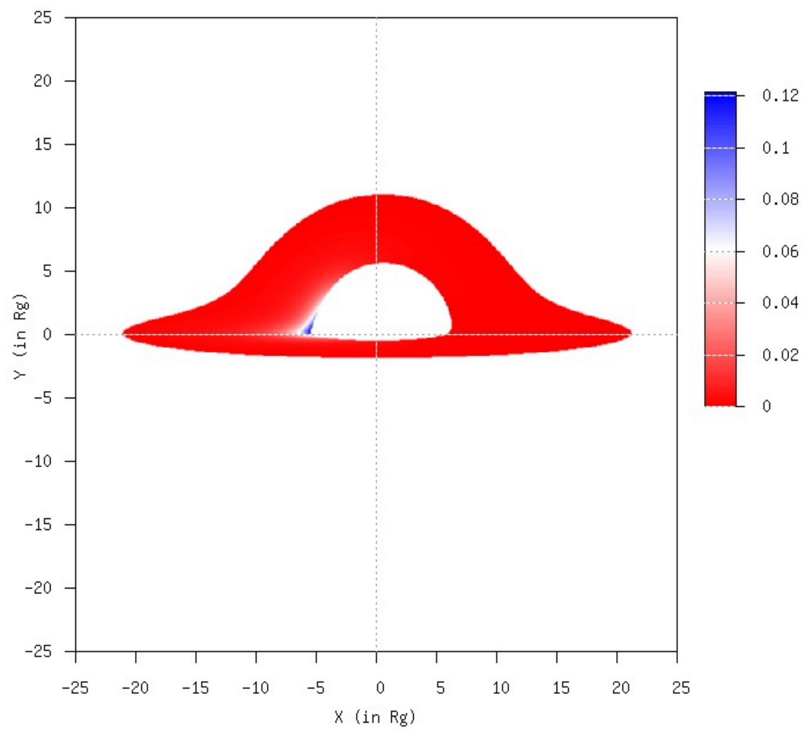

Kerr black hole images (a=0.5): **θ=89 deg**

- Redshift map
- Intensity map

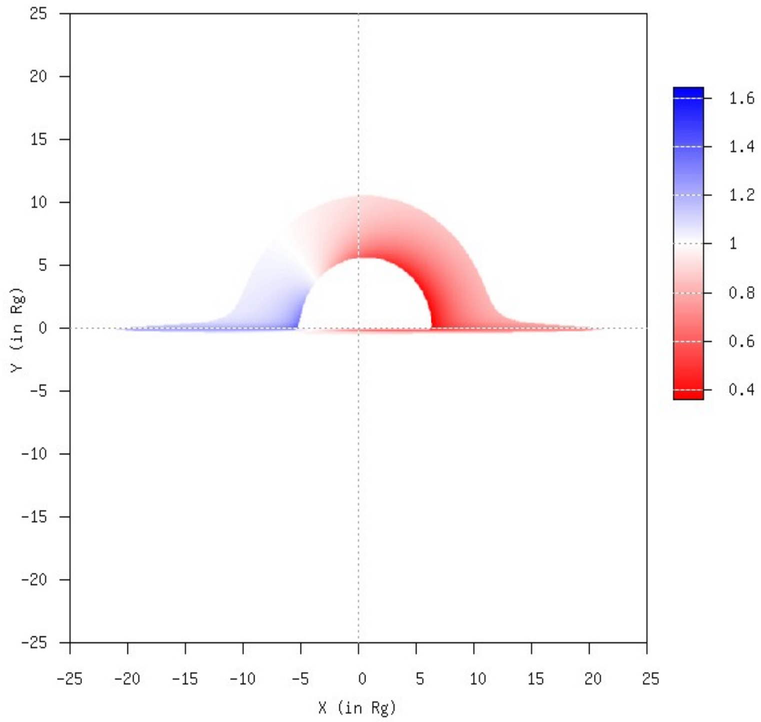

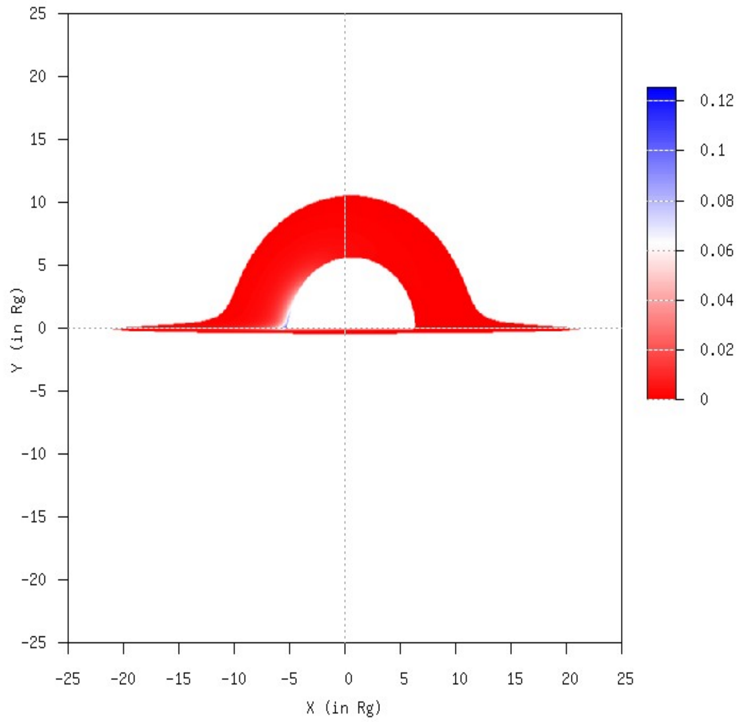

Kerr black hole images (a=0.75): **θ=15 deg**

- Redshift map
- Intensity map

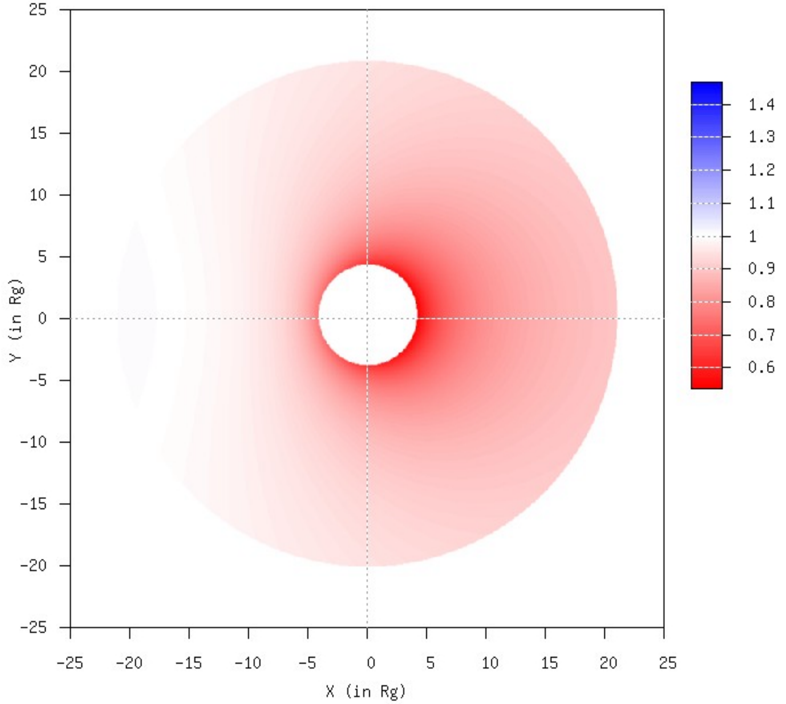

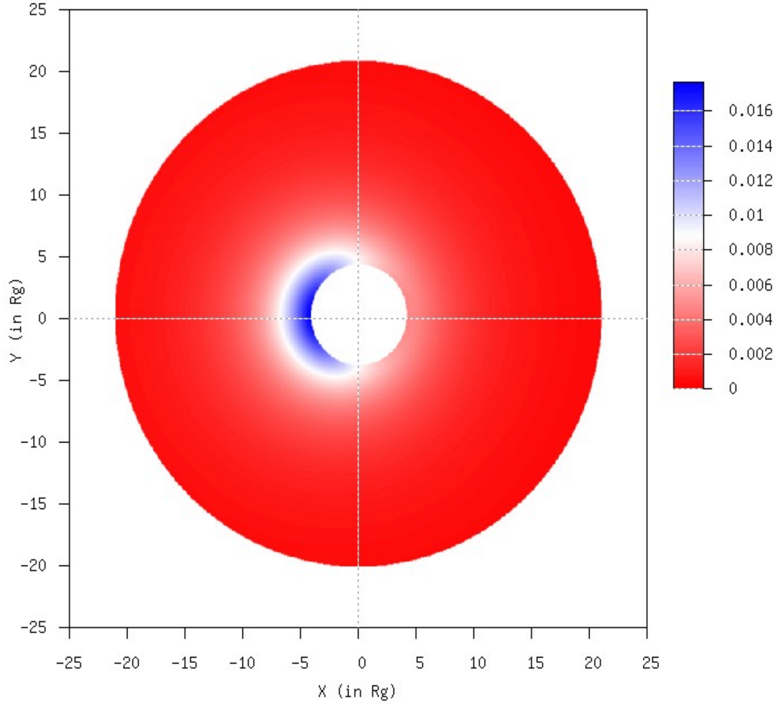

Kerr black hole images (a=0.75): **θ=30 deg**

- Redshift map
- Intensity map

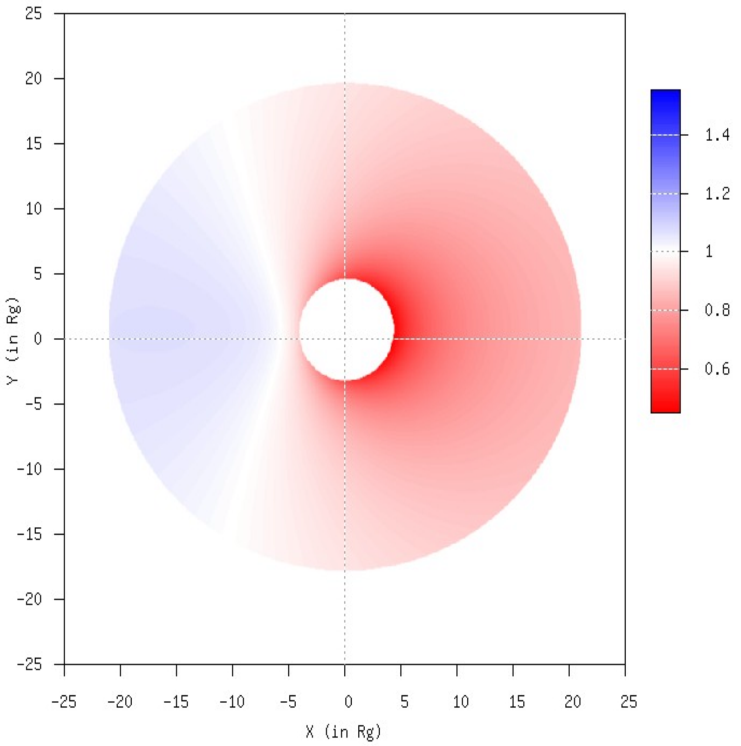

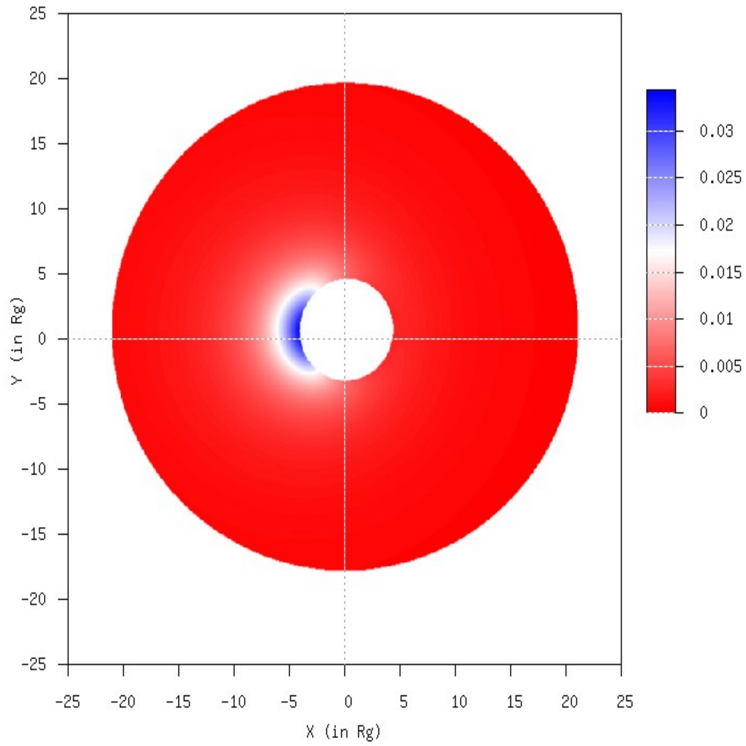

Kerr black hole images (a=0.75): **θ=45 deg**

- Redshift map
- Intensity map

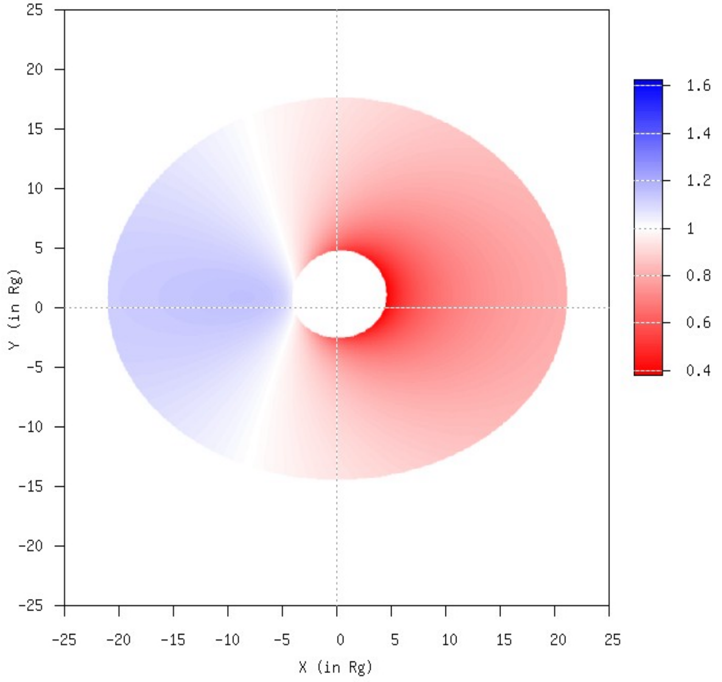

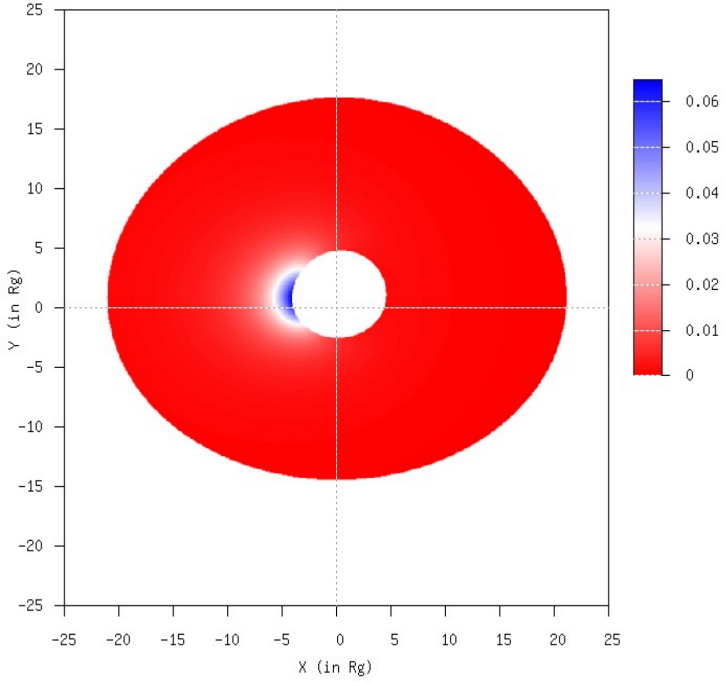

Kerr black hole images (a=0.75): **θ=60 deg**

- Redshift map
- Intensity map

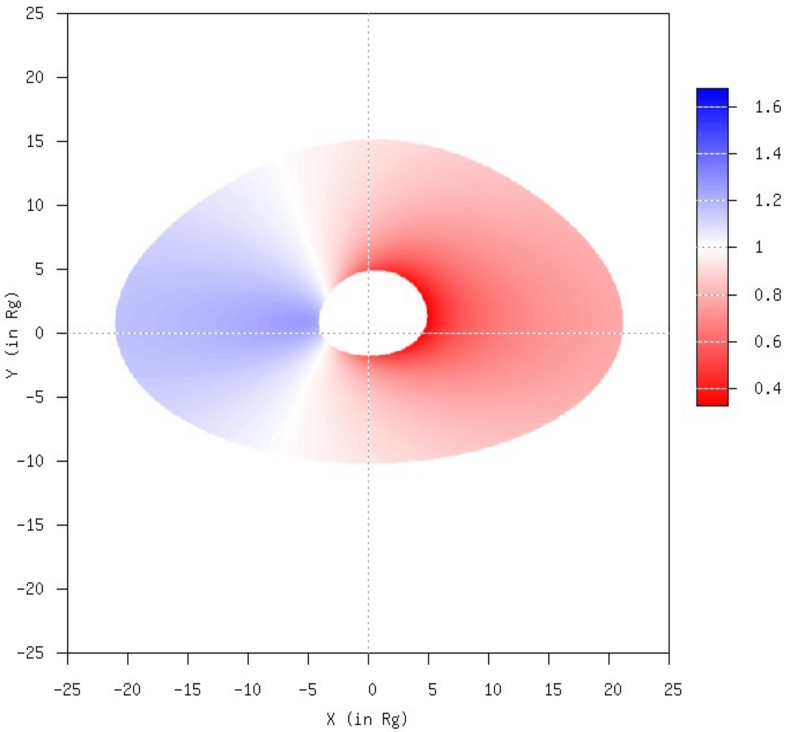

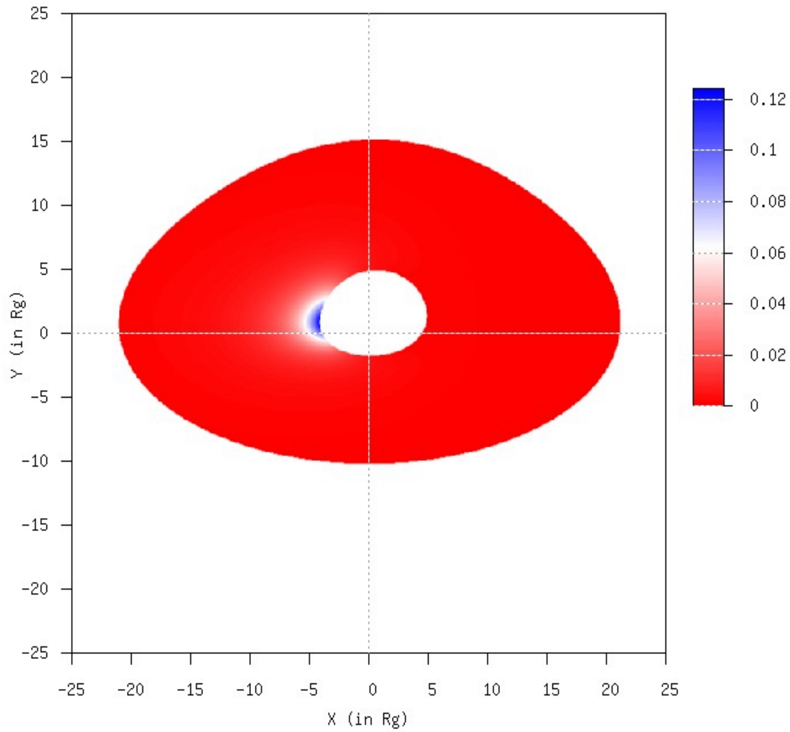

Kerr black hole images (a=0.75): **θ=75 deg**

- Redshift map
- Intensity map

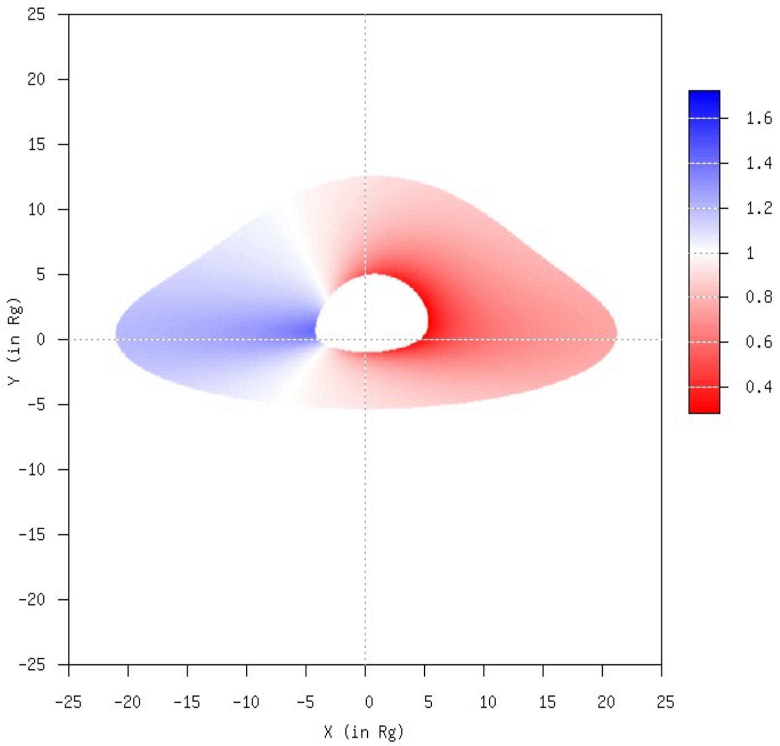

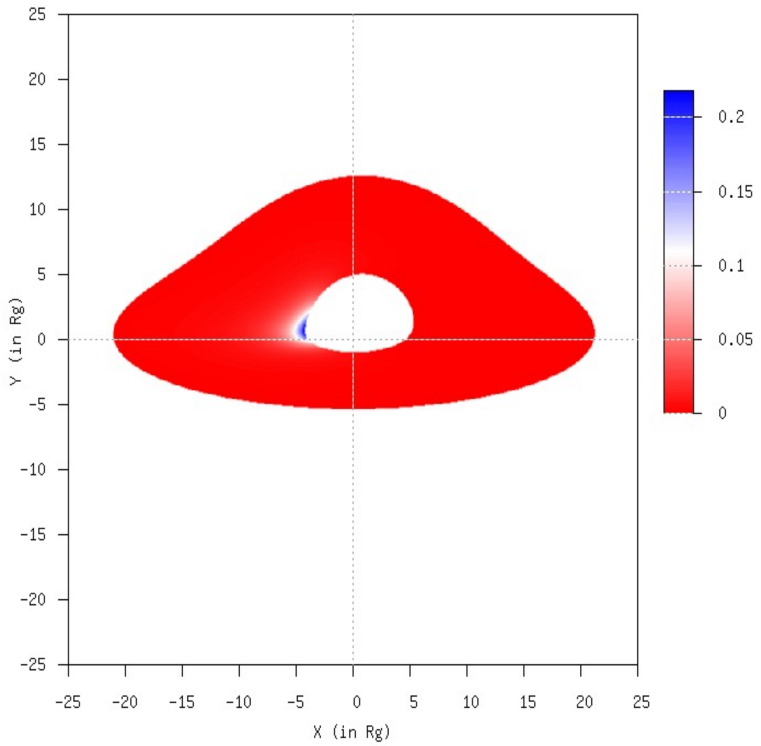

Kerr black hole images (a=0.75): **θ=85 deg**

- Redshift map

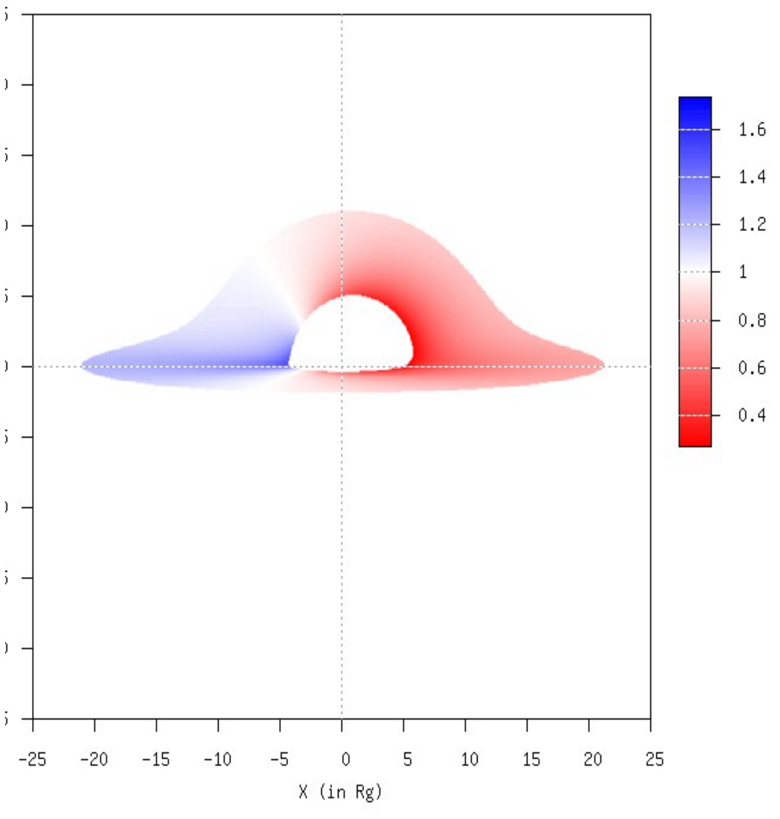

- Intensity map

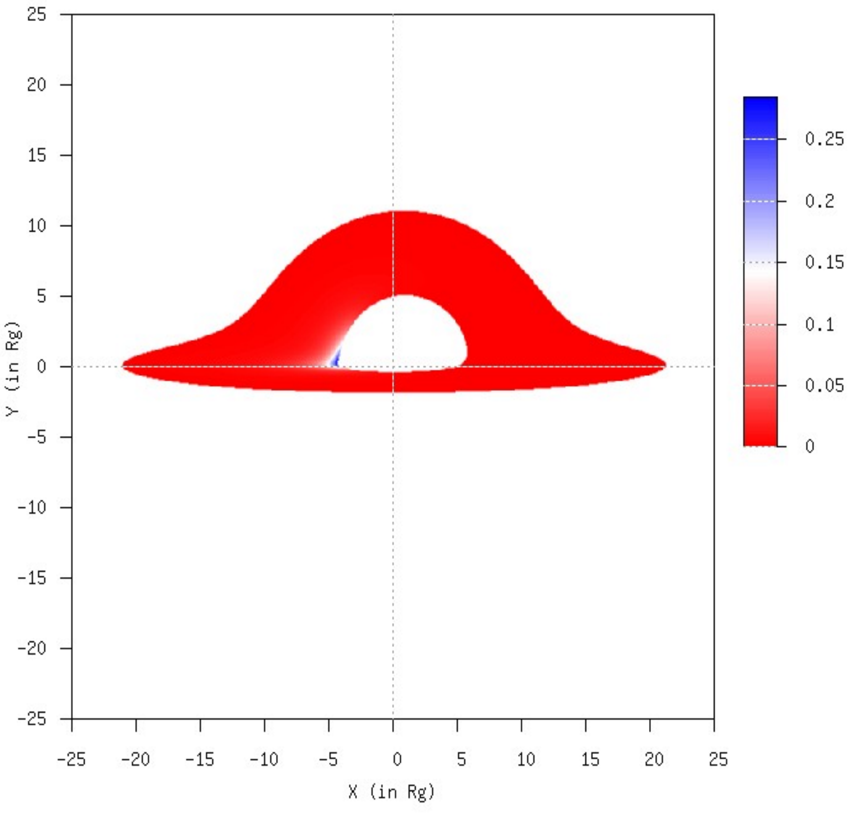

Kerr black hole images (a=0.75): **θ=89 deg**

- Redshift map

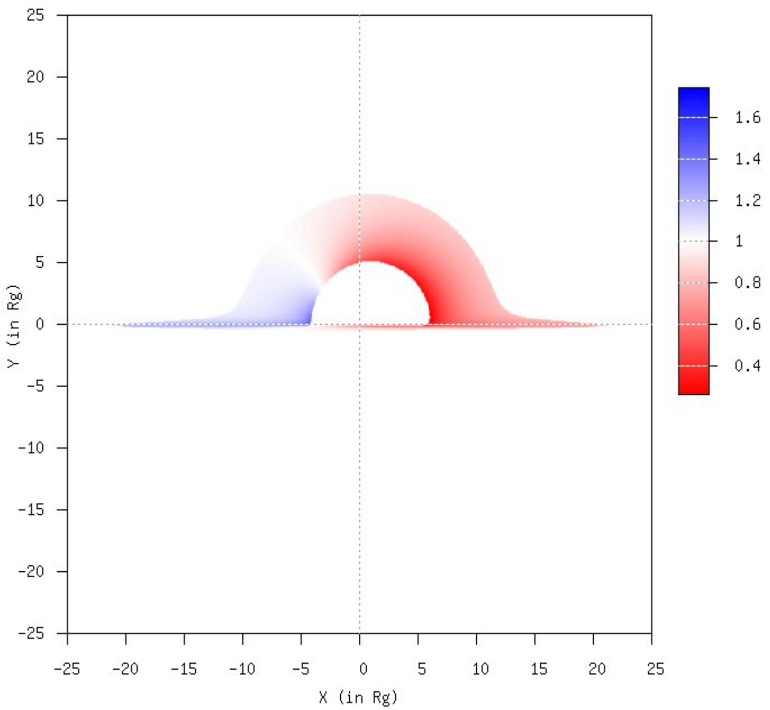

- Intensity map

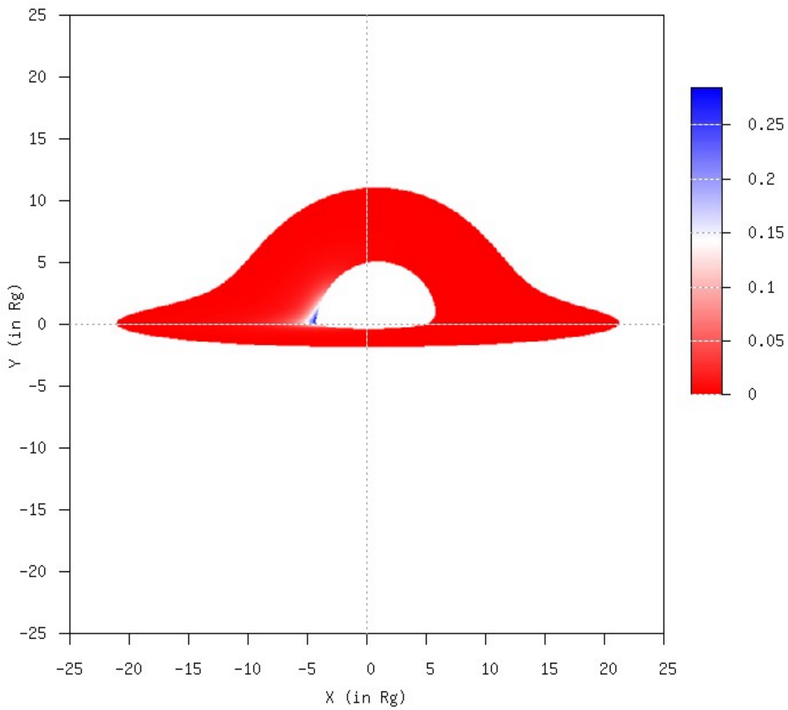

Kerr black hole images (*a*=0.99): **θ=15 deg**

- Redshift map
- Intensity map

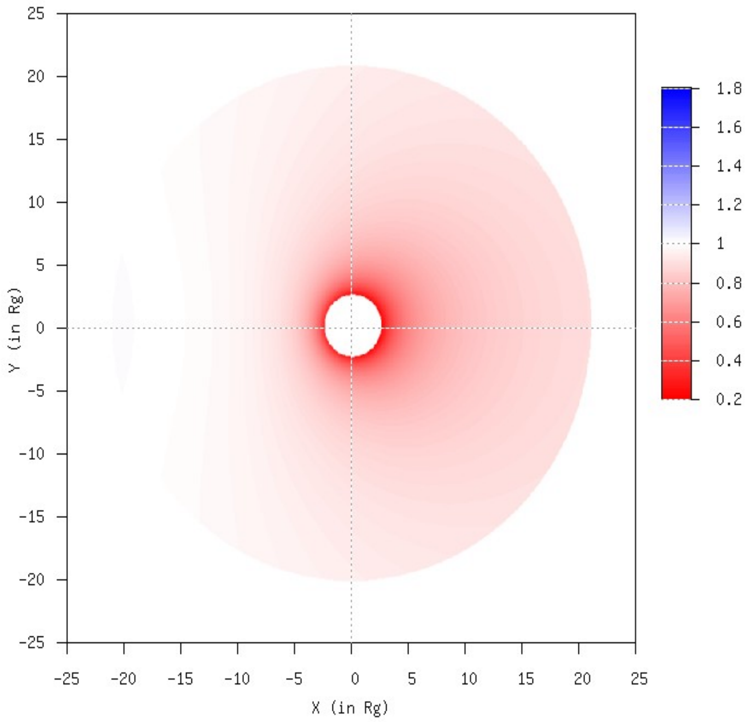

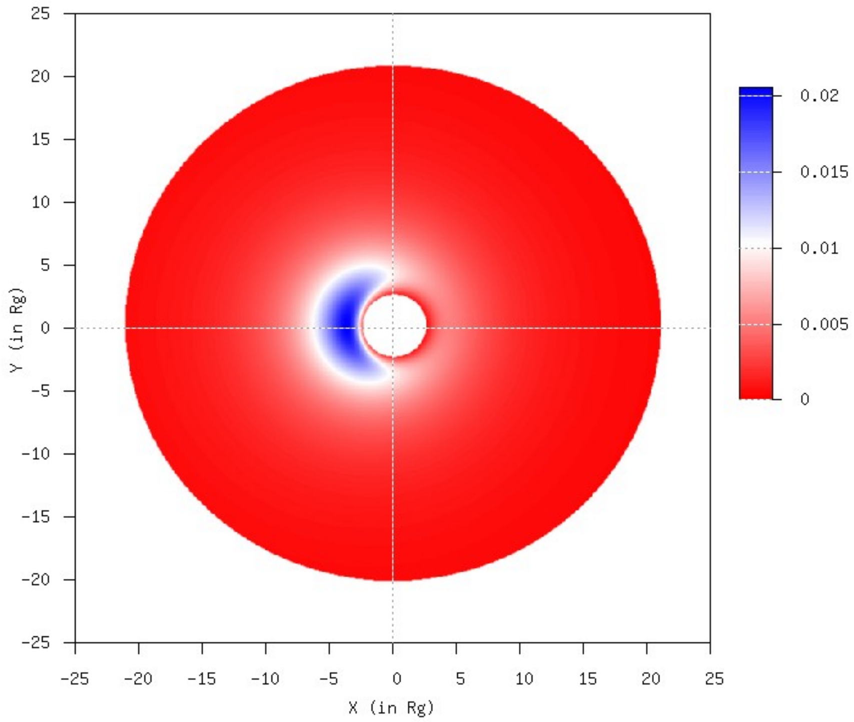

Kerr black hole images (a=0.99): **θ=30 deg**

- Redshift map
- Intensity map

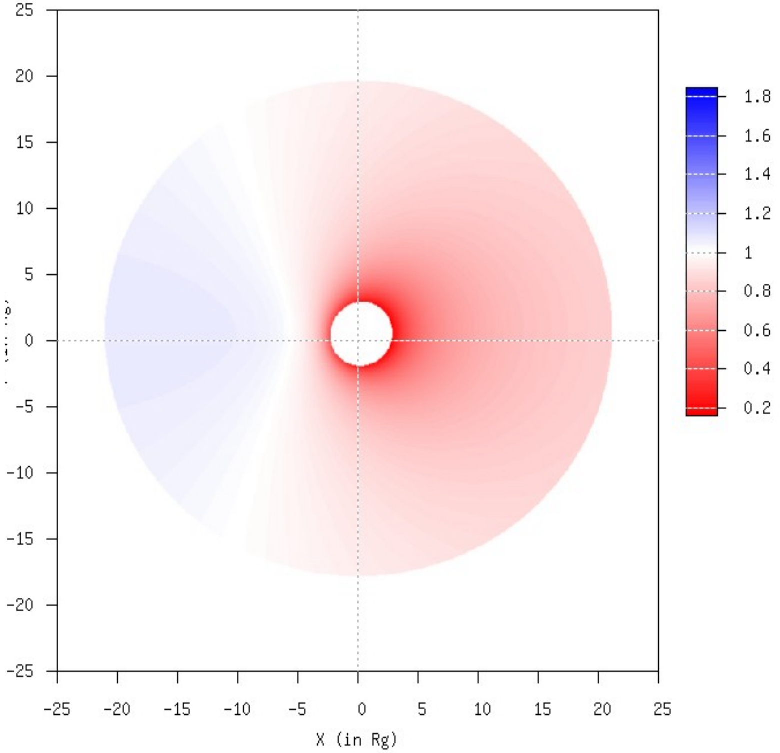

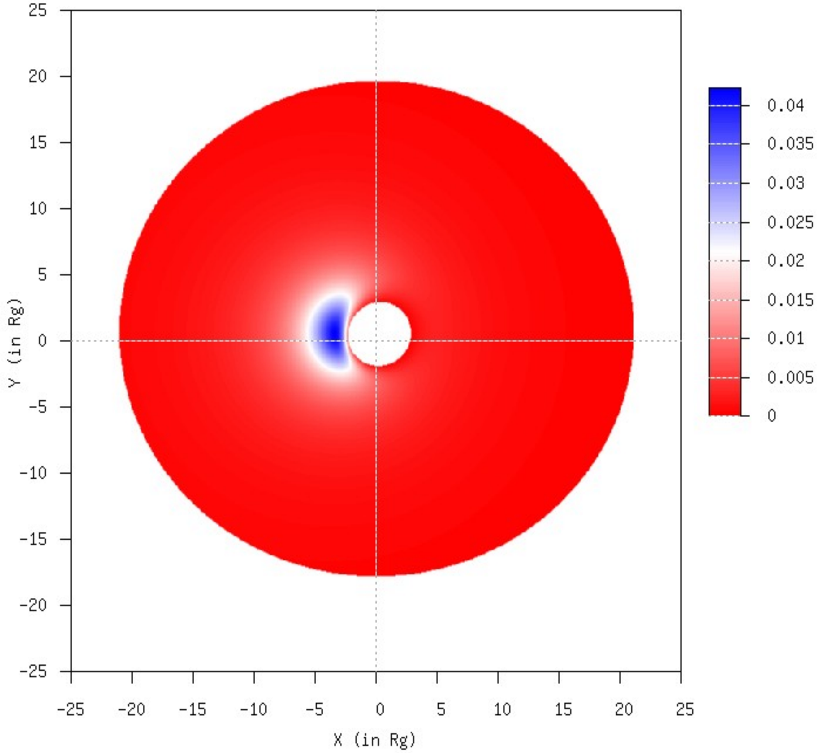

Kerr black hole images (a=0.99): **θ=45 deg**

- Redshift map
- Intensity map

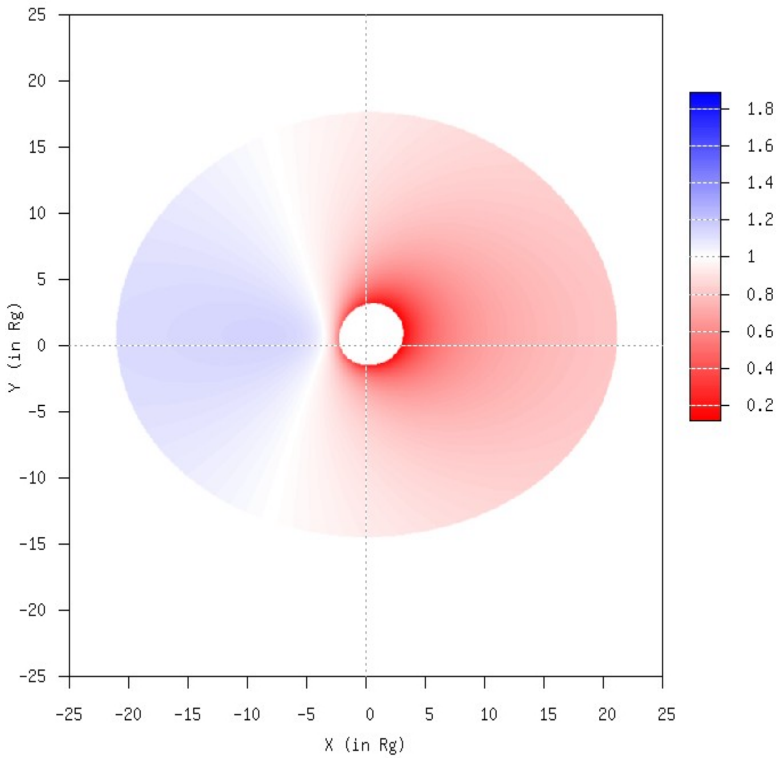

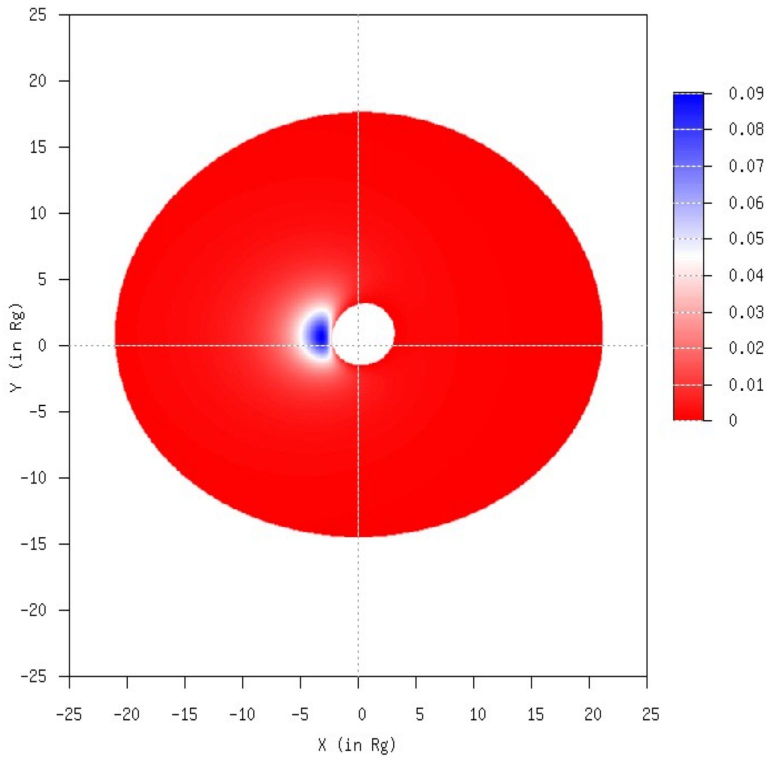

Kerr black hole images (*a*=0.99): **θ=60 deg**

- Redshift map
- Intensity map

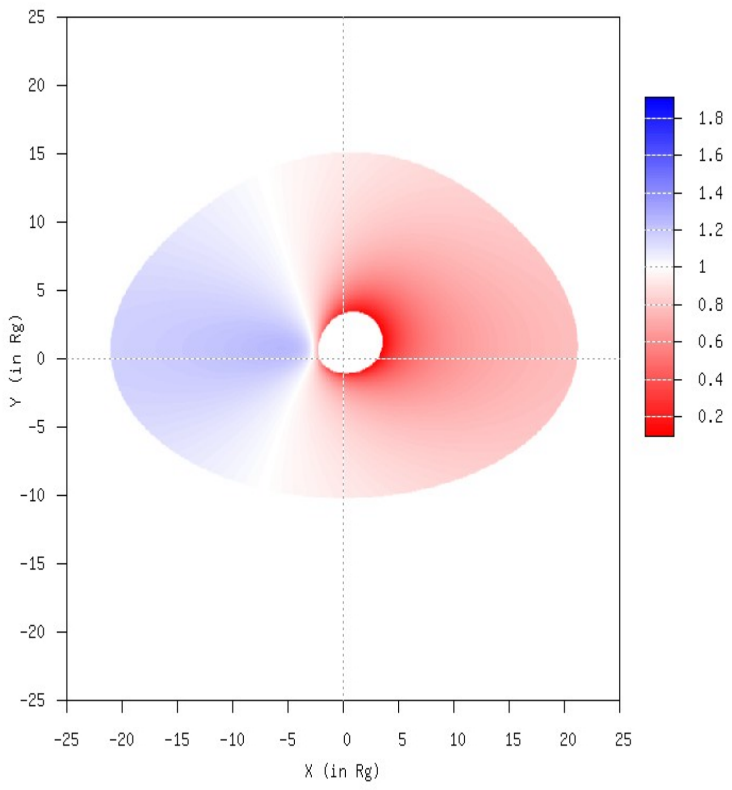

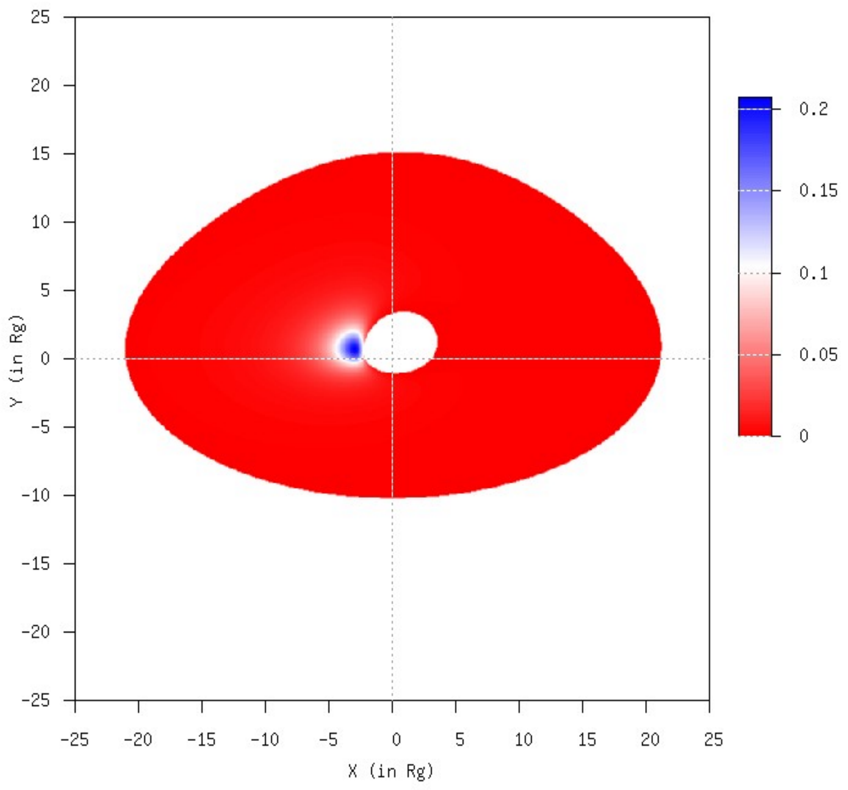

Kerr black hole images (a=0.99): **θ=75 deg**

- Redshift map
- Intensity map

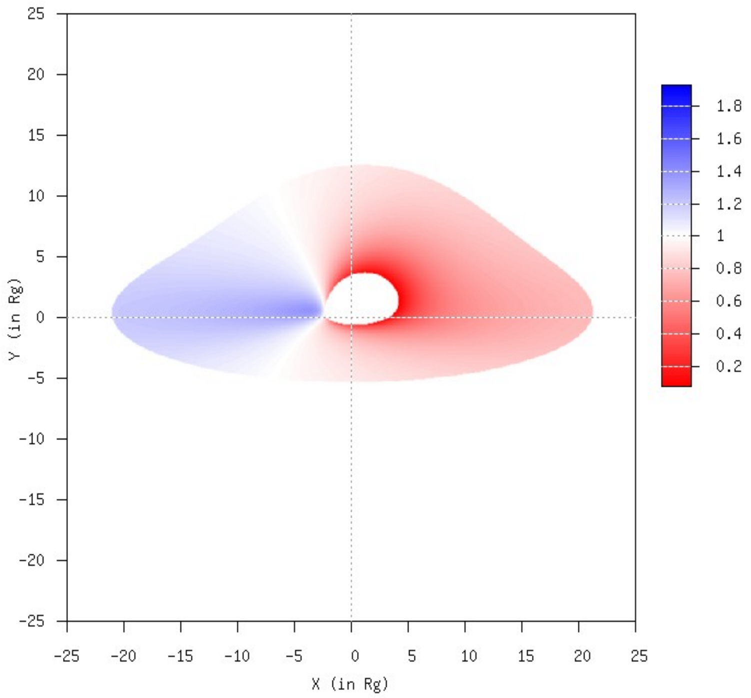

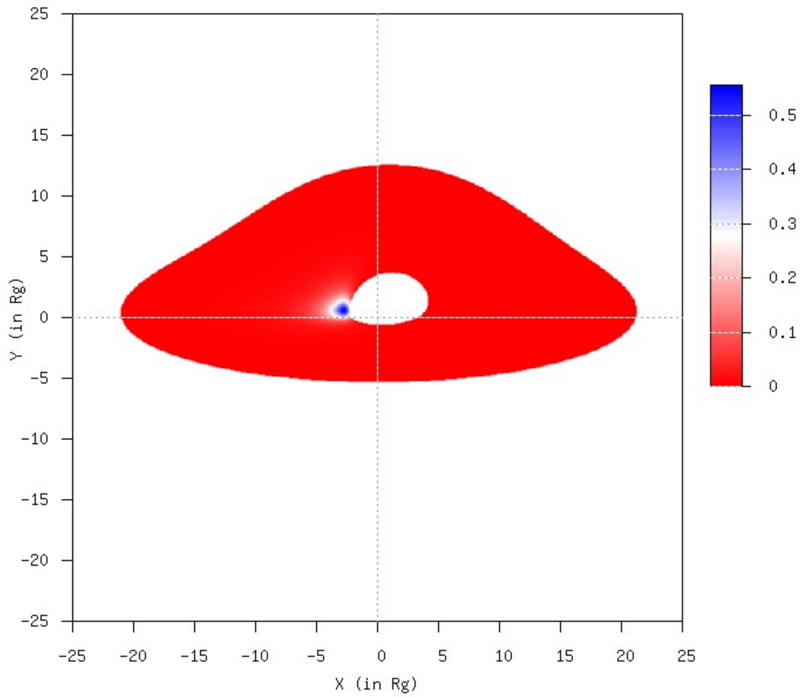

Kerr black hole images (a=0.99): **θ=85 deg**

- Redshift map
- Intensity map

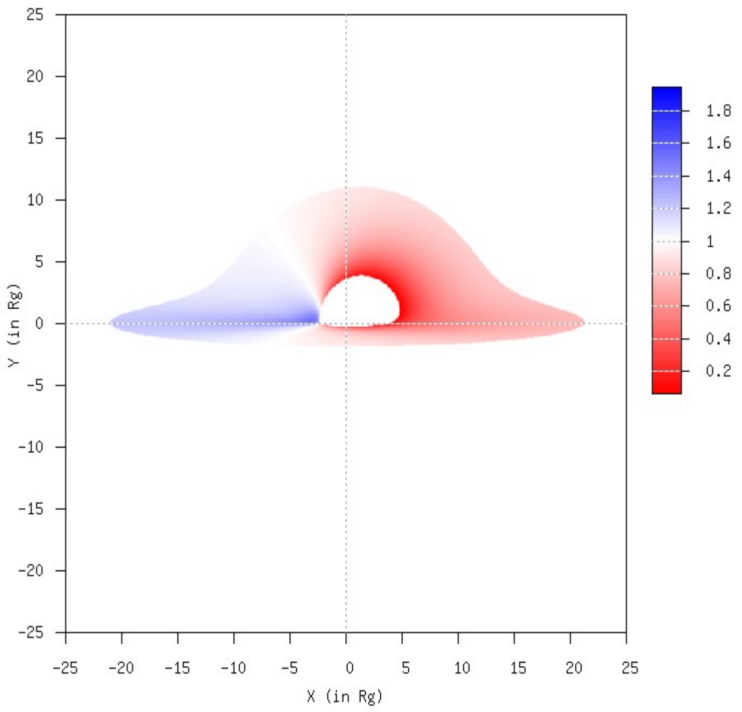

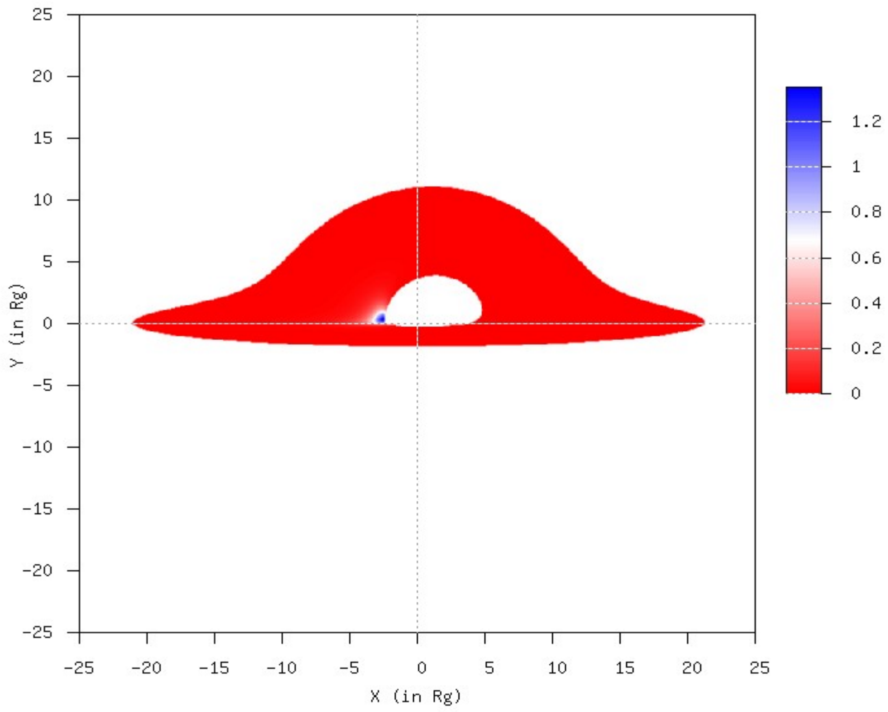

Kerr black hole images (*a*=0.99): **θ=89 deg**

- Redshift map
- Intensity map

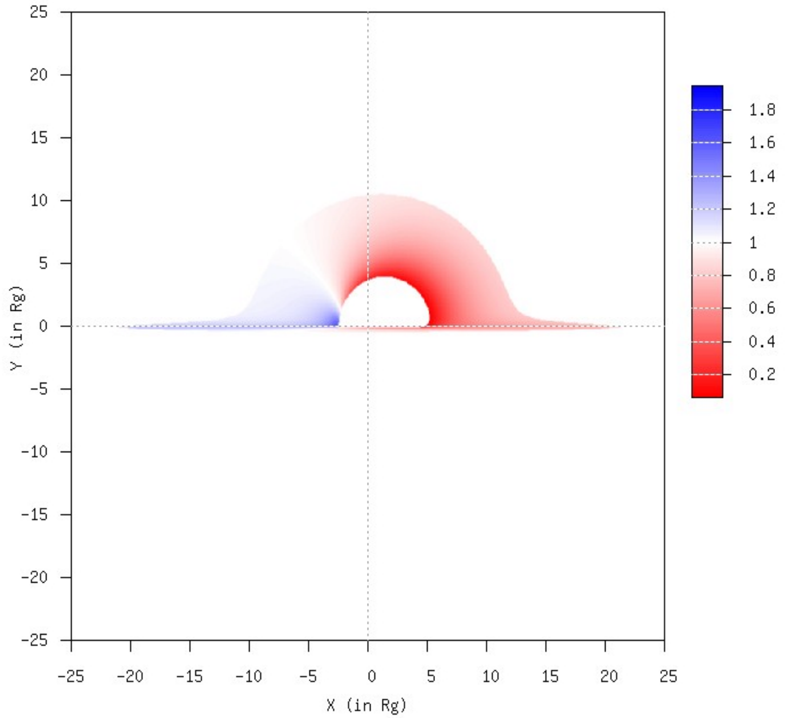

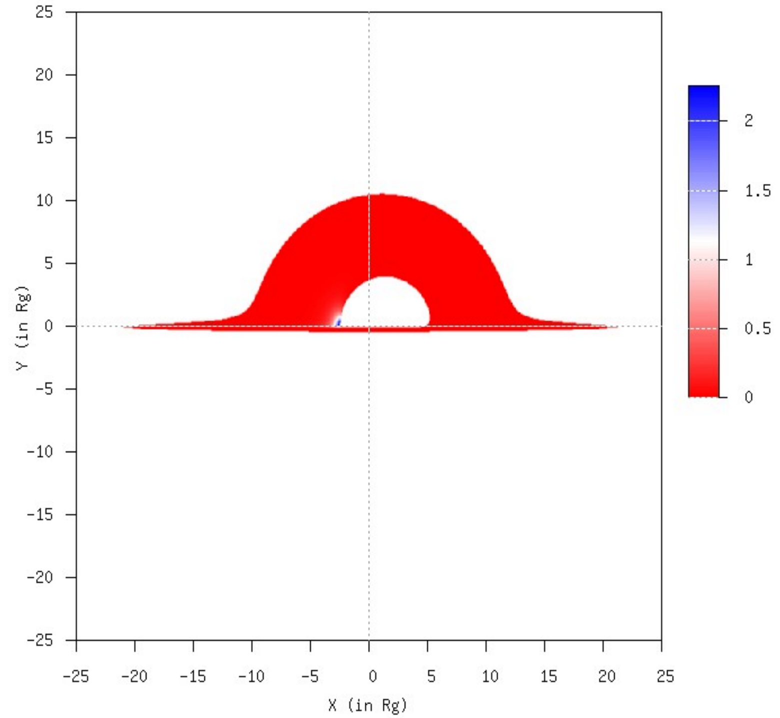

Conclusions

- Now the detailed structure of accretion disks is still unknown (in particular we do not know a thickness of accretion disks).
- Therefore, there is a possibility to observe highly inclinated accretion disks (about 1% of all AGNs snould have such high inclination. The situation is much better for microquasars; because of possible presession of accretion disks (for example, SS433).

  In this case this analysis could give us a useful tool for a determination

  of such high inclination angles, however another factors (which are behind of this simple model) could cause such line profiles.
- Distortion of iron line profiles could give essential information about magnetic fields near BH horizons in AGNs and GBHCs.

Searches for such features of spectral lines could useful to realize using present and future spacecrafts

such as

Chandra, XMM, Integral, Constellation.

- Radioastron could detect mirages (“faces”) around black holes.
- Shapes of images give an important information about BH parameters